THE FLUID DYNAMICS OF PRESSURE DIE CASTING PROCESSES

YING BIK LUI

Ph.D.

BRUNEL UNIVERSITY

1997

THE FLUID DYNAMICS OF PRESSURE DIE CASTING PROCESSES

A Thesis submitted for
the degree of Doctor of Philosophy

by

Ying Bik Lui

Department of Materials Engineering
Brunel University

September 1997

Abstract

Abstract

Title of thesis : **'The fluid dynamics of pressure die casting processes'**

submitted by : Ying Bik LUI

for : the degree of Doctor of Philosophy

at : Brunel University

in : September, 1997

The main text of the thesis consists of seven chapters. Following the literature survey, the work in Chapter 2 focuses on the study of the whole process of pressure die casting. The necessity of reclassification against the traditional 'three-stage' description is introduced in order to build a new basic tenet in constructing theoretical and practical investigations, which leads to the creation of fluid dynamic mathematical models of the process. On the basis of Chapter 2, Chapter 3 concentrates on dealing with the computer simulation of filling flow patterns occurring in the third stage that play the most important role in the process. The Simplified Marker And Cell (SMAC) method is used to obtain the computational results of the filling patterns of pressure die casting processes. On the basis of the computational analysis of typical examples, the viscosity, gravitational force and velocity effects on the overall filling pattern are examined, that lead to a validation of the important hypothesis that an ideal liquid can be used in numerical simulation of filling patterns and this enables one to achieve a more effective computer program for a complex cavity by quasi-3D or 3D models.

Chapter 4 treats a specific problem of the residual flow that exists in the final (fifth) stage of the process. Mathematical models of residual flow are derived.

Chapter 5 mainly consists of two parts. The first part deals with the application of similitude laws for simulating flows in pressure die casting processes. Detailed analyses and criteria on different relationships between model and prototype are given in order to correct previously offered formulae by Eckert (1989). The results of numerical simulation presented in Chapter 3 are also extended to validate the similitude criteria. The second part of Chapter 5 presents the use of a charge coupled device(CCD) for studying the diversity of fluid motion including the filling pattern, residual flow, thermals and air entrapment during cavity-fill and post cavity-fill within a one single shot cavity filling in water analogue experiments.

A discussion, conclusions and suggestions for further study of the subject concerned are presented in Chapters 6 and Chapter 7.

Acknowledgments

I wish to express my deeply appreciation to my supervisors, Professor Brian Ralph, Department of Materials Engineering, Brunel University and Professor W. B. Lee, Department of Manufacturing Engineering, Hong Kong Polytechnic University for their invaluable advice and guidance during my Ph.D. study.

Thanks also go to all my friends and colleagues for their support and encouragement throughout many years.

I would like to express my heartfelt gratitude to my whole family for their constant support, specially to my husband, Robert S. B. Lui, for his love, patience and continuous encouragement during my studies.

Table of Contents

Abstract ---------- i

Acknowledgements ---------- iv

Table of Contents ---------- v

List of Figures ---------- x

List of Tables ---------- xii

Nomenclature ---------- xiii

Chapter 1 Literature survey ---------- 1

1.1 The classification of a process of pressure die casting ---------- 2

1.2 The filling flow pattern of the die casting process ---------- 4

1.3 The numerical simulation of the filling pattern ---------- 8

1.4 The residual flow in the post-fill stage ---------- 14

1.5 The experimental studies of filling flow patterns ---------- 16

Chapter 2 A reclassification of the pressure die casting process ---------- 19

2.1 Introduction ---------- 20

2.2 The traditional classification of an injection process ---------- 21

2.2.1 The 'three-stage classification' of an injection process --------- 21

2.2.2 The problem of the traditional classification ---------- 21

2.3 A reclassification of the injection process ---------- 23

2.4 The equations governing the metal feeding system ---------- 24

2.4.1 The force balance equation ---------- 24

2.4.2 The continuity equation ---------- 24

2.5 The mathematical models applied in the reclassification ---------- 26

2.5.1 First stage: slow shot ---------- 26

2.5.2 Second stage: fast shot ---------- 27

2.5.3 Third stage: filling shot ---------- 27
(1) Flow rate and plunger speed ---------- 29
(2) Filling velocity of the molten metal ---------- 29
(3) Working pressure of molten metal ---------- 30
(4) Fill time ---------- 30
2.5.4 Fourth stage: pressure impact ---------- 33
(1) Peak pressure of the molten metal ---------- 34
(2) Peak pressure of the oil in the fluid power system ---------- 35
(3) Relation of dynamic pressures in the molten metal and oil ----- 35
(4) Bulk modulus of the molten metal ---------- 36
(5) Pressure impact time during the fourth stage ---------- 36
2.5.5 Fifth stage:final pressure setting ---------- 37
2.6 Conclusions ---------- 38

Chapter 3 The numerical simulation of filling flow pattern ---------- 40
3.1 Introduction ---------- 41
3.2 The governing differential equations ---------- 43
3.3 Highlight of the Simplified Marker And Cell (SMAC) technique ----- 43
3.3.1 Finite difference form of the equations ---------- 44
3.3.2 Solution scheme of the difference formulae ---------- 49
3.3.3 Free surface boundary conditions ---------- 51
3.3.4 Wall boundary condition ---------- 53
3.3.5 Marker particles movement ---------- 56
3.4 Turbulent viscosity model ---------- 57
3.5 Numerical stability conditions and accuracy ---------- 58
3.6 Computational results and analysis ---------- 59
3.6.1 The viscous effect on the overall filling pattern ---------- 60
3.6.2 The gravity effect on the overall filling pattern ---------- 61

3.6.3 The filling velocity effect on the overall filling pattern --------- 63
3.7 Simplification of computer program ---------- 66
3. 8 Conclusions ---------- 66
Annex 3-1 The vorticity field ---------- 67
Annex 3-2 The surface configuration ---------- 68
Annex 3-3 The basic surface cell configurations ---------- 71

Chapter 4 A study of the residual flow existing in pressure die casting processes ---------- 72
4.1 Introduction ---------- 73
4.2 The governing equation of residual flow ---------- 74
4.2.1 Hypotheses ---------- 74
4.2.2 The governing equations ---------- 76
4.3 Turbulent residual flow ---------- 76
4.3.1 Velocity profile ---------- 76
4.3.2 The maximum velocity of turbulent residual flow, $v_{r\max}$ -------- 77
4.3.3 The decaying velocity ---------- 78
4.4 Laminar residual flow ---------- 79
4.4.1 Velocity profile ---------- 80
4.4.2 The maximum velocity of laminar residual flow, $v_{r\max}$ -------- 80
4.5 The decay time of the residual flow ---------- 81
4.5.1 Water analogue experiments ---------- 81
(1) The decay time of turbulent residual flow ---------- 81
(2) The decay time of laminar residual flow ---------- 81
(3) The decay time for water analogue experiments, t_d ---------- 81
4.5.2 Solidification time of a pressure die casting process ---------- 82
4.5.3 Chvorinov's rule ---------- 86
4.6 Conclusions ---------- 87

Chapter 5 An experimental study of fluid dynamics in pressure die casting processes ---------- 88
5.1 The application of similitude laws to experiments ---------- 90
5.1.1 Similitude laws ---------- 90
(1) Hypothesis ---------- 90
(2) Geometric and kinematic similarity criteria ---------- 92
(i) Fill time scale ratio, S_t ---------- 92
(ii) Scale ratio of cavity thickness ---------- 92
(iii) Proper procedures for design practice ---------- 94
5.1.2 Dynamic similitude problems ---------- 96
5.1.3 Quasi-similitude ---------- 99
5.2 Flow visualization for simulating flow patterns & flow diversity ---- 103
5.2.1 Introduction ---------- 103
5.2.2 Experimental Apparatus ---------- 104
(1) Test rig ---------- 104
(2) Optical set up ---------- 104
5.3 Observations and analysis ---------- 107
5.3.1 Filling process ---------- 107
5.3.2 Thermals ---------- 114
5.3.3 The air entrapment ---------- 118
5.3.4 Residual flow ---------- 122
5.4 Conclusions ---------- 124
Annex 5-1 ---------- 125

Chapter 6 Discussion ---------- 126
6.1 Discussion on the study of reclassification of the processes ---------- 127
6.2 Discussion on the study of numerical simulation of filling pattern ----- 130

6.3 Discussion of the study of the residual flow in the post-fill stage ----- 133
6.4 Discussion of the experimental study ---------- 135

Chapter 7 Conclusions and suggestions for further work ---------- 139
7.1 Contributions of the theoretical study ---------- 141
7.2 Contributions of the experimental study ---------- 144
7.3 Recommendations for further study ---------- 144

References ---------- 146

List of Figures

Figure 1-1 Molten metal flow within a die by Frommer's (1933) concept -- 5

Figure 1-2 Molten metal flow within a die by Brandt's (1938) concept ----- 7

Figure 1-3 Molten metal flow within a die cavity by experimental demonstration (Koester and Goehring (1941)) ---------- 9

Figure 2-1 Reclassification of pressure die casting process ---------- 22

Figure 2-2 Hydraulic main circuit of molten metal feed system ---------- 25

Figure 2-3 The calculation relationship between filling velocity and pressure of the molten metal ---------- 28

Figure 2-4 Schematic diagram showing liquid compressibility in the metal feed system ---------- 31

Figure 3-1 Layout of velocity and pressure variables ---------- 45

Figure 3-2 Components of velocity and pressure values used in calculations of u^{n+1} and v^{n+1} - ---------- 47

Figure 3-3 Positions of field variables at a wall ---------- 54

Figure 3-4 Computed marker plots of the same overall filling patterns for different viscosity of $\upsilon = 1\times10^{-4} m^2 s^{-1}$, $\upsilon = 1\times10^{-6} m^2 s^{-1}$, and $\upsilon = 1\times10^{-9} m^2 s^{-1}$ ---------- 62

Figure 3-5 The gravity effect on the filling pattern ---------- 64

Figure 3-6 The filling velocity effect on the filling pattern ---------- 65

Figure 3A-2 Arrangement of different surface cell ---------- 69

Figure 3A-3 Four basic configurations of free surface cell ---------- 71

Figure 4-1 Velocity profile of turbulent residual flow ---------- 75

Figure 4-2 A typical velocity profile of a decay process of residual flow ---------- 83

Figure 4-3 A typical velocity profile of a decay process of residual flow without laminar flow ---------- 84

Figure 5-1 A typical history of molten metal pressure and flow rate of pressure die casting process ---------- 91

Figure 5-2 Schematic diagram for kinematic similarity flows ---------- 93
Figure 5-3 Relationship between dimensional scale, flow rate scale and cavity fill time scale for model and die ---------- 101
Figure 5-4 Relationship between velocity scale, flow rate scale and cavity fill time scale for model and die ---------- 102
Figure 5-5 Experimental apparatus set up ---------- 105
Figure 5-6 Optical layout ---------- 106
Figure 5-7 The configuration and filling sketch of the test model ---------- 108
Figure 5-8 Filling pattern in a circular cavity from video-print ---------- 109
Figure 5-9 Filling pattern in a rectangular cavity from video-print --------- 110
Figure 5-10 Filling pattern in a rectangular cavity with a full weir gate from video-print ---------- 111
Figure 5-11 Filling pattern in a circular cavity from computation---------- 112
Figure 5-12 Filling pattern in a rectangular cavity from computation ---------- 113
Figure 5-13 Thermal flow patterns ---------- 116
Figure 5-14 Dynamic behaviours of air entrapment from computer image processing ---------- 119
Figure 5-15 Dynamic behaviours of air bubble from video-print ---------- 120
Figure 5-16 Smaller bubbles become blisters that stick onto the inner wall of the cavity ---------- 121
Figure 5-17 The relation between decay time, cavity thickness and kinematic viscosity ---------- 123
Figure 6-1 The molten metal feed system ---------- 129

List of Tables

Table 3-1 Viscosity data ---------- 60

Table 4-1 Examples of the decaying nature of the velocity during residual flow ---------- 78

Table 4-2 Examples of the decaying nature for different cavity thickness after one second of residual flow initiated and assuming $(v_{r\max})_g = 20 ms^{-1}$ ---------- 79

Table 5-1 Typical examples of the model-prototype scale ---------- 95

Table 5-2 The formulae, definition and significance of dimensionless numbers ---------- 97

Table 5-3 Dimensions of the model and/or die calculated from Eckert's criteria ---------- 98

Table 5-4 The decay time of residual flow obtained from experiments ---------- 122

Nomenclature

a	area of plunger
a_c	cross-sectional area of rectangular die cavity
a_g	area of gate
A	projected area of cavity
A_a	working area of actuator
A_b	area of back surface of actuator
b	width of the gate
B	width of the cavity
c_c	coefficient of contraction
c_d	discharge coefficient of the metal feed system
c_f	combined friction factor of actuator with plunger
c_p	specific heat at constant pressure
c_r	decay time coefficient of residual flow
c_s	coefficient of solidification time
c_v	velocity coefficient of the jet
d_h	hydraulic diameter of the gate
D	divergence
$\overline{D}$	divergence in tentative field
D_h	hydraulic diameter of the cavity cross section
E_u	Euler number
F_r	Froude number
f	friction factor
g	gravitational acceleration
G_r	Grashof number
H	thickness of cavity

H_a	average casting thickness
H_g	height of the ingate
H_{min}	minimum casting thickness
h	average casting thickness of the molten metal
I	strain rate
K	damping coefficient
K_o	damping coefficient of residual flow
K_{ol}	damping coefficient of laminar residual flow
K_{ot}	damping coefficient of turbulent residual flow
l_{com}	total compressed length of molten metal in the plunger
l_m	characteristic mixing length
L	characteristic length
L_p	stroke of plunger
m_x , m_y	x, y component of unit tangential stress to the surface
M_0	Morton number
n_x , n_y	x, y component of unit outward normal stress to the surface
p	pressure of molten metal
p_a	oil pressure of actuator
p_{af}	pressure of the oil in the third filling stage
p_{ao}	air pressure in the cavity; with proper venting $p_{ao} = 0$
p_b	oil back pressure of actuator
p_f	pressure of the molten metal flow in the third filling stage
p_{max}	stable maximum pressure of the molten metal
$(p_p)_{met}$	peak pressure of the molten metal
$(p_p)_{oil}$	peak pressure of the oil
P_r	Prandtl number

p_{rel}	stable setting pressure of the pressure relief valve
$\sum \Delta p$	total pressure loss of the metal feed system.
$\sum \Delta p_b$	total pressure loss in the oil return circuit
$\sum \Delta p_f$	total pressure loss in the metal feed system
q	flow rate of molten metal
q_1	unit width flow rate of the molten metal
Q	flow rate
Q_a	inlet flow rate of the actuator, $Q_a = \mathrm{A}_a\ \dot{x}$
Q_b	return flow rate of the actuator
Q_{accu}	flow rate generated by the accumulator
Q_{pump}	flow rate of the oil pump
R_e	Reynolds number
R_{ef}	Reynolds number based on the filling velocity
R_f	fluid ratio of molten metal
S_l	dimensional scale
S_p	pressure scale
S_q	flow rate scale
S_ϱ	density scale
S_t	fill time scale
S_v	velocity scale
t	time
t_d	decay time of residual flow
$t_{d\ l}$	decay time of laminar residual flow
$t_{d\ t}$	decay time of turbulent residual flow
t_f	fill time
t_p	pressure impact time

t_s	solidification time
Δt	time increment
T_w	water temperature
ΔT	temperature difference of wall surface & bulk fluid
U_i , U_j	mean velocity components
u, v, w	velocity components in x, y, z coordinates respectively
u^*, v^*, w^*	dimensionless velocity components u, v, w respectively
$\overline{u}, \overline{v}$	tentative velocity components in x, y coordinates respectively
u_0, v_0	marker velocity components in x, y coordinates respectively
v_{accu}	the portion of plunger speed periodically generated by the accumulator
v_b	outlet velocity of oil
v_c	critical velocity of turbulent flow transiting to laminar flow
v_f	filling velocity
v_p	plunger speed ($= \dot{x}$), $v_p = \frac{Q_a}{A_a}$
v_{pump}	the portion of plunger speed continuously generated by the oil pump
v_r	velocity of residual flow
$v_{r\max}$	maximum velocity of residual flow
$(v_{r\max})_g$	maximum available velocity of residual flow at gate
$v_{r\,s}$	velocity of residual flow during solidifying process
V	velocity magnitute
$\overline{V}$	volume of the cavity
$\overline{V_{cav}}$	total volume of the cavity including volume of overflow
$\overline{V_{met}}$	total volume of molten metal including volumes of gooseneck, runner, cavity of castings and overflow.
$\overline{V_{oil}}$	total oil volume in the high pressure side of the fluid power system

$\Sigma\Delta V$	total volume including volumes of gooseneck, runner, casting cavity and overflow wells
$\overline{\Delta V_{met}}$	relative volume of the compressed molten metal
$\overline{\Delta V_{oil}}$	relative volume of the compressed oil
W	weight of actuator with plunger
x	plunger displacement
$\dot{x}$	plunger speed
$\ddot{x}$	plunger acceleration
x, y, z	spacial coordinates
x^*, y^*, z^*	dimensionless spacial coordinates x, y, z respectively
X, Y, Z	x, y, z components of body force respectively
Z_o	molten metal level inside cavity above gate centre line.

Greek symbols

β_{oil}	bulk modulus of the oil (approximately 17.5 kbar)
β_{met}	bulk modulus of the molten metal
τ	shear stress of molten metal
ω	vorticity
$\overline{\omega}$	vorticity in tentative field
Γ	arbitrary pressure field
φ	potential function
ϱ	density of liquid
μ	dynamic viscosity
λ	cavity height of test model
υ	kinematic viscosity

υ_e	effective viscosity
υ_t	turbulent viscosity
υ^*	effective kinematic viscosity
σ	surface tension of liquid
∇	Laplace operator

Suffix

m	model
d	die
k	marker
i, i+1/2;	
j, j+1/2 etc.	position of field variables

Superscripts

n, n+1	time inteval

Chapter 1

Literature survey

Chapter 1

Literature survey

Pressure die casting is one of the most efficient and important techniques for metal processing. It can be applied to produce nearly net-shape, thin, geometrically complicated parts in large quantities with a short process cycle. The successful production of die castings for about 60 years (1920s-1980s) relied mostly on experience and there was a lack of a mathematical framework to relate all the important variables in die casting. In the last fifteen years combined fluid flow and heat transfer analysis for the filling of castings has received a great deal of attention. It is an accepted fact that computer simulation is an effective way to understand the complex nature of the filling flow and the associated solidification process. The development of such software that predicts flow patterns is commercially available although it is necessary to refine the programs to increase the accuracy.

1.1 The Classification of a Process of Pressure Die Casting

A correct classification of the pressure die casting processes is important in a better understanding of the nature of a process and in establishing mathematical models to present the process, and consequently in achieving quality castings.

Barton presented several articles from 1944-1952 and collected these into a review chapter in 1964. The chapter discussed the effect of injection pressure, the effect of temperature gradients, and velocity variations within the molten metal and in the layer adjacent to the metal-die interface throughout the whole casting cycle. Barton divided the process of die filling into three phases:

Phase I: A jet traverses the cavity, impinges on the opposite wall, then

spreads over the major portion of the die surfaces. An initial projected skin is thus formed and small accumulations of turbulent metal occur at points where the direction of flow changes abruptly.

Phase II: The shell formed then fills by deposition of further metal upon its inner surface. The turbulent accumulations enlarge at this stage.

Phase III: As the cavity is completely filled, the full injection pressure is uniformly exerted upon the casting through its still fluid core.

Barton pointed out that the characteristics of injection in the first phase govern the surface finish; the second phase controls the solidity, and in the third phase the strength of the casting is determined.

Sachs (1952) presented a theoretical and complexity analysis of the molten metal flow process. He considered steady flow status in the process and also derived equations for non-steady flow of the liquid metal injection in a cold chamber casting system section by section in six sequences without classification of the liquid metal filling process.

Many experimental studies have monitored the process parameters and provide useful information for process control of quality cast products. These data are valuable for analysis and classification of filling stages (Doehler, 1951; Veinik, 1958; Davis and Siauw, 1977; Davis *et al.*, 1977a, b; Robinson, 1977; Randolph *et al.*, 1977; Segawa, 1977; Allsop and Kennedy, 1983; Andersen and Ingerslev, 1983; Hernandez and Hamar 1985; Fink, 1987; Zeleniak, 1993). These experiments presented the fundamentals of shot monitoring in a pressure die casting machine operation, in which three stages of slow shot, fast shot and filling shot are applied for the interpretation of shot traces.

Stuhrke and Wallace (1965) reported the research outcomes of the fluid flow patterns in simulated die cavities. A classification with four periods of the die casting operation was introduced: (i) slow shot, (ii) free or fast shot, (iii) fill and (iv) packing periods.

Sanders *et al.* (1970) illustrated a four-stage: (i) pre-injection, (ii) die filling (injection), (iii) packing and (iv) damping that was identified on the monitored pressure curve for a hot-chamber die casting machine. Shawki and Kandell (1988) re-illustrated the same four-stage classification of the die casting operation in their review paper.

Minaie (1989) divided the die casting process into a two-stage model for fluid flow and solidification in which the second stage commences at the completion of filling stage.

Jonsson *et al.* (1991) proposed that the filling flow in castings can be divided in two: (i) The Newtonian fluid flow (molten metal) in turbulent motion at the filling stage, and (ii) The non-Newtonian fluid (melt-solid slurry) flow behaviour at the solidification stage.

Unfortunately, the above works attempted to classify a process of pressure die casting into a so-called three-stage or four-stage process which could not completely disclose the nature of the process and therefore could not represent the complete mathematical model of each stage.

1.2 The Filling Flow Pattern of the Die Casting Process

It is well known that the flow pattern in the filling stage of a die casting process is directly concerned with the quality of casting products. The two earliest publications about the analytical approach for calculating the metal velocity and the die filling time were Frommer (1933) and Jacobi (1950). Frommer postulated the molten metal flow in a die cavity to be an ideal flow that follows the laws of fluid mechanics. Frommer's concept of metal flow within a die is shown in Figure 1-1. The molten metal to be injected into a die of a rectangular cross-section, traverses the cavity in a jet with a cross-section identical to the shape of the gate, as shown in Figure 1-1(a). The jet strikes the opposite wall where it gathers into a pulsating pool. As the pool fills, it becomes

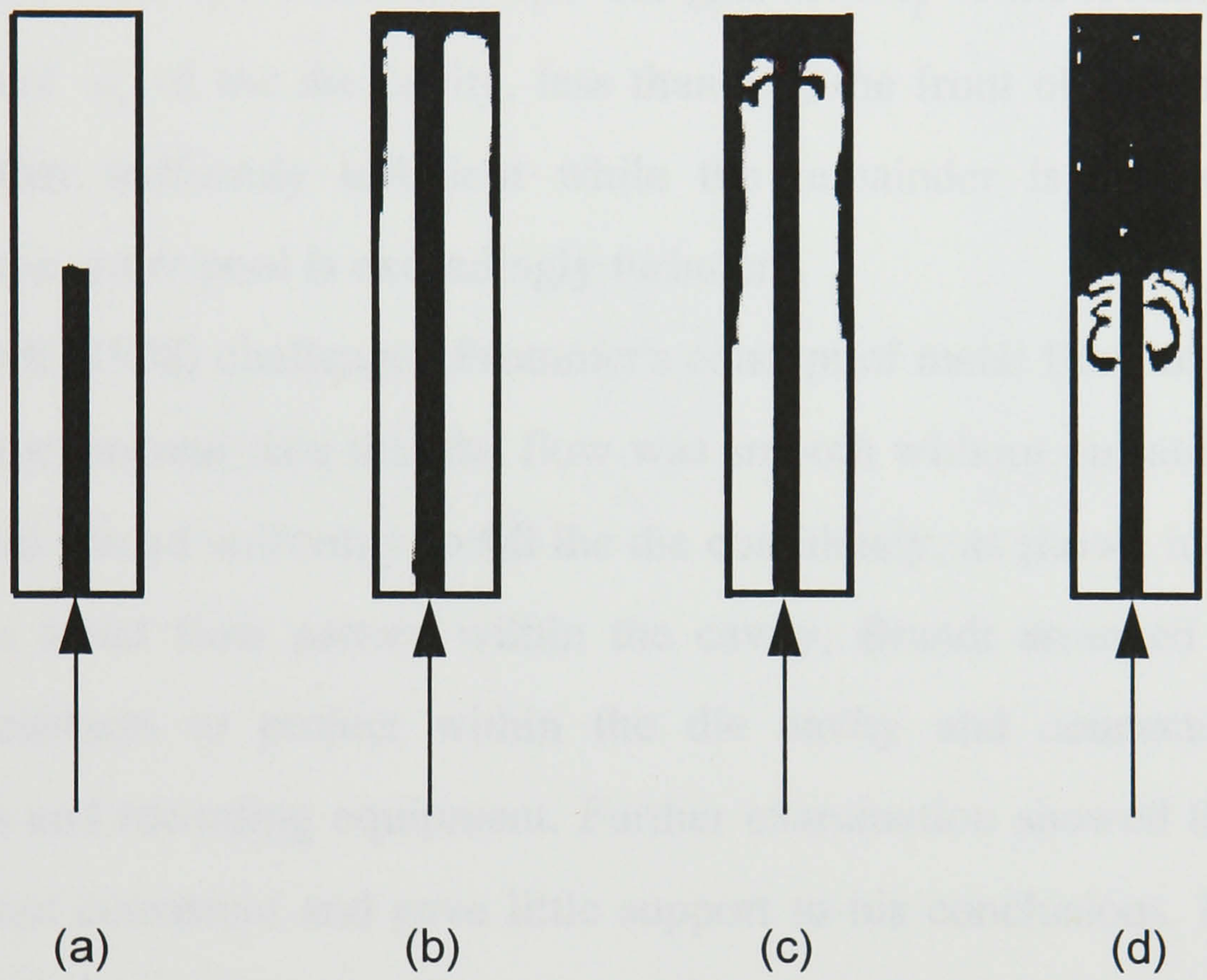

Figure 1-1 Molten metal flow within a die following Frommer's (1933) concept.

more turbulent; portions of it flow back along the walls of the cavity ahead of the filled-pool, as shown in Figure 1-1(b). Finally considerable turbulence at the filled-pool holds the incoming stream and the portions of metal along the walls that slow down due to friction and heat loss to the cavity walls, as shown in Figure 1-1(c). All the metal on the die walls is taken in at the filled-pool and then gradually fills the die, as shown in Figure 1-1(d). With a small injection velocity of the molten metal and a ratio (a_g/a_c), the gate area a_g to the rectangular cross-sectional area a_c of the die cavity, less than 1/3, the front of the molten metal pool is rather uniformly turbulent while the remainder is relatively stable; otherwise, the entire pool is exceedingly turbulent.

Brandt (1938) challenged Frommer's concept of metal flow and concluded from his experimental data that the flow was smooth without pulsation's and the molten metal spread uniformly to fill the die completely, as shown in Figure 1-2. To indicate metal flow pattern within the cavity, Brandt arranged a series of electrical contacts to project within the die cavity and connected them to instruments and recording equipment. Further examination showed that Brandt's data were not consistent and gave little support to his conclusions. Koester and Gohring (1941) maintained, splattering rather than flowing could have closed Brandt's test circuits prematurely. Although Brandt's experiments failed, the approach was valuable because it focused the attention of Koester and Gohring on Frommer's work, and inspired them to design an experiment to resolve the opposing views of Frommer and Brandt.

Koester and Gohring concluded that the metal flow into a die was basically in line with that presented by Frommer. Their experimental result, shown in Figure 1-3, proves that Frommer's concept of cavity filling is a major contribution to the formulation of a theory of metal flow in die casting.

Bennett (1961) used a water model with gate velocity about 22 $m\ s^{-1}$. The experimental results were remarkably similar to Frommer's ideal fluid

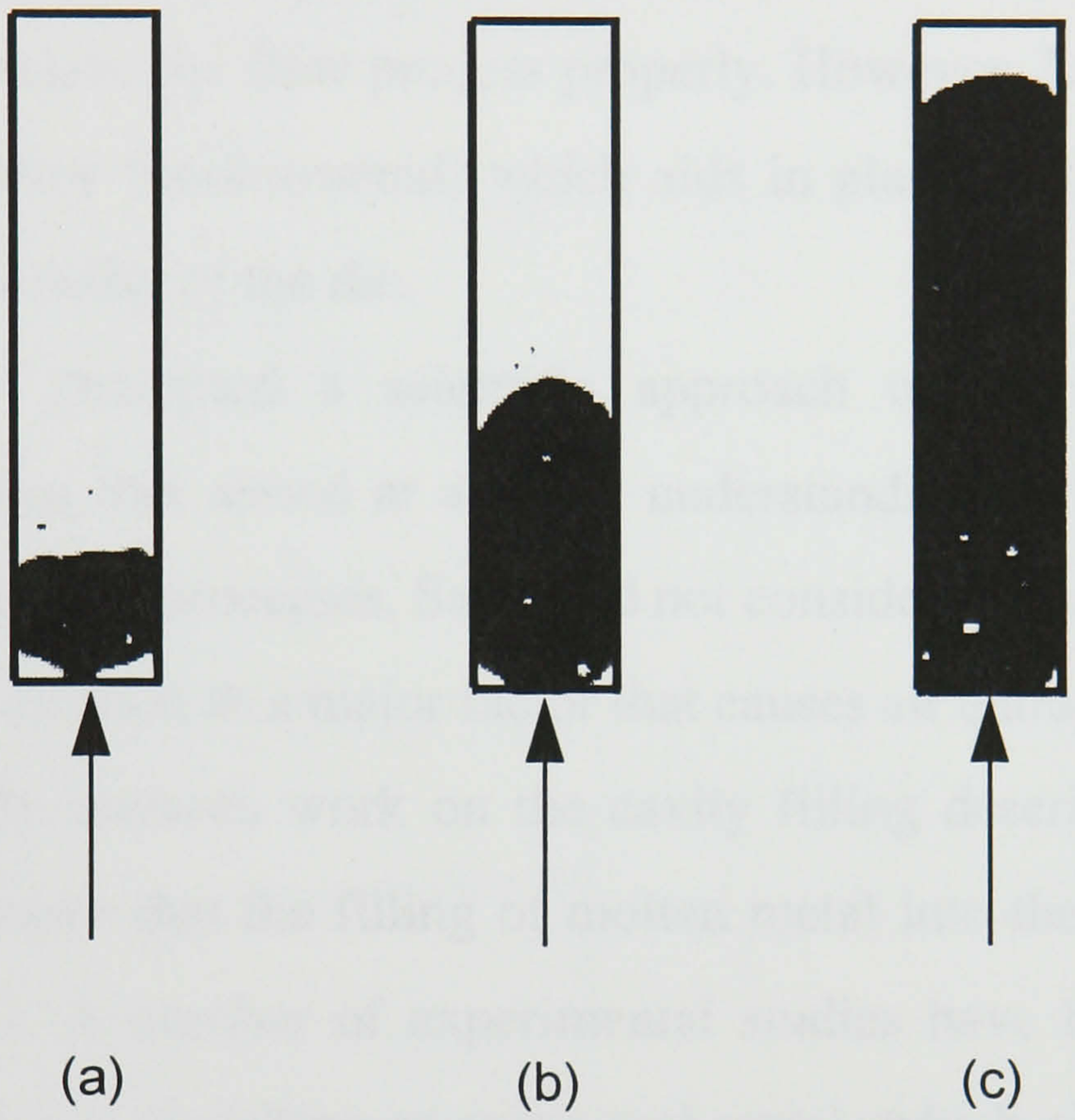

Figure 1-2 Molten metal flow within a die following Brandt's (1938) concept.

flow pattern. Barton in 1952, Plyatskii in 1953 and Belopukov in 1958 (Nussey and Kondic, 1964) supported Frommer's theory.

Doehler (1951) observed the metal melt flow phenomena and pointed that shrinkage most often occurs close to the gate.

Lieby (1957) stated that the idealized free jet often changes character after striking an oblique wall or diverges and divides at corners or edges of the die and so it is difficult to analyze the flow process properly. However, Lieby introduced the concept of free flow (unobstructed) which aids in planning the parting line, runner location and venting of the die.

Sachs (1967) attempted a scientific approach using one-dimensional applied fluid dynamics that aimed at a better understanding and control of the variables in the die casting processes. Sachs did not consider the turbulent flow of the molten metal at injection as a major factor that causes air entrapment.

From the early research work on the cavity filling described above, the conclusion can be drawn that the filling of molten metal into the die cavity is a free jet flow process. A number of experimental studies have been performed either by water analogue modelling or using real metal, which aimed to find an adequate flow pattern and to optimize the gating system geometry. The Reynolds number of the fluids varied from 20,000 to 800,000 in these experimental studies, that were in an extreme turbulent flow regime. These experiments showed the filling patterns under different filling parameters, gate and cavity configuration, also the machine data and operation (Smith and Wallace, 1963; Sheptak, 1963; Stuhrke and Wallace, 1965; Davis *et al*., 1980; Booth and Allsop, 1983).

1.3 The Numerical Simulation of the Filling Pattern

The application of computer modelling to investigate the mould filling has changed the long history of the gating system and mould design that mainly relied on experience of engineers and designers. In the last fifteen years,

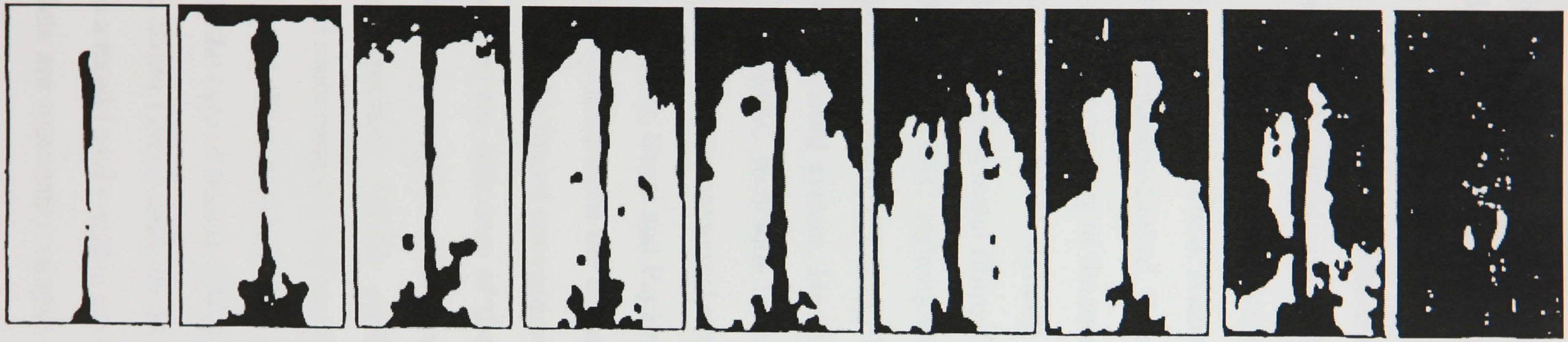

(a) 0.04s (b) 0.08s (c) 0.11s (d) 0.15s (e) 0.19s (f) 0.26s (g) 0.30s (h) 0.35s (i) 0.48s

Figure 1-3 Molten metal flow within a die cavity by experimental demonstration (Koester and Goehring , 1941).

increasing efforts have been put into the development of numerical methods which can simulate the molten metal filling process properly in achieving a quality casting.

The most popular and successful techniques such as MAC (Marker and Cell, Welch *et al.*, 1965); SMAC (Simplified Marker and Cell, Amsden and Harlow, 1970); SOLA (Solution algorithm, Hirt *et al.*, 1975); SOL-VOF (Solution algorithm-Volume of Fluid, Nichols *et al.*, 1980) and SIMPLE (Semi-Implicit Method for Pressure-Linked Equations; Patankar, 1980) have been modified and applied in modelling of the mould filling flow.

Hwang and Stoehr (1983) initially reported the application of MAC technique to model 2-D liquid metal filling flow. Then Stoehr and Hwang (1983) modified the MAC and SMAC techniques for sand moulding to predict 2-D liquid metal filling into a rectangular cavity horizontally and vertically; a stepped plate and a complete mould system. Hwang and Stoehr (1987a, 1987b, 1988) further modified the SMAC technique in matching the actual casting operation more closely and improved the numerical stability and accuracy.

Desai *et al.* (1984); Desai and Pagalthivarthi (1987) studied the transient thermal contact problems between the hot metal filling the system and the cold mould wall, calculated the forced convection temperature distribution in a runner channel, and examined the influence of the post-fill buoyancy-induced natural convection on a planar rectangular mould cavity.

Stoehr and Ingerslev (1986) applied the SMAC and SOLA-VOF techniques to model more complex and realistic shape casting, a pulley with three spokes, and compared the computed flow patterns with physical experiments. Good agreement in the case of bottom filling was obtained.

Walter and Sahm (1986) used the SOLA-VOF technique to model liquid metal flowing into a mould cavity with a top ingate.

Some models are reasonably simple to program, can be run on personal

computers and give results quickly. Usually the complex fluid flow status is ignored and the liquid metal is assumed to be at a uniform temperature in the mould at the beginning of solidification as the following three programs for optimum die runner and gate system design: (i) Metflow (Davis *et al.*, 1985); (ii) Meltflow (Andresen, 1986 and 1987); (iii) A user-friendly computer program of Castfeed (Salloum *et al.*, 1987), and (iv) DMT-Castflow (CSIRO, 1992).

Salloum *et al.* (1989) reported the use of C I D C (Computer Indegrated Die Casting) that treats all aspects of product and process analysis of the automotive industry. Mould filling is one part of this which simulates molten metal entering the mould cavities.

Minaie *et al.* (1991) developed a two-stage numerical model for the filling patterns and the subsequent solidification phenomena in the pressure die casting process. This is a 2-D model and the liquid metal is assumed to flow in a laminar manner. The first stage of filling patterns is modeled by the VOF method where solidification has not yet begun. The second stage, after the cavity is completely filled, is where the solidification analysis begins with an initial convection representing the residual flow field from the filling stage.

Lewis et al., (1992) reported a finite element method for mould filling simulation that is based on the VOF technique (Hirt and Nichols, 1981) and where the molten metal flow is assumed to be laminar.

Domanus *et al.* (1984) presented a model of fluid flow coupled with heat transfer of a liquid melt for casting processes. The use of the COMMIX code (COMponent MIXing), which was originally used in nuclear engineering, and with the filling flow simulation based on the VOF-3D, was then to be extended to track the liquid/gas and liquid/solid interface for die castings.

A hybrid computing technique has been developed by Wang *et al.* (1988), from which the SOLA-VOF technique was extended into 3-D and a new fast solution procedure was suggested. This hybrid code was merged with the

preprocessing code GEOMESH-a geometry meshing software for castings and a post-processing code for the filling flow pattern and temperature field.

Anzai *et al.* (1988, 1990) proposed the Front Marker Tracing (FMT) method to trace the portion of fluid front, and employed a new type cell named FS Cell (Anzai and Uchida, 1990) to improve the accuracy of simulation by SMAC technique. Furthermore, Anzai and Uchida (1991) adopted the hypothesis of ideal fluid in a quasi-3-D simulation model successfully.

Ohtsuka *et al.* (1990) proposed a new analysis method called the Flow Analysis Network Method (FAN) to deal with 3-D problems of filling flow, complex geometric shapes and solidification calculations for thin-walled die castings. The simulation model has been verified by an actual die cast parts.

Lu *et al.* (1992) adopted the SMAC technique to model quasi-3-D filling flow of molten metal into a thin-walled die cavity of (i) a square plate shape, (ii) a cylindrical sleeve shape, and (iii) a half cylindrical sleeve shape with different gate designs. To verify the numerical simulation, a physical model has been designed using water analogue flow visualization. A high speed camera was used to record the flow patterns. Very good agreement between simulation and experiments has been obtained.

Hu *et al.* (1992a) reported an effective simplified mathematical model to solve directly the distribution of liquid metal mass and for the computation of heat transfer, solidification coupled with the flow in both filling and residual period. This work pointed that the metal droplets produced during cavity filling and the irregularities of the liquid surface would affect the casting porosity. The properties of the mixture of liquid (or solid) and air is taken as having volume-averaged values and a computer model was set up to predict such flows. Ignoring the effect of air in the cavity and the gravitational effect in the model design would lead to unreasonable conclusions.

Jong and Hwang (1991b) and Yeh *et al.* (1993) developed a 3-D model by

combining the features of SOLA and MAC-3D (Lin and Hwang, 1988; Jong and Hwang, 1991a). The model has increased the capability, accuracy and efficiency of modelling fluid flow in castings of complex geometry by improvement of the calculation of the turbulent model and the pressure field. Verifications of the model have been made.

Lipinski *et al.* (1991) presented a model combining heat transfer and molten metal flow for real complex shaped castings through the MAGMA-soft computer program. The MAGMA-soft program was developed by the MAGMA Giessereitechnologie GmbH, Germany. For filling sequence simulation (FSS), the finite difference method is used, and the VOF function was adopted to track the free surface of the liquid melt. The complex 3-D domain was automatically subdivided by the built-in mesh generater into 200,000-1,000,000 control volume elements. The filling sequence simulation can be used to detect conditions under which the mould cavity cannot be filled correctly and then casting defects arise. For the first time a real complex shape of engine block casting has been simulated for both the filling sequance and the cooling of the mould cavity filled with liquid metal (Hansen,1991). The MAGMAsoft program has been applied to predict the centreline shrinkage and fine porosity of a roller casting that were reported by Pickin and Travers (1991).

Although a number of 3-D mould filling models have been developed, just a few of them have the capability of handling the turbulent flow of molten metal filling, and for actual castings with complex geometry. Also their accuracy and efficiency remains to be improved(Piwonka, 1995).The problems are: (i) the 3-D analysis systems can handle regular geometrical castings and require a powerful computer workstation in treating actual castings' geometry; (ii) the filling is assumed to be laminar flow and this is not true for most die castings; (iii) quite a number of the models need to be verified; (iv) the mathematical models need to be further simplified, for example, Anzai and Uchida (1991) assumed that the

molten metal is an ideal fluid and used a simplified model in a quasi-3-D filling flow simulation.

1.4 The Residual Flow in the Post-Fill Stage

In pressure die casting processes, the superheated liquid metal flows with high speed and small viscosity, and is forced into a mould cavity by the plunger of the casting machine. In solidification processing, forced convection heat transfer predominates during the transient initial filling stages, once the mould cavity is filled, the buoyancy-generated natural convection heat transfer prevails within the mould cavity until the liquidus temperature is reached (Desai *et al.*, 1984). The buoyancy-generated natural convective mass transfer is realized as the residual flow phenomena in post-fill stage. The phase change of the metal melt within the cavity is greatly affected by the forced convection filling flow and the residual natural convection post-fill flow (Desai and Pagalthivarthi, 1987).

Flemings (1974) systematically introduced the mechanism of the solidification process of the molten metal that provides a background to study the nature of the post-fill stage of pressure die casting processes.

In recent years increasing efforts have been undertaken to develop numerical models to simulate not only the filling flow, but also the heat transfer and the solidification process for pressure die castings. It is found that the residual flow fields existing in the post-fill stage of the pressure die casting process is important in influencing the rate of phase change, the varying interface of the solid/liquid mushy zone with time and the formation of porosity due to air entrapment and shrinkage (Chiang and Tsai, 1992a,b; Chen, 1990; Chen and Im, 1990).

Minaie (1989, 1991 and 1992) and Minaie *et al.* (1991) emphasised that at the end of cavity filling stage, the residual flow fields have a strong influence on

the solidification pattern. The numerical models and the prediction of the phase change pattern need to be proved by experiments.

Hu *et al*. (1992a) reported a mathematical model to show the residual flow field that influences the solidification process and the porosity formation. Although the computing visualization needs experimental verification, it provides useful information for further attempt on modelling of the residual flow.

Huppert (1990) pointed out that intense fluid motions can be generated by the solidification of a binary liquid and presented quantitative calculations for the fluid motion from laboratory experiments.

Chiang (1990) reported that the convective flow (residual flow) in the liquid metal within the cavity has a great influence on the rate of solidification. It is found that the shrinkage-induced fluid flow enhances convective heat transfer, and the global solidification time is smaller than that predicted without the shrinkage effect. Chiou and Tsai (1990) found that castings with narrower mushy zones, higher heat capacity of casting and mould materials, smaller casting length, lower initial mould temperature could decrease the development of microporosity. In the literature, computer software SOLCAST (Scott *et al*., 1991) is used to predict the location of shrinkage porosity in metal castings.

Maxworthy *et al.* (1996) performed a number of new experiments on the rise of air bubbles, and presented the relevant parameter with a huge range of Morton number ($M_0 = g\upsilon^4 \varrho^3 / \sigma^3$) of 10^{13} that provides basic information for the study of the influence to air entrapment on residual flow.

Beckermann (1997) presented a summary of selected experimental and theoretical studies aimed at understanding the convection transport processes both for a single grain and at the scale of a casting. A comparison of model prediction with experiments was shown and predicted liquid residual velocity vectors ($|v_{r\,\max}| = 1.7\ cms^{-1}$). Koster (1997) presented an X-ray flow visualization method for visualizing convection and solidification in metallic alloys.

1.5 The Experimental Studies of Filling Flow Patterns

The measurement and direct observation of liquid metal filling a die cavity are very difficult, because the mould/die is opaque, and the molten metal is at high temperature and the fill time is very fast (milliseconds).

Eckert in 1989 applied the laws of similitude and dimensional analysis to the design of experiments to study the fluid flow through a water analogue method in the die casting process. The present study uses a different approach to that of Eckert and this is given in Chapter 5.

In the past, several ways were used to measure the flow pattern for the mould filling of castings.

(I) Using analogue liquid metal or real molten metal:

(i) Using analogue liquid metal:

From 1938 to 1964, experimental work conducted by Brandt (1938); Koester and Gohring (1941); Erickson (1945); Kayama and Ichida (1953) used an analogue metal having a low melting temperature. Brandt's (1938) contact time method is described in Section 1.2. Koester and Gohring (1941) did some experimental observations of cinematographic trials in which Wood's metal was injected into dies with transparent walls and the test results were edited by Sachs and Barton (Nussey and Kondic, 1964) to substantiate Frommer's theory of the filling pattern. This is shown in Figure 1.3.

(ii) Using real molten metal:

In this method, heat-resistant pyrex glass is used to form a transparent section of the mould/die cavity and ingate system, and a high speed camera is applied to record the filling phenomena.

The filling sequence of molten cast iron entering a sand mould to produce a three-spoke wheel casting with different ingate designs has been obtained by Andersen and Ingerslev (1983) to verify flow modelling using the MAC method.

Stoehr and Ingerslev (1986), and Hwang and Stoehr (1987a,b) performed similar tests to verify the numerical simulation of the SOLA-VOF technique.

Jong and Hwang (1991a,b) used molten metal and developed two variations of the contact time measuring method: (i) using LEDs (light emitting diodes), which are connected to copper wire sensors set in the mould cavity; (ii) using a computerized data acquisition system to record the time and pick up the signals. These methods have the capability to measure the 3-D filling pattern.

Lingberg *et al.* (1991) reported the high speed filming of a mould filling process with aluminium alloys in a cold chamber die casting machine. The films showed three types of flow: (i) continuous jet flow, (ii) course particle jet flow and (iii) atomized jet flow. The films presented clearly the air inclusions in the melt jet flow, and showed that the filling pattern is significantly influenced by the air inclusions. This report provides a direct observation and understanding of the mould filling process and gives valuable information for experimental verification of numerical models.

Yamamoto *et al.* (1988, 1989) used molten aluminium alloy to study the flow behaviour during fast shot injection for two thin-walled pressure die castings. They also tested the last filled portion of the cavity and its correlation to cast defects.

(II) Using a water model:

In this method, water or water with additives is used to replace the molten metal. Plexiglass (perspex) is used to form the casting die and a high-speed camera is coupled to film the filling phenomena. In the sixties and seventies, a number of water analogue experiments have been performed to study the fluid flow patterns in simulated die casting cavities in order to advance knowledge of gating system design (Smith and Wallace, 1963; Sheptak, 1963; Stuhrke and Wallace, 1965; Davis and Siauw 1977; Davis *et al.*, 1977a, b, 1980; Booth and Allsop, 1983). The water analogue method has been applied in pressure die

casting to study the wave formation correlated to air entrapment and casting porosity during filling (Davis *et al.*, 1980; Garber, 1981 and 1982; Iwata and Yamamoto, 1986; Xue *et al.*, 1993a,b; Thome and Brevick, 1993). Xue *et al.*, (1993a,b) added plastic particles to the water in order to model the inclusion behaviour in the melt and to study the mould filling control.

Street (1986) noted an interesting feature in water analogue work (Booth and Allsop, 1983) by placing an overflow pocket in the place opposite the gate, they frequently found more air being swept into the cavity.

Nomura *et al.*, (1991a, b) studied the filling patterns in a water analogue test and compared the results with a SMAC 3-D simulation technique.

Booth and Allsop (1983) recorded gate velocities ranging from 5 to 50 $m\ s^{-1}$ in a flat plate perspex (plexiglass) die cavity. The results showed a negligible effect of gate velocity on the overall filling pattern within the die cavity. On the basis of the dynamic similarity applied to a die casting process (Eckert, 1989), Minaie *et al.*, (1991) and Hu *et al.*, (1992c) reported the filling flow visualization of the water model experiments, in which highly irregular liquid surfaces and liquid breakup have been observed.

Lu (1993) carried water analogue experiments of a thin-walled die-model. A plexiglass die was designed and a high speed camera was employed with a speed of 4,000 frames per second to film the flow phenomena. Good consistency of modelling and experiments have been obtained.

(III) Other methods:

Sauki and Onada (1960) used radioactive tracers as additives to the die lubricant to study the location of turbulent metal flow within die cavities.

Ashton and Buhr (1973) used x-ray cinematography to observe the flow of actual metals into moulds.

Chapter 2

A reclassification of the pressure die casting process

Chapter 2

A Reclassification of the Pressure Die Casting Process

Abstract

In this chapter, the basics of the die filling stages in pressure die casting processes are discussed. Sections 2.1 and 2.3 of this chapter give a general introduction of die casting processes and the necessity of reclassification against the traditional 'three-stage' to a 'five-stage' process is introduced. The other sections of this chapter explain in more detail some of the concepts and derived formulae of the peak pressures of the molten metal and oil in the power system, bulk modulus of the molten metal, and impact time during the fourth stage.

2.1 Introduction

Pressure die castings are produced by forcing the liquid metal under high pressure into metallic moulds called dies. The die consists of two halves that are held together by a mechanism with a large locking force. In a pressure die casting process, after the die halves have been closed and locked, molten metal is driven by a plunger quickly through the feeding system into the die cavities while the air in the die escapes through vents. The locking force closes up the two die halves firmly during the molten metal filling and subsequent application of the high pressure to the molten metal in the cavity. When the metal is solidified due to heat transfer to the cooled mould, the die halves are open and the solidified casting is then ejected and removed from the die. While the die halves are open, it is cleaned and lubricated for a longer die life. Then the die halves are closed and locked, and another operation cycle is repeated.

2.2 The Traditional Classification of an Injection Process

2.2.1 The 'Three-Stage Classification' of an Injection Process

The injection of molten metal in die casting is a complex process. A great deal of work has been done in an attempt to correlate the empirical knowledge of the die casting process with scientific principles. A knowledge of the injection phase is necessary to determine the optimum machine setting and gating parameters in die design. Traditionally, pressure die casting engineers and researchers classify the cavity filling process into a 'three-stage' process as shown in Figure 2-1, which has become a basic tenet in constructing theoretical and practical investigations. In the first stage, the plunger advances slowly until the base of the shot sleeve is fully covered with molten metal. In the second stage, the die cavity is being filled at a virtually constant pressure, whilst a greater force is applied to the piston to overcome the friction. The last stage is typified by a high rise in packing pressure when the die cavity is fully filled.

There seems no doubt that the third stage is the most important, and plays a key role in completing the whole function of a pressure die casting process.

2.2.2 The Problem of the Traditional Classification

Many experimental studies have monitored the process parameters and provided useful information (Allsop and Kennedy, 1983; Andersen and Ingerslev, 1983; Davis and Siauw, 1977; Davis, *et al.*, 1977a, b; Stuhrke and Wallace, 1965; Doehler, 1951; Hernandez and Hamar, 1985; Robinson, 1977; Veinik 1958; Zeleniak, 1993) for further study. While most of the results show the variations of the oil pressure with the travel of the plunger, measurement of the metal pressure in the die cavity indicates a rapid pressure build up at the end of die cavity filling. Unfortunately, the concept of a third stage of the traditional classification incorrectly combines two physical phenomena into one and does not differentiate

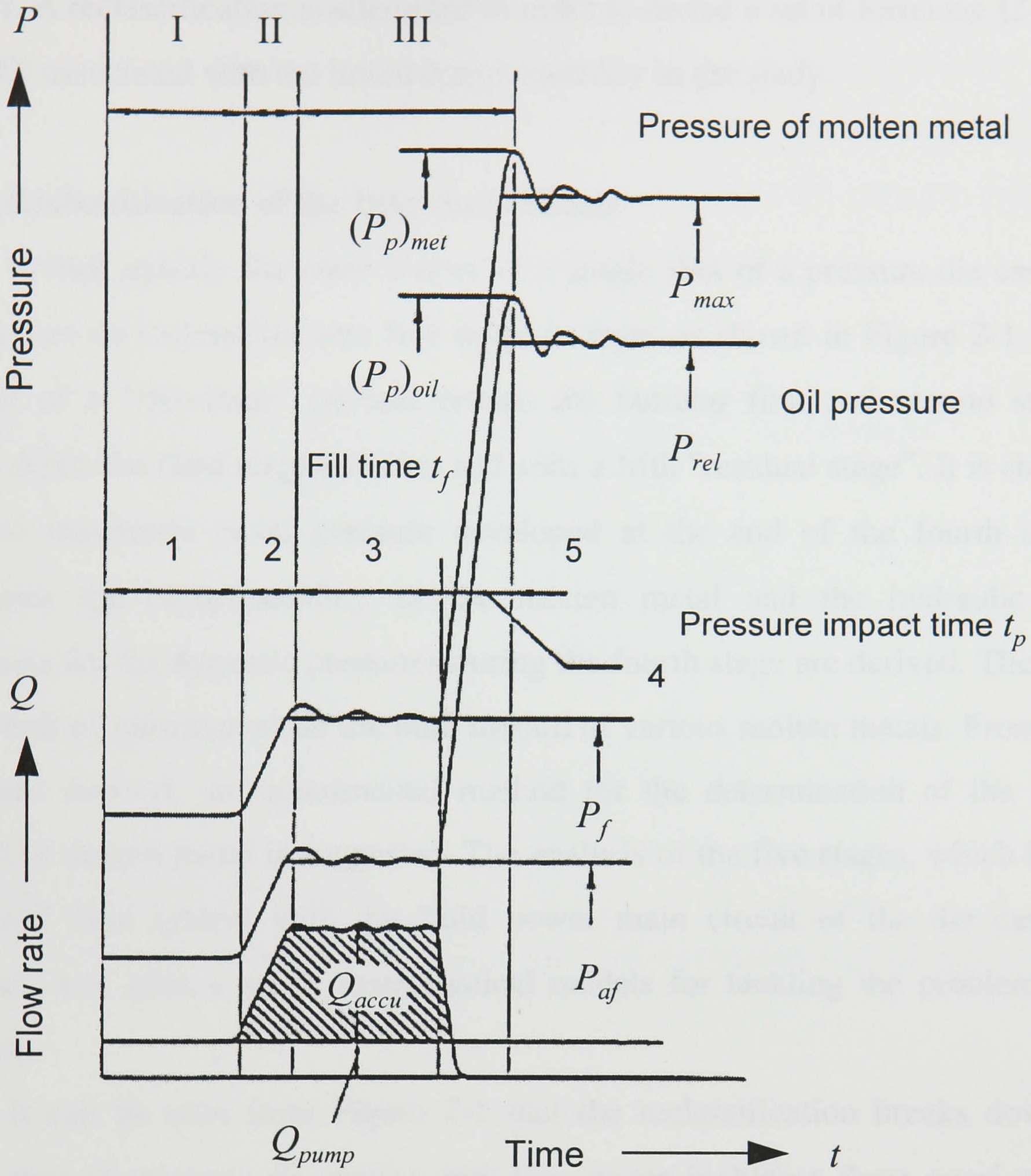

Figure 2-1 Reclassification of pressure die casting process.

Traditional 'three stages'	Reclassification 'five stage'
I. Slow shot	1. Slow shot
II. Fast shot	2. Fast shot
III. Filling shot	3. Filling shot
	4. Pressure impact
	5. Final pressure setting

liquid incompressibility and liquid compressibility at the end of an injection process. A reclassification is attempted in order to derive a set of formulae (2-22) to (2-40) associated with the liquid compressibility in the study.

2.3 A Reclassification of the Injection Process

In fact, exactly the same history of a single shot of a pressure die casting process can be reclassified into five distinct stages as shown in Figure 2-1. The concept of a "five-stage" process retains the familiar first and second stage, breaks down the third stage into two and adds a fifth "residual stage". It is shown that the maximum metal pressure developed at the end of the fourth stage represents the compressibility of the molten metal and the hydraulic oil. Equations for the dynamic pressures during the fourth stage are derived. There is still a lack of information on the bulk moduli of various molten metals. From the equations derived, an experimental method for the determination of the bulk moduli of molten metal is suggested. The analysis of the five stages, which links the metal feed system with the fluid power main circuit of the die casting machine, will give a set of mathematical models for tackling the problems in question.

It can be seen from Figure 2-1 that the reclassification breaks down a single shot of pressure die casting into five stages including three quasi-stable stages, i.e., the first, third and fifth stage and two transient stages, i.e., the second and fourth stages.

The aim of the reclassification of pressure die casting processes is to create a set of mathematical models especially for the filling and pressure impact stages, i.e., the third and fourth stages in order to tackle the problems encountered in design and performance prediction applied in pressure die casting processes.

2.4 The Equations Governing the Metal Feeding System

2.4.1 The Force Balance Equation

A schematic diagram of the hydraulic system of a high pressure die casting machine is shown in Figure 2-2, which shows the various components of the hydraulic circuit starting from the accumulator then to the plunger cylinder and to the die cavity. The force balance equation can be written as:

$$\frac{W}{g}\ddot{x} + c_f \dot{x} = p_a A_a - p_b A_b - pa \tag{2-1}$$

At quasi-steady state: $\dot{x}$ = constant; $\ddot{x} = 0$; and equation (2-1) becomes:

$$p = \frac{A_a}{a} p_a - \frac{A_b}{a} p_b - \frac{c_f}{a} \dot{x} \tag{2-2}$$

In comparison to pressure forces, the friction force can be neglected normally, then equation (2-2) can be simplified as:

$$p = \frac{A_a}{a} p_a - \frac{A_b}{a} p_b \tag{2-3}$$

2.4.2 The Continuity Equation

The continuity equation in the average form associated with plunger speed is:

$$Q_a = A_a \dot{x} \tag{2-4}$$

or $$q = \alpha \dot{x} \tag{2-5}$$

and $$q = \frac{a}{A_a} Q_a \tag{2-6}$$

At quasi-steady state: $\dot{x}$ = constant, Q_a = constant, and the flow rate of molten metal q = constant.

The Bernoulli equation representing the energy balance law in fluid motion is obeyed in dealing with a specified problem in the following sections.

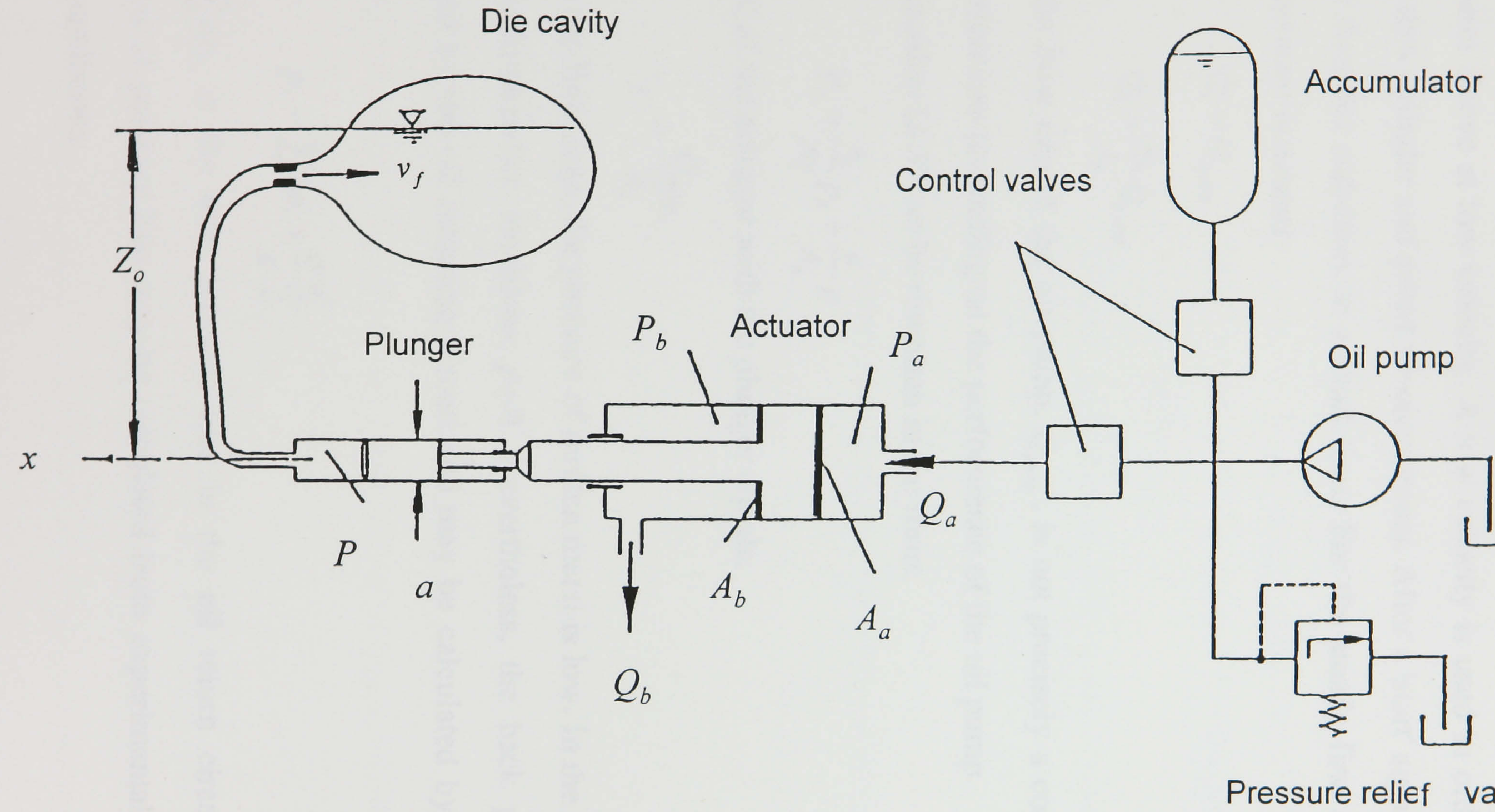

Figure 2-2 Hydraulic main circuit of molten metal feed system.

2.5 The Mathematical Models Applied in the Reclassification

2.5.1 First Stage: Slow Shot

The first stage is sometimes called the pre-fill stage where molten metal fills the shot sleeve at low velocity. A low velocity is used in order to expel air from the shot cylinder and avoid air entrapment. After a 'start' signal is given, the hydraulic actuator stabilizes in a short time. For the steady first stage, a quasi-stable flow state is treated:

$$Q_a = Q_{pump} \tag{2-7}$$

$$Q_b = \frac{A_a}{A_b} Q_{pump} \tag{2-8}$$

In fact, the flow rate of the oil pump, Q_{pump}, is not precisely a constant and has small fluctuations depending on the performance of the oil pump.

Equation (2-3) can be rewritten in the form:

$$p_a = \frac{A_b}{A_a} p_b + \frac{a}{A_a} p \tag{2-9}$$

The speed of the actuator with the plunger equals:

$$v_p = \frac{Q_{pump}}{A_a} \tag{2-10}$$

In the first stage, the pressure of molten metal is low. In the cases of a dry shot or cold-chamber machines, p=0. Nevertheless, the back pressure p_b is determined by the oil returning circuit and may be calculated by the Bernoulli equation.

$$p_b = \sum \Delta p_b + \frac{\varrho}{g} \frac{v_b^2}{2} \tag{2-11}$$

where $\sum \Delta p_b$ is the total pressure loss in the oil return circuit, and every component of pressure loss may be calculated from experimental data given in relevant handbooks.

From an energy conservation point-of-view, p_b should be designed to be as low as possible. On the other hand, keeping a certain amount of back pressure is beneficial to the working stability of the actuator.

2.5.2 Second Stage: Fast Shot

The second stage follows the first stage and continues until the molten metal arrives at the filling gate. In this unsteady stage, the oil surges from the accumulator to the hydraulic system. This causes fluctuations of working pressure and back pressure on the actuator.

The force balance equation (2-1) stands, and the oil working pressure can be gained by rewriting equation (2-1) as:

$$p_a = \frac{1}{A_a}[\frac{W}{g}\ddot{x} + c_f\dot{x} - (A_b p_b + pa)] \tag{2-12}$$

The oil inlet flow rate can be obtained from a modification of equation (2-7) as:

$$Q_a = Q_{pump} + Q_{accu} f(t) \tag{2-13}$$

The speed of the actuator is:

$$v_p = \frac{1}{A_a}[Q_{pump} + Q_{accu} f(t)] \tag{2-14}$$

The dynamic performance of flow rates, speed of the actuator and oil working pressure, back pressure of actuator and molten metal pressure during the second stage mainly depends upon the dynamic performance of the control valves, accumulator and other boundary conditions of the metal feed system.

2.5.3 Third Stage: Filling Shot

According to the new classification, the third stage ends at the instant when the pressure begins to build up. The gate velocity and pressure in the cavity are maintained approximately constant and the flow can be treated as quasi-steady state in order to derive the flow formulae for the third stage.

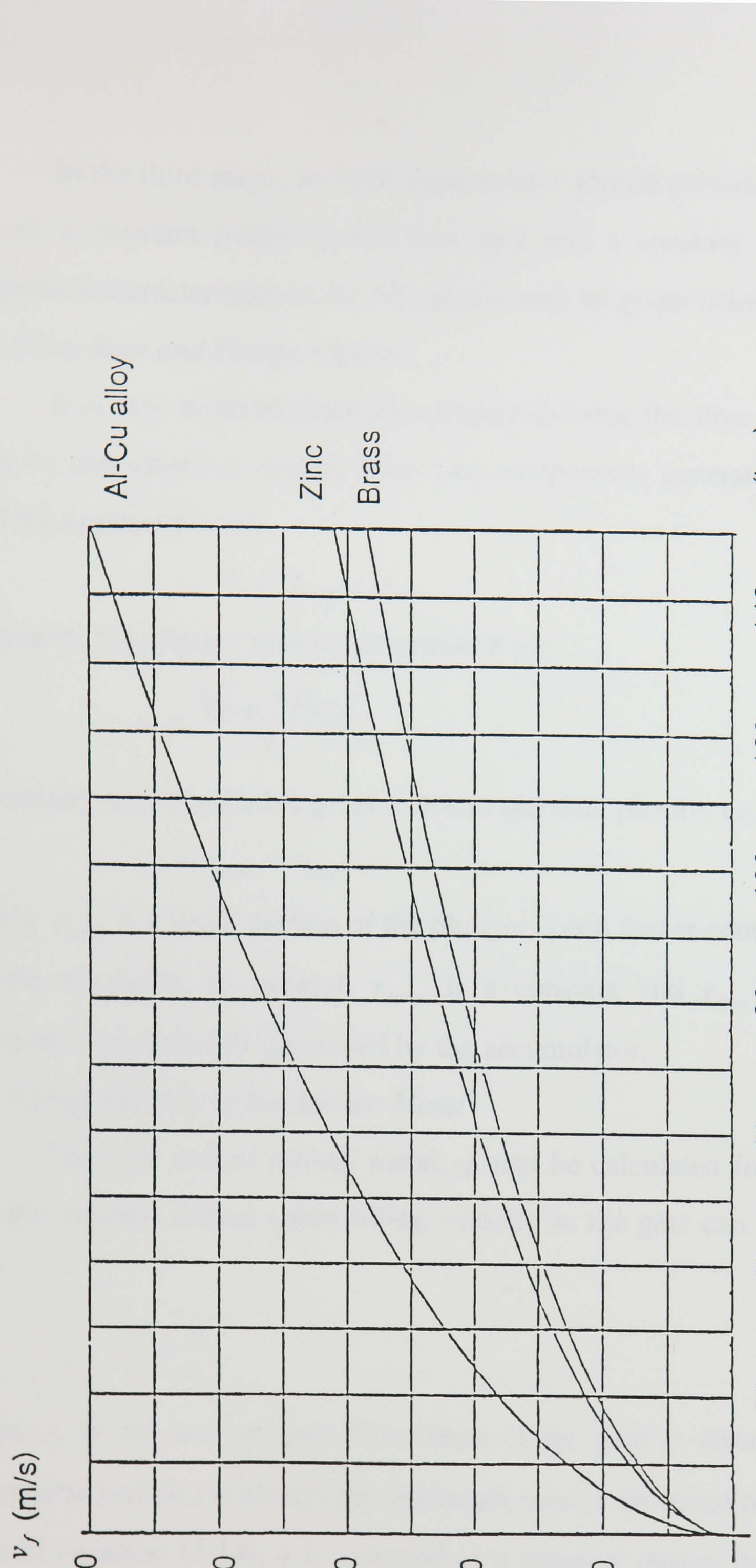

Figure 2-3 The calculation relationship between filling velocity and pressure of the molten metal.

In the third stage, an ideal accumulator should provide a constant plunger speed, a constant molten metal flow rate and a constant gate velocity. Four important characteristics of the filling shot may be given below:

(1) Flow Rate and Plunger Speed

It is easy to understand from Figure 2-1 that the flow rate of the actuator may be considered as arising from two components generated by the oil pump and the accumulator as:

$$Q_a = Q_{pump} + Q_{accu} \tag{2-15}$$

Similarly, the plunger speed is determined by:

$$v_p = \frac{Q_{pump} + Q_{accu}}{A_a} \tag{2-16}$$

Re-writing equation (2-16) gives a clearer physical picture, i.e.,

$$v_p = v_{pump} + v_{accu} \tag{2-17}$$

where v_{pump} is a small portion of the plunger speed that is continuously generated by the oil pump. In general, v_{pump} is a constant and v_{accu} is a much larger component periodically generated by the accumulator.

(2) Filling Velocity of the Molten Metal

The flow rate of molten metal, q, can be calculated from equation (2-5), and the average molten metal filling velocity in the gate can be obtained below as:

$$v_f = \frac{q}{a_g} \tag{2-18}$$

where a_g is the area of gate. The shape of the gate is always designed to be rectangular and also is always the minimum area of the metal feed system. On the basis of equation (2-18), q is assumed as a constant during the injection period, $v_f \propto \frac{1}{a_g}$. It should be noted that a small area of the gate will cause a large filling velocity and a high working pressure.

(3) Working Pressure of Molten Metal

From Bernoulli's equation, with known cross sections at the plunger surface and filling gate as in Figure 2-2, the pressure of molten metal can be expressed as:

$$p = \frac{\varrho}{2g}(v_f{}^2 - v_p{}^2) + p_{ao} + \varrho Z_o + \sum \Delta p \qquad (2\text{-}19)$$

Equation (2-19) can be reduced to a simpler form:

$$v_f = c_d \sqrt{\frac{2g}{\varrho} p} \qquad (2\text{-}20)$$

where $c_d = \sqrt{1-(\sum \Delta p / p)}$, and $\sum \Delta p$ is the total pressure loss of the metal feed system. Every component of the pressure loss can be determined from relevant handbooks.

From equation (2-20), when the pressure and other conditions of the metal feed system remain unchanged, a lighter metal will result in a larger filling velocity. Assuming c_d = 0.97 and applying equation (2-20), the relation between filling velocity and pressure is shown in the Figure 2-3, from which the velocity of molten brass flow is equal to 57% of that of an Al-Cu alloy.

Equation (2-20) also shows $p \propto v_f^2$ or $p \propto q^2$. Excessive gate velocity, v_f, will not only cause liquid splash, influencing the quality of castings, but also waste energy by increasing the working pressure. The CSIRO* (Allsop and Kennedy, 1983) recommended a gate velocity of 40 ms^{-1} in order to make a zinc casting with a good surface finish. Unfortunately, many of the pneumatic hot chamber machines are not capable of producing sufficient metal pressure during injection to achieve a 40 ms^{-1} gate velocity.

(4) Fill time

The fill time of the die cavity is equal to the volume of the cavity to be filled divided by the flow rate of molten metal driven by the plunger as:

*Commonwealth Scientific Industrial Research Organization, Australia

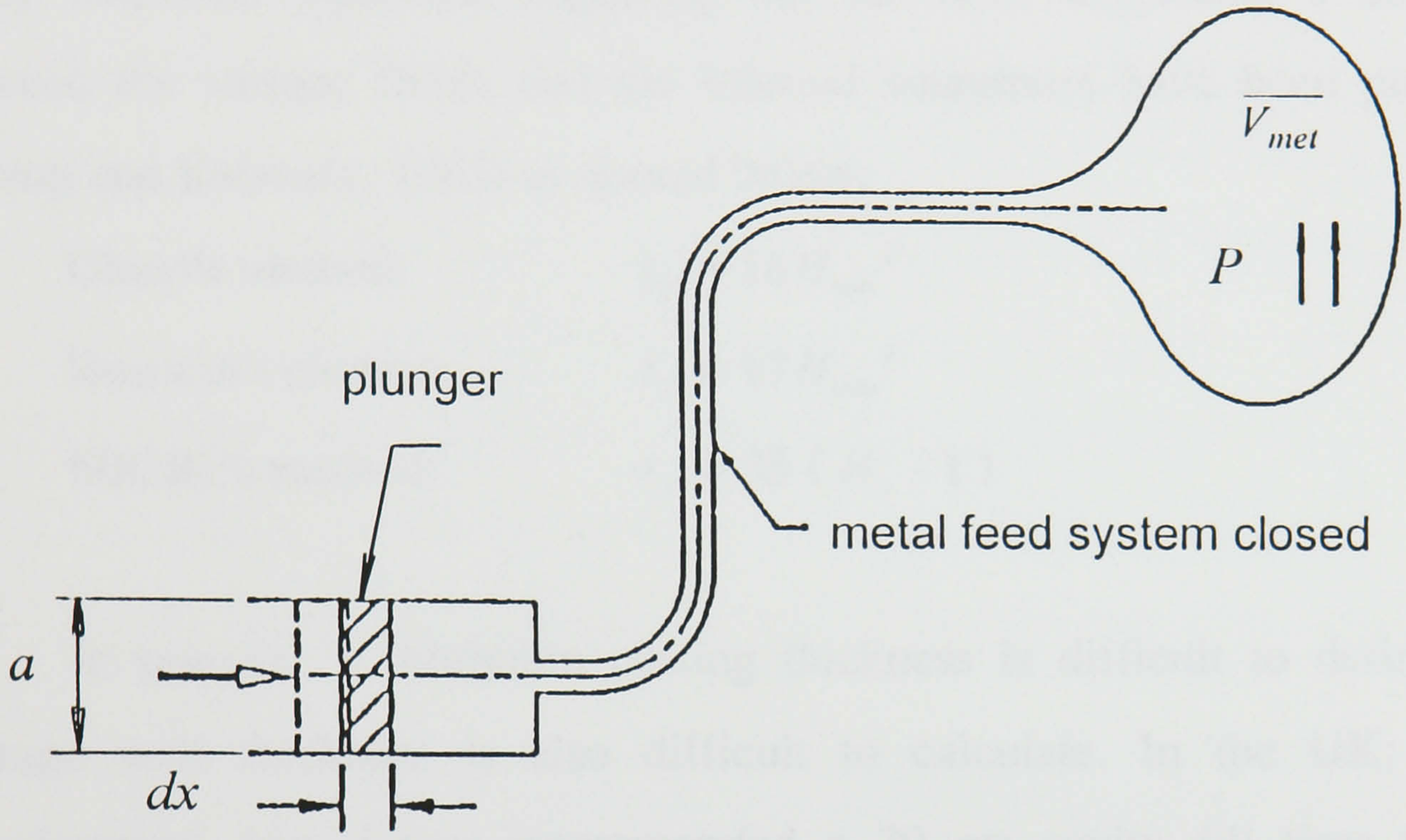

Figure 2-4 Schematic diagram showing liquid compressibility in the metal feed system.

dx	elemental compressed length
$\overline{V_{met}}$	total volume of molten metal in the metal feed system
p	pressure of molten metal
a	area of plunger

$$t_f = \frac{\overline{V_{cav}}}{q} \tag{2-21}$$

Equation (2-21) is simple but important in stating that the fill time $t_f \propto \overline{V_{cav}}$ the total volume of the cavity, including the volume of overflow and $t_f \propto \frac{1}{q}$. Many empirical equations regarding the fill time suggesting a compromise between the surface finish and the internal soundness have been put forward (Allsop and Kennedy, 1983) as quoted below:

Ulmer's method: $t_f = 16 H_{\min}^{\ 2}$ (2-21a)

Rearwin's method: $t_f = 17 H_{\min}^{\ 2}$ (2-21b)

*DCRF's method: $t_f = 35\ (\ H_a\ -\ 1\ )$ (2-21c)

In practice, a minimum casting thickness is difficult to define and an average wall thickness is also difficult to calculate. In the UK, the Zinc Development Association recommended a 20 *ms* cavity fill time for plated castings and 40 *ms* for non-plated castings(Allsop and Kennedy, 1983). This is a sensible recommendation since there is a limited variation in casting sizes and a surprisingly small variation in casting wall thickness.

From results collected from a wide range of foundry research and practice in the UK, Europe and the USA, the BNF**Metals Technology Centre found the best relationship between cavity fill time and average wall thickness that is recommended as below (Allsop and Kennedy, 1983):

For Al, $t_f = 40\,H$ (2-21d)

For Zn, high quality chrome finish $t_f = 6\,H + 7$ (2-21e)

For Zn, low quality non or chrome finish $t_f = 7\,H + 13$ (2-21f)

*Die Casting Research Federation

** British Non-Ferrous Metals Technology Centre

As the metal feed system has been designed and fabricated with a fixed capacity oil pump, the fill time t_f should be calculated from equation (2-21). Once a casting die has been designed, the total volume $\overline{V_{cav}}$ will be fixed. The only way to change the fill time is to alter the plunger speed (which is directly proportion to the flow rate, q, of the molten metal) by a flow control valve in the fluid power system. Therefore, when the flow rate of the oil pump is fixed, the plunger speed is also fixed. According to the continuity equation and Bernoulli's equation, the area of gate, a_g, the shape of gate and its location associated with the value of c_d can only affect the filling velocity and pressure, but cannot affect the flow rate of the oil pump, i.e., the fill time is independent of c_d. Similarly, it should be noted that a reduction in gate area will result in an increase in the gate velocity and the pressure of the molten metal, but this also cannot reduce the fill time.

Owing to the very complex flow pattern appearing in the die cavity during the injection period, the third stage greatly influences the air entrapment and porosity associated with pressure die castings. Therefore, the third stage is a key feature of the process, and a specific research topic, to be covered in detail in Chapter 3.

2.5.4 Fourth Stage: Pressure Impact

The fourth stage lasts only from one to five milliseconds immediately followed the third stage (Stuhrke and Wallace, 1965; Robinson, 1977; Segawa, 1977; Zeleniak, 1993; and Rollez, 1993). The reason to separate such a short time period into a separate stage is that this stage represents a special set of fluid mechanics conditions, which in turn requires its own mathematical solutions.

The above equations from (2-1) to (2-21) represent the fundamental behaviour in the first three stages. These equations have a common background which assumes the incompressibility of the liquid. At the last moment of the third

BRUNEL UNIVERSITY LIBRARY

stage, the cavity and overflow are completely filled with molten metal. The metal feed system and the hydraulic power system become two separated closed spaces. If oil is continuously driven by the oil pump and forced into the actuator, the compressibility of the fluids becomes a dominating factor in the hydraulic power system and in the metal feed system as well. Accordingly, the pressure in the actuator and the pressure in the cavity will build up rapidly (1-5 *ms* has been reported for a number of different test machines) to a high peak value about 2-4 *times* that of the normal filling pressure (Stuhrke and Wallace 1965; Robinson, 1977; Segawa, 1977; Zeleniak, 1993; and Rollez, 1993). This is, in reality, the pressure impact stage in pressure die casting processes, which is similar to the water hammer phenomenon in fluid mechanics.

(1) Peak pressure of the molten metal

By reference to Figure 2-4, when the actuator moves forwards together with the plunger an elemental displacement, dx, the molten metal with the elemental volume, adx, is compressed into the whole metal feed system and the resulting peak pressure may be derived according to the definition of fluid compressibility:

$$adx = \frac{\overline{V_{met}}}{\beta_{met}} dp \tag{2-22}$$

The rate of pressure increase with time is found by rewriting (2-22) as:

$$\frac{dp}{dt} = \beta_{met} \frac{a}{\overline{V_{met}}} \frac{dx}{dt} \tag{2-23}$$

The rate of pressure increase with displacement is:

$$\frac{dp}{dx} = \frac{a}{\overline{V_{met}}} \beta_{met} \tag{2-24}$$

By integrating equation (2-24) the total peak pressure of the molten metal, $(P_p)_{met}$, is obtained:

$$(P_p)_{met} = \frac{al_{com}}{\overline{V_{met}}} \beta_{met} \tag{2-25}$$

where al_{com} is the total compressed volume of the molten metal. Furthermore, equation (2-25) can be rewritten as:

$$(P_p)_{met} = \Delta\overline{V_{met}}\ \beta_{met} \tag{2-26}$$

where $$\Delta\overline{V_{met}} = \frac{al_{com}}{\overline{V_{met}}} \tag{2-27}$$

It is clear that the maximum pressure of the molten metal, $(P_p)_{met}$, is proportional to β_{met}, the bulk modulus of the molten metal and $\Delta\overline{V_{met}}$, the relative volume of the compressed molten metal. It is, therefore, necessary to obtain the value of β_{met} from experiment.

(2) Peak pressure of the oil in the fluid power system

Similar to the above section, the peak pressure at the actuator can be deduced from the following:

$$\frac{dp_a}{dt} = \beta_{oil}\frac{A_a}{\overline{V_{oil}}}\frac{dx}{dt} \tag{2-28}$$

$$\frac{dp_a}{dx} = \frac{A_a}{\overline{V_{oil}}}\beta_{oil} \tag{2-29}$$

$$(P_p)_{oil} = \Delta\overline{V_{oil}}\ \beta_{oil} \tag{2-30}$$

where $$\Delta\overline{V_{oil}} = \frac{A_a l_{com}}{\overline{V_{oil}}} \tag{2-31}$$

(3) Relation of dynamic pressures in the molten metal and oil

Combining equations (2-23) and (2-28) permits the relation between the dynamic pressure of the working oil in the fluid power system and the molten metal in the metal feed system to be obtained:

$$\frac{dp}{dt} = \frac{\beta_{met}}{\beta_{oil}}\frac{a}{A_a}\frac{\overline{V_{oil}}}{\overline{V_{met}}}\frac{dp_a}{dt} \tag{2-32}$$

Integrating equation (2-32) gives:

$$\int_{p_f}^{p} dp = \int_{p_{af}}^{p_a}\frac{\beta_{met}}{\beta_{oil}}\frac{a}{A_a}\frac{\overline{V_{oil}}}{\overline{V_{met}}} \tag{2-33}$$

Assuming β_{met} and β_{oil} are constant, a solution can be found from equation (2-33) to establish the relation between the two dynamic pressures in the fourth stage as:

$$p = p_f + \frac{\beta_{met}}{\beta_{oil}} \frac{a}{A_a} \frac{\overline{V_{oil}}}{\overline{V_{met}}} (p_a - p_{af}) \tag{2-34}$$

At the end of the fourth stage, as shown in Figure 2-1, the oil pressure reaches a peak value, then decays to the stable setting pressure of the pressure relief valve. Similarly to the trend of the oil pressure, the stable maximum pressure of the molten metal is given by:

$$p_{\max} = p_f + \frac{\beta_{met}}{\beta_{oil}} \frac{a}{A_a} \frac{\overline{V_{oil}}}{\overline{V_{met}}} (p_{rel} - p_{af}) \tag{2-35}$$

(4) Bulk modulus of the molten metal

The bulk modulus, β_{met}, of the molten metal is very large, and actual values are difficult to obtain experimentally. However, an experimental method is suggested here which may permit the determination of the bulk modulus of various molten metals. On the basis of equation (2-35), the area of plunger and actuator, the total volume of the molten metal, $\overline{V_{met}}$, and the total oil volume in the high pressure side of the fluid power system, $\overline{V_{oil}}$, as well as the oil bulk modulus β_{oil} are known. If $p_{\max}, p_f, p_{rel}, p_{af}$ can be measured simultaneously during the fourth filling stage, then β_{met} may be obtained from:

$$\beta_{met} = \beta_{oil} \frac{A_a}{a} \frac{\overline{V_{met}}}{\overline{V_{oil}}} \frac{(p_{\max} - p_f)}{(p_{rel} - p_{af})} \tag{2-36}$$

(5) Pressure impact time during the fourth stage

The duration of the fourth stage is very short (e.g. 1-5 *ms*), and may be derived on the basis of volume balance. Substituting $qdt=adx$ in equation (2-22) gives:

$$qdt = \frac{\overline{V_{met}}}{\beta_{met}} dp \tag{2-37}$$

The flow rate of the molten metal, q, is reduced to zero at the end of the filling in the fourth stage which is approximately linear and can be expressed as:

PAGE
MISSING
IN
ORIGINAL

(ii) A high pressure impact encourages penetration of the liquid through the film into residual air spaces and converts these to solids, which strengthens the casting;

(iii) A high pressure impact has a densifying effect on the casting surface, and produces a sound surface on the casting.

Nevertheless, excessive pressure peak will cause negative effects such as:

(i) A high pressure impact may damage machine parts;

(ii) A high pressure impact may cause flash to be formed;

(iii) A pressure impact may be associated with noise.

2.6 Conclusions

On the basis of breaking through the restrictions of the concept of a 'three-stage' process and replacing this with a 'five-stage' process, a systematic system of equations from (2-1) to (2-40) covering the necessary mathematical models for the die filling process have been generated.

Equations (2-1) to (2-21) present the nature of the first to third stages of the filling process. Those equations are used for evaluation of pressure die casting processes, machine selection, design and calculations of the metal feed system, etc. It is best to get the basic information on the plunger speed history by a dry shot test (Robinson, 1977) in order to obtain more accurate information of oil pump, plunger and accumulator, etc. In addition, the most important and simple task in design of dies and metal feed system or machine setting, or machine selection is to ensure the molten flow supply is equal to the volume of cavities:

$$a L_p = \sum \Delta V \tag{2-41}$$

where $\sum \Delta V$ is the total volume including volumes of gooseneck, runner, casting cavity and overflow wells. By computer aided design, the stroke of the plunger, L_p, can be determined precisely. In the case of ($a L_p < \sum \Delta V$), porosity will be

generated in the castings due to lack of molten flow supply. Therefore, it is reasonable for a quality casting to amend equation(2-41) to be:

$$a L_p = (1.05\text{-}1.10)\sum \Delta V \tag{2-42}$$

Equations from (2-22) to (2-40) expose the nature of the pressure impact in the fourth stage to be a manifestation of the compressibility of molten metal, which provides a sound basis using these formulae to attack the problems of pressure impact and associated air entrapment, porosity, and machine settings.

In addition, the above results of the reclassification for one shot of a pressure die casting process provide a fundamental understanding of the flow of the molten metal through a metal feed system in order to have a sound background for the design, research and development of pressure die casting machines.

Chapter 3

The numerical simulation of filling flow pattern

Chapter 3

The Numerical Simulation of Filling Flow Pattern

Abstract

This chapter aims to model the filling pattern of molten metal within the mould cavity of the pressure die casting process. By applying the Simplified Marker And Cell (SMAC) computational fluid dynamics technique in the finite difference form of the Navier-Stokes equations, the highly transient fluid flow of which the location of the fluid and the orientation of its free surface can be treated as an integral part for modelling and calculation. On the basis of the computational analysis for some typical examples, the influence of parameters such as viscosity, gravitational force and gate velocity on the overall filling pattern are examined from which the role played by each parameter is clearly discerned. These conclusions suggest the application of the hypothesis of an ideal liquid into the mathematical equations for modelling of filling flow pattern. The numerical simulation programme can then be further simplified to achieve an accurate and cost-effective computation for the complex geometrical cavity filling by quasi-3-D or 3-D model.

3.1 Introduction

Following the rapid development of computer technologies (specifically increases in the computing speed and the size of storage) many computational methods have been proposed, examined and refined to a level that significantly impacts on the research and development for all fields of science and engineering.

Molten metal flow within the mould cavity during filling is highly transient. The amount and the orientation of the free surface of the molten metal

changes rapidly. Models of this kind of fluid flow are based on the momentum balance principle.

Modelling and simulating such flow is difficult since the free surface continuously changes spatially with time. Consequently, the computational domain is not fixed. Since the mid-1960's, computational prediction of free surface flow at a relatively low Reynolds number has been developed progressively by the Los Alamos Scientific Laboratory. A series of computing techniques for solving viscous, incompressible, transient fluid flow problems involving free surfaces was developed, such as the Marker and Cell (MAC) method, by Welch *et al.* in 1966; Simplified Marker and Cell (SMAC) method, by Amsden and Harlow in 1970; the Solution Algorithm (SOLA) method, by Hirt *et al*. in 1975; the Volume of Fluid (VOF) method, by Hirt and Nichols in 1981 and the Solution Algorithm-Volume Of Fluid (SOLA-VOF) method, by Nichols *et al*. in 1980.

The most popular and successful techniques for computing incompressible flows have been those of SMAC, VOF, SOLA-VOF and SIMPLE (Semi-Implicit Method for Pressure-Linked Equations, Patankar, 1980). The technique allows the evolution of the molten metal domain as well as the velocity profile and pressure distribution within the molten metal to be computed. Based on the same principles, these methodologies differ from each other in the way they keep track of the free surface location and satisfy the free surface boundary conditions. However, all of them use the finite difference scheme. Their major advantage lies in their ability to deal with free surface and unsteady flow for a wide range of fluid flow problems such as broken dam, flow onto or over a step, tank draining, splash drop, instability of a liquid column and extrusion of immiscible fluid etc. More recently, many researchers have developed specific codes for filling flows in die casting: Stoehr and Hwang, 1983; Hwang, 1985; Wang *et al.*, 1988; Minaie, 1989; Anzai and Uchida, 1990; Hu *et al*., 1992a; and Lu, 1993.

3.2 The Governing Differential Equations

The basic differential equations used in the present study are the continuity equation and the Navier-Stokes equations shown in equation (3-1), equation (3-2) and (3-3) respectively for the two dimensional cartesian co-ordinate form (Hwang, 1985). These three equations are appied to calculate the flow behaviour in the interior region.

$$D = \frac{\partial u}{\partial x} + \frac{\partial v}{\partial y} = 0 \tag{3-1}$$

where the divergence is denoted as D.

$$\frac{\partial u}{\partial t} + u\frac{\partial u}{\partial x} + v\frac{\partial u}{\partial y} = X - \frac{\partial p}{\partial x} + \upsilon\left(\frac{\partial^2 u}{\partial x^2} + \frac{\partial^2 u}{\partial y^2}\right) \tag{3-2}$$

$$\frac{\partial v}{\partial t} + u\frac{\partial v}{\partial x} + v\frac{\partial v}{\partial y} = Y - \frac{\partial p}{\partial y} + \upsilon\left(\frac{\partial^2 v}{\partial x^2} + \frac{\partial^2 v}{\partial y^2}\right) \tag{3-3}$$

where p = pressure/ density.

If the continuity equation is incorporated into the momentum equation, equations (3-4) and (3-5) will be obtained. These are derived from the conservation of momentum in a control volume of the incompressible fluid.

$$\frac{\partial u}{\partial t} + \frac{\partial u^2}{\partial x} + \frac{\partial uv}{\partial y} = X - \frac{\partial p}{\partial x} + \upsilon\left(\frac{\partial^2 u}{\partial x^2} + \frac{\partial^2 u}{\partial y^2}\right) \tag{3-4}$$

$$\frac{\partial v}{\partial t} + \frac{\partial uv}{\partial x} + \frac{\partial v^2}{\partial y} = Y - \frac{\partial p}{\partial y} + \upsilon\left(\frac{\partial^2 v}{\partial x^2} + \frac{\partial^2 v}{\partial y^2}\right) \tag{3-5}$$

3.3 Highlight of the Simplified Marker and Cell (SMAC) Technique

The present study uses SMAC technique in the finite difference method, FDM, to solve the partial differential equations (3-1), (3-4) and (3-5).

First, the configuration of the casting cavity is divided into a number of rectangular subdivisions, called cells, which remain at rest. Second, a set of massless markers (particles), which move at local velocity, are introduced into those cells. Typically, 20 imaginary markers are evenly distributed into the mesh system to represent the location of the molten metal at any instant.

The SMAC system designated the cells in the interior and surface regions as full, surface, and empty cells respectively. A full cell is one that contains at least one marker and all of its neighbouring cells containing marker as well. A surface cell lies at the boundary between regions which contain at least one marker but having at least one neighbouring cell without any marker. An empty cell is any cell not containing marker. The flow domain as well as the corresponding interior and surface regions of the domain are then identified. Initial velocities and pressure are specified for each fluid cell together with appropriate boundary conditions. The continuity and momentum equations are made discrete by the finite difference scheme and solved iteratively to obtain the velocity and pressure fields. All cells are then examined and reflagged as full, empty, or surface so that a new configuration of fluid is determined. Because the cavity thickness of pressure die casting is usualy much smaller than the length and width, the filling flow pattern within the cavity will be treated as 2D-motion which is identified inside two parallel plates in the present work. The z-axis of the flow is ignored.

3.3.1 Finite Difference Form of the Equations

The first step is transforming the governing partial differential continuity and momentum equations into finite difference form (Hwang, 1985).

As shown in Figure 3-1, the field variables are defined such that u is the horizontal velocity component at the centre of the vertical (y) side face and v is the vertical velocity component at the centre of the horizontal (x) side face respectively while the pressure p, which is at the centre of each mesh cell. The field is discretized into cells of size $\Delta x \times \Delta y$ with the cell centres being designated by i in the x direction and j in the y direction. The cells do not change in size or position and the calculations are designed to find appropriate velocities and pressures for each cell at any point in time. Thus this approach is Eulerian.

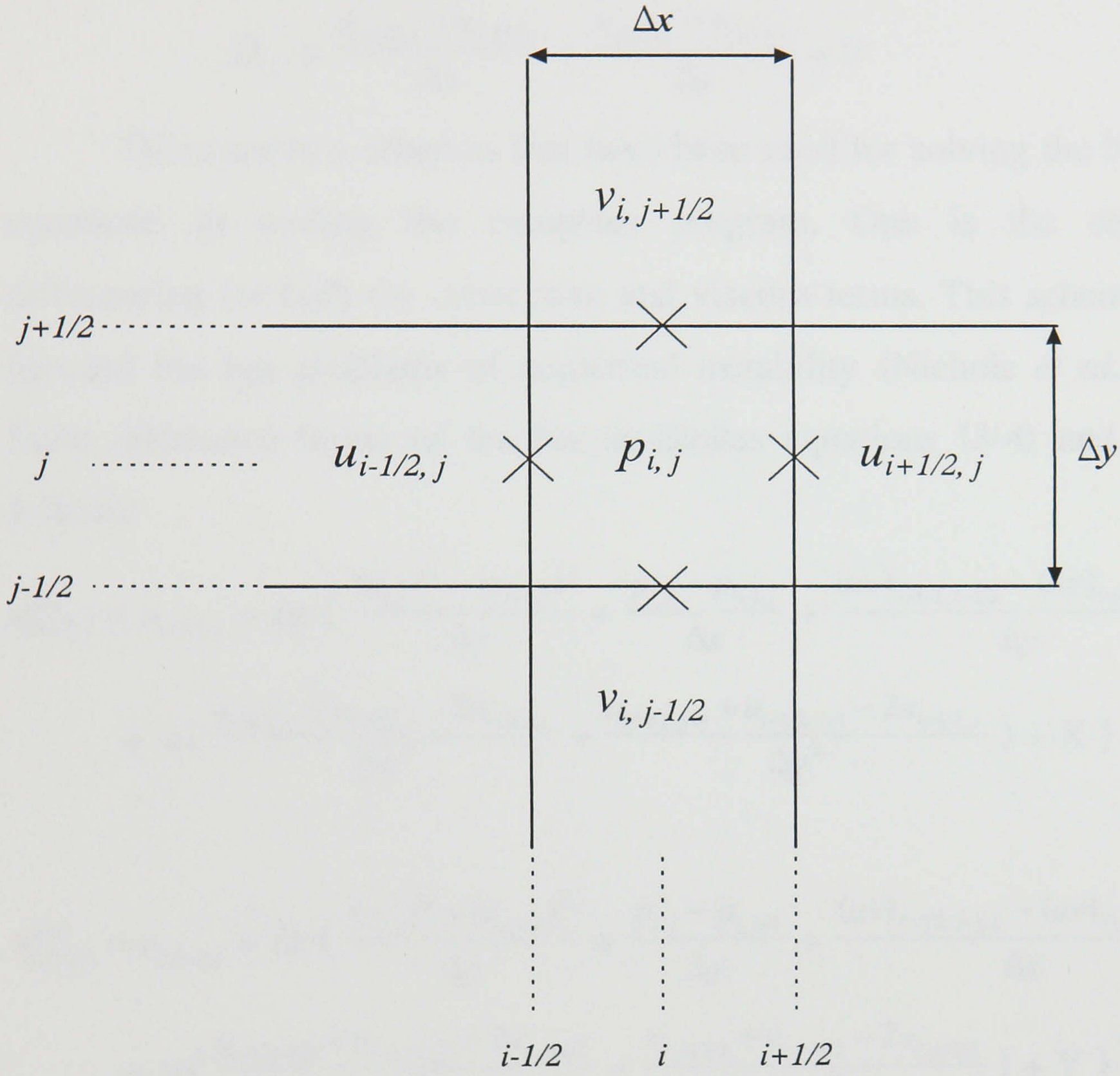

Figure 3-1 Layout of velocity and pressure variables.

The finite difference form of divergence associated with the continuity equation for the incompressibility condition according to the definition of the field variables becomes:

$$D_{i,j} = \frac{u_{i+1/2,j} - u_{i-1/2,j}}{\Delta x} + \frac{v_{i,j+1/2} - v_{i,j-1/2}}{\Delta y} = 0 \qquad (3\text{-}6)$$

There are two schemes that have been used for solving the Navier-Stokes equations in writing the computer program. One is the centre-in-space differencing for both the convective and viscous terms. This scheme is straight-forward but has problems of numerical instability (Nichols *et al.*, 1980). The finite difference forms of the Navier-Stokes equations (3-4) and (3-5) are as follows:

$$u^{n+1}_{i+1/2,j} = u_{i+1/2,j} + \Delta t \{ \frac{(u_{i,j})^2 - (u_{i+1,j})^2}{\Delta x} + \frac{p_{i,j} - p_{i+1,j}}{\Delta x} + \frac{(uv)_{i+1/2,j-1/2} - (uv)_{i+1/2,j+1/2}}{\Delta y}$$

$$+ \upsilon (\frac{u_{i+3/2,j} + u_{i-1/2,j} - 2u_{i+1/2,j}}{\Delta x^2} + \frac{u_{i+1/2,j+1} + u_{i+1/2,j-1} - 2u_{i+1/2,j}}{\Delta y^2}) + X \} \qquad (3\text{-}7)$$

$$v^{n+1}_{i,j+1/2} = v_{i,j+1/2} + \Delta t \{ \frac{(v_{i,j})^2 - (v_{i,j+1})^2}{\Delta y} + \frac{p_{i,j} - p_{i,j+1}}{\Delta y} + \frac{(uv)_{i-1/2,j+1/2} - (uv)_{i+1/2,j+1/2}}{\Delta x}$$

$$+ \upsilon (\frac{v_{i+1,j+1/2} + v_{i-1,j+1/2} - 2v_{i,j+1/2}}{\Delta x^2} + \frac{v_{i,j+3/2} + v_{i,j-1/2} - 2v_{i,j+1/2}}{\Delta y^2}) + Y \} \qquad (3\text{-}8)$$

Note that in equations (3-7) and (3-8), for convenience the terms are expressed without denoting that the time intervals are at "n" time intervals. Also, the velocities of u and v in the calculation of new step values are symmetrical about the point (i+1/2, j) and point (i, j+1/2) respectively as shown in Figure 3-1 for the location of field variables $u_{i+1/2,j}$ and $v_{i,j+1/2}$. Figure 3-2 gives the rest of the quantities involved in the calculations. In the SMAC method, the central difference scheme is used in both the convection terms and the viscous terms. The definition of the convection terms is as follows:

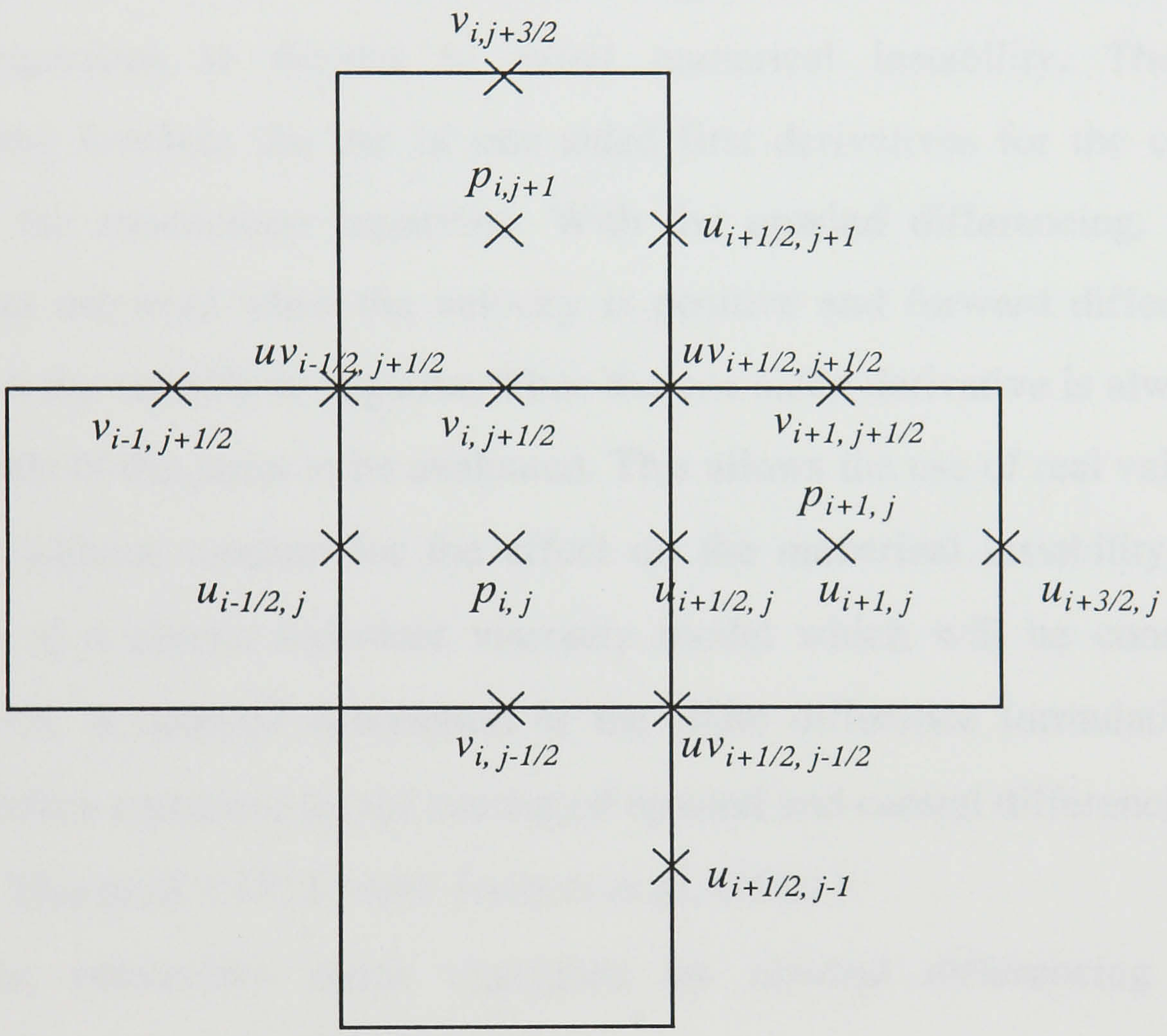

Figure 3-2 Components of velocity and pressure values used in calculations of u^{n+1} and v^{n+1}.

$$u_{i,j}{}^2 = u_{i-1/2,j\cdot} \cdot u_{i+1/2,j} \tag{3-9}$$

$$(uv)_{i+1/2,j+1/2} = \frac{1}{2}(u_{i+1/2,j} + u_{i+1/2,j+1}) \cdot \frac{1}{2}(v_{i,j+1/2} + v_{i+1,j+1}) \tag{3-10}$$

For solving the numerical instability problems, a large viscosity (so called "artificial viscosity") instead of the real viscosity of molten metal is used in the calculation in the original MAC method. The use of upwind differencing for convective terms and the central differencing for viscous terms of the Navier-Stokes equations is desired to avoid numerical instability. The upwind differencing involves the use of one sided first derivatives for the convection terms in the momentum equations. With the upwind differencing, backward differences are used when the velocity is positive and forward differences are used when the velocity is negative. Thus the one sided derivative is always in the upwind side of the point to be evaluated. This allows the use of real value for the viscosity without concern for the effect on the numerical instability, also the inclusion of a simple turbulent viscosity model which will be considered in Section 3.4. A detailed description of the finite difference formulation of the Navier-Stokes equations by the combined upwind and central differencing can be found in Hirt *et al.* (1975) and Nichols *et al.* (1980).

The convective terms expressed by upwind differencing in finite difference equations (3-11) and (3-12) are

$$\frac{\partial u^2}{\partial x} = \frac{u_{i+1,j}(u_{i+1,j})}{\Delta x} - \frac{u_{i,j}(u_{i,j})}{\Delta x} \tag{3-11}$$

where $(u_{i,j}) = (u_{i-1/2,j} + u_{i+1/2,j})/2$

$(u_{i,j}) = (u_{i-1/2,j})$ if $u_{i,j} > 0$

$(u_{i,j}) = (u_{i+1/2,j})$ if $u_{i,j} < 0$

and
$$\frac{\partial uv}{\partial y} = \frac{v_{i+1/2,j+1/2}\,(u_{i+1/2,j+1/2})}{\Delta y} - \frac{v_{i+1/2,j-1/2}\,(u_{i+1/2,j-1/2})}{\Delta y} \qquad (3\text{-}12)$$

where
$$(u_{i+1/2,j+1/2}) = u_{j+1/2,j} \quad \text{if} \quad v_{i+1/2,j+1/2} > 0$$
$$(u_{i+1/2,j+1/2}) = u_{i+1/2,j+1} \quad \text{if} \quad v_{i+1/2,j+1/2} < 0$$

The combined central and upwind differencing is expected to have a higher accuracy calculation results than upwind differencing alone.

All the terms contained in equation (3-6), that is the present time step of divergence, are already known quantities. Thus a continuity equation for the new time step n+1 is taken and shown by equation (3-13):

$$\frac{u^{n+1}_{i+1/2,j} - u^{n+1}_{i-1/2,j}}{\Delta x} + \frac{v^{n+1}_{i,j+1/2} - v^{n+1}_{i,j-1/2}}{\Delta y} = 0 \qquad (3\text{-}13)$$

The discretization of the governing equations have been completed. The solution scheme follows in the next section.

3.3.2 Solution Scheme of the Difference Formulae

In the MAC algorithms, the velocities and pressures are solved simultaneously. In the SMAC method, the pressure does not need to be calculated and a fluid motion system was uniquely defined by using velocity and vorticity physical quantities (Amsden and Harlow, 1970). The Navier-Stokes equations can be transformed into the vorticity equation of the form:

$$\frac{\partial \omega}{\partial t} + u\frac{\partial \omega}{\partial x} + v\frac{\partial \omega}{\partial y} = \upsilon\left(\frac{\partial^2 \omega}{\partial x^2} + \frac{\partial^2 \omega}{\partial y^2}\right) \qquad (3\text{-}14)$$

where
$$\omega = \frac{\partial u}{\partial y} - \frac{\partial v}{\partial x} \qquad (3\text{-}15)$$

From equations (3-14) and (3-15), we can see that the vorticity field of a flow domain is independent of the pressure field. Therefore, any pressure field put into momentum equations (3-7) and (3-8) will assure that the resulting velocity field carries the correct vorticity. However, an arbitrary pressure field cannot guarantee the vanishing of the divergence D because the continuity equation is not involved in the velocity field. Therefore the velocity field is tentative only. A tentative velocity field can be written with an arbitrary pressure field Γ for the centre-in-space differencing form as below:

$$\bar{u}^{n+1}_{i+1/2,j} = u_{i+1/2,j} + \Delta t \{ \frac{(u_{i,j})^2 - (u_{i+1,j})^2}{\Delta x} + \frac{\Gamma_{i,j} - \Gamma_{i-1,j}}{\Delta x} + \frac{(uv)_{i+1/2,j-1/2} - (uv)_{i+1/2,j+1/2}}{\Delta y}$$

$$+ \upsilon(\frac{u_{i+3/2,j} + u_{i-1/2,j} - 2u_{i+1/2,j}}{\Delta x^2} + \frac{u_{i+1/2,j+1} + u_{i+1/2,j-1} - 2u_{i+1/2,j}}{\Delta y^2}) + X) \qquad (3\text{-}16)$$

$$\bar{v}^{n+1}_{i,j+1/2} = v_{i,j+1/2} + \Delta t(\frac{(v_{i,j})^2 - (v_{i,j+1})^2}{\Delta y} + \frac{\Gamma_{i,j} - \Gamma_{i,j+1}}{\Delta y} + \frac{(uv)_{i-1/2,j+1/2} - (uv)_{i+1/2,j+1/2}}{\Delta x}$$

$$+ \upsilon(\frac{v_{i+1,j+1/2} + v_{i-1,j+1/2} - 2v_{i,j+1/2}}{\Delta x^2} + \frac{v_{i,j+3/2} + v_{i,j-1/2} - 2v_{i,j+1/2}}{\Delta y^2}) + Y) \qquad (3\text{-}17)$$

Furthermore, if the tentative velocity field is adjusted by employing an appropriated potential function, φ, the velocity field will carry the correct vorticity and satisfy the continuity equation in the fluid region under investigation. Thus the final velocity is given by:

$$u^{n+1}_{i+1/2,j} = \bar{u}^{n+1}{}_{i+1/2,j} - \frac{\varphi_{i+1,j} - \varphi_{i,j}}{\Delta x} \qquad (3\text{-}18)$$

$$v_{i,j+1/2}^{n+1} = \overline{v}^{n+1}{}_{i,j+1/2} - \frac{\varphi_{i,j+1} - \varphi_{i,j}}{\Delta y} \tag{3-19}$$

The final velocity is dependent on the tentative velocity $\overline{u}$ and $\overline{v}$, and potential function φ, which is shown in equations (3-18) and (3-19).

Equations (3-7) and (3-8) are expressions for $u^{n+1}{}_{i+1/2,j}$ and $v^{n+1}{}_{i,j+1/2}$ respectively. Similar equations for $u_{i-1/2,j}^{n+1}$ and $v_{i,j-1/2}^{n+1}$ can be written. These four expressions are substituted all together into the continuity equation (3-13), then a Poisson type equation for the pressure field (Welch *et al.*, 1965) can be obtained:

$$\overline{D}_{i,j}^{n+1} = \frac{\varphi_{i+1,j} + \varphi_{i-1,j} - 2\varphi_{i,j}}{\Delta x^2} + \frac{\varphi_{i,j+1} + \varphi_{i,j-1} - 2\varphi_{i,j}}{\Delta y^2} \tag{3-20}$$

The relaxation method is successively used to iterate for the solution of equation (3-20). Then the values of the potential function φ will be put back into equations (3-18) and (3-19) in order to get the final velocities of u^{n+1} and v^{n+1}. Since the value of potential function φ is determined by the equation (3-20) which satisfied the condition of $\overline{D}_{i,j}^{n+1} = 0$, therefore the final velocity field have vanishing the divergence. Annex 3-1 gives the details of the tentative and final velocity fields which carries the same vorticity. This assures that the correct final velocity field is obtained.

3.3.3 Free Surface Boundary Conditions

In the last section, the calculation of the full region (interior region) has been introduced. An important part of the numerical solution is to determine the field variables in the free surface region. For the surface-region flow calculation, equation (3-4) and (3-5) are applied, but equation (3-1) is not valid since the

divergence is not vanishing. The calculation of the free surface region depends on its boundary conditions.

The boundary conditions at the free surface should be the vanishing of the normal and tangential stresses, for a 2-D surface, equations (3-21) and (3-22) should be followed (Hirt and Shannon, 1968):

(1) the vanishing of the tangential stress on the free surface:

$$\upsilon\left(2n_x m_x \frac{\partial u}{\partial x} + \left(n_x m_y + n_y m_x \right) \left(\frac{\partial u}{\partial y} + \frac{\partial v}{\partial x} \right) + 2n_y m_y \frac{\partial v}{\partial y} \right) = 0 \qquad (3\text{-}21)$$

(2) the vanishing of the normal stress on the free surface:

$$p - 2\upsilon\left(n_x n_x \frac{\partial u}{\partial x} + n_x n_y \left(\frac{\partial u}{\partial y} + \frac{\partial v}{\partial x} \right) + n_y n_y \frac{\partial v}{\partial y} \right) = 0 \qquad (3\text{-}22)$$

where n_x, n_y are the x, y components of the unit outward normal stress to the free surface; and m_x, m_y are the x, y components of unit tangential stress to the free surface.

The free surface boundary conditions require accurate information about the orientation of the free surface. The cell reflagging scheme can be used to determine the free surface orientation. The SMAC system uses the approximation method, that is (i) the tangential stress condition is replaced by zero divergence on a surface cell and the vanishing of the normal derivative of fluid velocity tangential to the free surface while (ii) a zero surface pressure is applied to the normal stress condition. There are three cases of the surface cell to be considered, which corresponds to a surface cell having empty cells on one, two, or three sides of it.

If a surface cell lies to the empty cell neighbour to the left or right, the pressure can be determined as:

$$p_{i,j} = \frac{2\upsilon}{\Delta x}(u_{i+1/2,j} .- u_{i-1/2,j}) \tag{3-23}$$

If the empty neighbour lies to the above or below, the pressure is:

$$p_{i,j} = \frac{2\upsilon}{\Delta y}(v_{i,j+1/2} - v_{i,j-1/2}) \tag{3-24}$$

For a surface cell with three open sides or for a cell with two open sides that opposite to each other, the pressure for the surface cell is set zero.

For a corner cell, the pressure is also set zero in the SMAC system.

Annex 3-2 shows detailed surface configuration and the calculation of velocities. Annex 3-3 gives four basic surface cell configurations.

3.3.4 Wall Boundary Condition

Figure 3-3 shows the field variable positions at a wall. The SMAC method in finite difference form assigned some quantities on exterior regions (cells) which are needed for the computation. Various boundary conditions may be applied at the walls of the computing mesh. The conditions for a boundary at the left wall will be discussed (Figure 3-3) as a typical example, while other wall conditions are similar.

(1) Free-slip wall conditions (slip factor = 1)

A free-slip wall represents no drag on the fluid from the wall. Thus, we have

$$\left.\begin{aligned} &u_{i-1/2,j} = 0, \text{ then } u_{i-3/2,j} = u_{i+1/2,j} \\ &v_{i-1,j+1/2} = \text{slip factor} \times v_{i,j+1/2}\ (= v_{i,j+1/2}) \\ &v_{i-1,j-1/2} = \text{slip factor} \times v_{i,j-1/2}\ (= v_{i,j-1/2}) \\ &\varphi_{i-1,j} = \varphi_{i,j} \end{aligned}\right\} \tag{3-25}$$

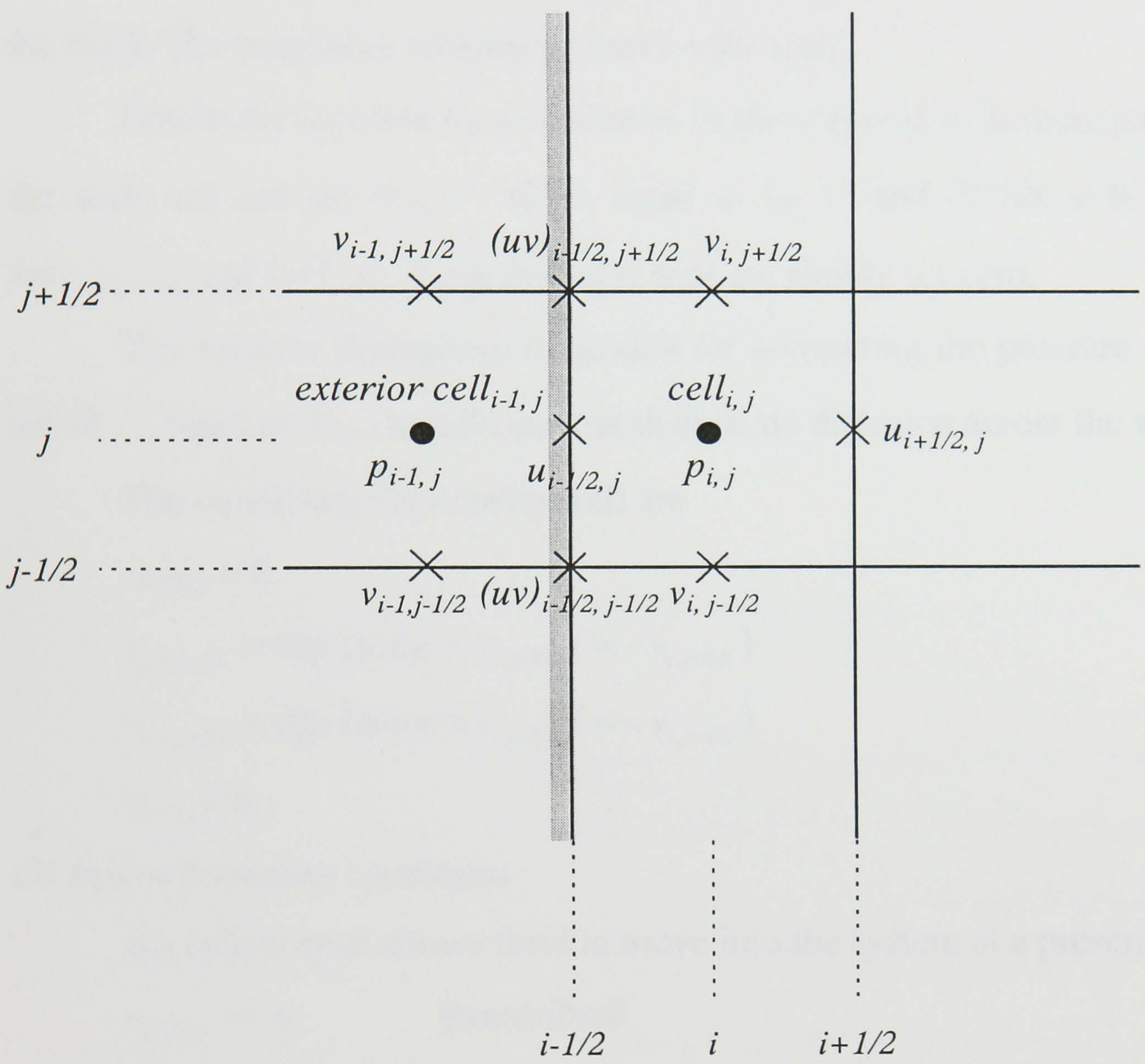

Figure 3-3 Positions of field variables at a wall

The velocity component u in the x direction (normal to the wall) vanishes at the wall. There is no gradient in either tangential velocity or in the potential function φ.

(2) Nonslip wall conditions (Slip factor = -1)

A nonslip boundary represents a viscous boundary that exerts a drag upon the fluid. The tangential velocity is zero on the wall.

Due to the fact that no momentum in the x-axis is to be transported across the wall, we can set $(u_{i-1,j})^2$ to be equal to $(u_{i,j})^2$ and $\partial u^2/\partial x = 0$. The terms $(uv)_{i-1/2,j+1/2}$ and $(uv)_{i-1/2,j-1/2}$.on the solid wall are simply set zero.

The exterior divergence is needed for computing the pressure data. Thus, set $D_{i-1,j}$ equal to $D_{i,j}$ to indicate that there is no diffusion across the wall.

The conditions for nonslip wall are

$$\left.\begin{aligned} u_{i-1/2,j} &= 0 \\ v_{i-1,j+1/2} &= \text{slip factor} \times v_{i,j+1/2} \ (= - \ v_{i,j+1/2} \ ) \\ v_{i-1,j-1/2} &= \text{slip factor} \times v_{i,j-1/2} \ (= - \ v_{i,j-1/2} \ ) \\ \varphi_{i-1,j} &= \varphi_{i,j} \end{aligned}\right\} \quad (3\text{-}26)$$

(3) Inflow boundary conditions

An inflow wall allows fluid to move into the system at a prescribed rate.

$$\left.\begin{aligned} u_{i-1/2,j} &= u \qquad \text{(prescribed)} \\ v_{i-1,j+1/2} &= - \ v_{i,j+1/2} \\ v_{i-1,j-1/2} &= - \ v_{i,j-1/2} \\ \varphi_{i-1,j} &= \varphi_{i,j} \end{aligned}\right\} \quad (3\text{-}27)$$

The free-slip boundary conditions in a real fluid implies the development of a boundary layer in which the fluid is accelerated from the wall velocity to a free stream value some distance from the wall. In fact, the no-slip condition forces an artificially large drag on the fluid, while a free-slip condition represents no boundary drag. Therefore, the slip factor is expected to lie between -1 to 1.

Intermediate values of slip factor represent the conditions between the two extremes.

3.3.5 Marker Particle Movements

As the velocity field is computed, each marker particle is travelling with a velocity taken as the average from the nearest cell velocities. For example, marker velocity component u_0 is determined as the mean value of the four nearest horizontal cell velocities. Similarly the marker velocity component v_0 is calculated as an interpolated value of its nearest four vertical cell velocities.

After determining the marker velocity u_0 and v_0, the new position of each marker can be calculated. For example of marker *k*:

$$x_k^{n+1} = x_k^n + u_0 \cdot \Delta t \tag{3-28}$$

$$y_k^{n+1} = y_k^n + v_0 \cdot \Delta t \tag{3-29}$$

where the left sides of the equations give the new coordinates of the marker position.

The new marker positions gives the new configuration of the molten metal. Cells also can then be reflagged such as full or empty or surface and so on.

The actual location of the free surface must be determined by some additional computation on the distribution of markers within the cell. Obviously, storage requirements increase significantly with this method because of the large increase in the number of point coordinates that must be stored for the markers' positions. In order to achieve stable and accurate calculations, the computation requires that the fluid travels no more than one cell dimension during each time increment. The markers on the interior cells which are not next to the surface cells do not really have practical importance in determining the evolution of the free surface. Thus, the number of marker particles can be reduced, and computational efficiency can be improved. In conclusion, the marker particles method is logically simple and computationally efficient.

3.4 Turbulent Viscosity Model

Due to the complexity of the turbulent flow during the filling of castings, a simple turbulent viscosity model is adopted to evaluate the effects of the turbulence on the calculated flow patterns. The effective viscosity υ_e is given as follows:

$$\upsilon_e = \upsilon + \upsilon_t \tag{3-30}$$

where υ_t is the turbulent viscosity and υ is the viscosity of the material in the laminar flow.

Turbulent viscosity is a local property, depending on the flow system configuration and velocity field at each point in the system. The model chosen for this calculation is based on Prandtl's mixing length hypothesis (Launder and Spalding, 1972), in which the turbulent viscosity is given by

$$\upsilon_t = l_m{}^2 |I| \tag{3-31}$$

where strain rate

$$I = \frac{\partial U_i}{\partial x_j} + \frac{\partial U_j}{\partial x_i} \tag{3-32}$$

and U_i and U_j are mean velocity components (detailed in Hwang, 1985).

The strain rate I is determined locally by the mean velocity field, and the characteristic mixing length, l_m, must be prescribed. In comparison with the turbulence stress corresponding to the stress caused by the viscosity effect, it is tempting to assume that the turbulence stress acts like the viscous stress, i.e., that they are proportional to the velocity gradient of the mean velocity field. Thus the turbulent effect is considered in the calculation model.

3.5 Numerical stability Conditions and Accuracy

Numerical calculations often have computed quantities that develop large, high frequency oscillations in space, time, or both. This behaviour is usually referred to as numerical instability. In solving for the Navier-Stokes difference equations, the source of the numerical instability comes mainly from the convection terms calculation. The SMAC algorithm takes the central difference form for convection terms which is sensitive to the instability.

The present calculation uses the upwind differencing for convective terms and the central differencing for viscous terms of the Navier-Stokes equations which avoid numerical instability and also assure accuracy.

A stability conditon associated with the upwind differencing scheme is

$$\Delta t < \text{Min}\left(\frac{\Delta x}{|u_{\max}|}, \frac{\Delta y}{|v_{\max}|}\right) \tag{3-33}$$

Equation (3-33) means that the fluid cannot move through more than one cell in one time step, because the difference equations assume that there are fluxes only between adjacent cells. The minimum is applied to every cell in the mesh. Once a mesh has been prescribed, the time increment necessary for stability is chosen according to this criterion. Typically, Δt is chosen to be one-third of the minimum cell transit time in the computation and the stability is improved.

The condition necessary to ensure stability for the viscous diffusion terms in the finite difference momentum equations is

$$\nu \Delta t < \frac{1}{2} \frac{\Delta x^2 \Delta y^2}{\Delta x^2 + \Delta y^2} \tag{3-34}$$

where Δt is chosen to satisfy the inequalities in equations (3-33) and (3-34).

Equation (3-34) means the momentum must not diffuse more than one cell in one time step.

Obvious requirements for accurate computation include the necessity for a cell resolution fine enough and a time increment small enough to resolve the feature of interest and still avoid instability.

Numerical simulation technique gives only approximate solutions. In a numerical method, round-off error and truncation error influence the computational output.

A truncation error will occur in a computation since the differential equations are replaced by the difference equations. The error (higher order terms) can be evaluated from the residual term of a Taylor's series expansion. In general for a mesh system, finer meshs with appropriate smaller time steps, contribute to improve computation accuracy. The test conclusion shows that a finer mesh would give a more accurate result than the coarser mesh. The use of a finer mesh can reveal more accurately the contour of the free surface.

It is very important to make a consistency accuracy check between the numerical simulation and experimental information provided by the real die casting process or from a water-analogue test. The consistency check will verify the validation of the mathematical modelling.

3.6 Computational Results and Analysis

This section gives the computational results of the study on the important effect of viscosity and gravitational force in association with filling patterns that aims to make a further simplification to the preceding equation set, and improve the effectiveness of the computational technique. Furthermore, the computational results are used to analyze the effect of the filling velocity on filling pattern. The computational results are also delivered in Chapter 5 for comparison against experimental information in order to verify the truly theoretical treatments.

3.6.1 The Viscous Effect on the Overall Filling Pattern

The Table 3-1 below provides the viscosity data of some molten metal (Eckert, 1989 and Porter, 1991):

Table 3-1 Viscosity data.

	T $^{\circ}C$	ϱ $kg\,m^{-3}$	$10^3\mu$ $kg\,m^{-1}s^{-1}$	$10^6\upsilon$ m^2s^{-1}	$\frac{\upsilon}{(\upsilon)_{water}}$
Water (20 $^{\circ}C$)	0	1000	1.006	1.006	1.000
Aluminium (660 $^{\circ}C$)	660	2385	1.30	0.545	0.54
Magnesium (650 $^{\circ}C$)	650	1590	1.25	0.786	0.78
Bismuth (271$^{\circ}C$)	271	10070	1.62	0.61	0.61
Zinc (420 $^{\circ}C$)	420	7150	1.74	0.393	0.391
Woods* Metal(332 $^{\circ}C$)	70	10400	1.7	0.163	0.162

Tables 3-1 shows the kinematic viscosity of materials used commonly in pressure die casting processes is equal to $(0.163\text{-}0.786)\times10^{-6}m^2s^{-1}$, and that all are smaller than the viscosity of water at 20 $^{\circ}C$ that is used for water analogue simulation. Thus, various molten metals have a fluidity that is even better than water.

In order to find the viscous effect on the filling pattern, a rectangular cavity of size $10\times10\times1mm$ was designated for computing. The filling velocity was taken as a constant $v_f=0.75ms^{-1}$, a very low filling velocity, in order to lower

*Woods Metal: 50% Bismuth, 25% Lead, 12.5% Cadmium, 12.5% Tin

its influence. To put viscosity as an obvious consideration, other parameters were maintained as constant inputs into the computer for three different inputs of kinematic viscosity as:

$$\upsilon = 1\times10^{-6} m^2 s^{-1} \text{ (water, } T_w = 20^{\circ}C) \text{ ,}$$

$$\upsilon = 1\times10^{-9} m^2 s^{-1}$$

and $$\upsilon = 1\times10^{-4} m^2 s^{-1}.$$

The computational output (marker plots) illustrated in Figure 3-4 represent the same overall filling pattern for the above three different cases although the maximum difference in kinematic viscosity is equal to 100,000 times.

Note that $\upsilon = 1\times10^{-9} m^2 s^{-1}$ is a very small value, so we can assumed υ=0, thereby ignoring the kinematic viscosity.

This was empirically confirmed by Iwahori *et al.* (1986).

3.6.2 The Gravity Effect on the Overall Filling Pattern

A symmetrical filling pattern is always conducted under the condition of a symmetrical filling injection and has been reported computationally and experimentally in some of literature (Hwang, 1985; Hu, 1992a, b). However, it is still necessary to investigate the effect of the gravitational force on the filling pattern when the mould is assembled vertically.

A rectangular cavity of size 12.4×12.4×13.5*mm* was designated for the computational study of gravity effects on the filling pattern. The model was placed vertically in order to see how the gravitational force acts on fluid motion with a free surface. The density, kinematic viscosity, and other parameters were entered as before into the computer for three different inputs of filling velocity as follows: (i) $v_f = 0.75\, ms^{-1}$,

(ii) $v_f = 1.93\, ms^{-1}$,

and (iii) $v_f = 5.00\, ms^{-1}$.

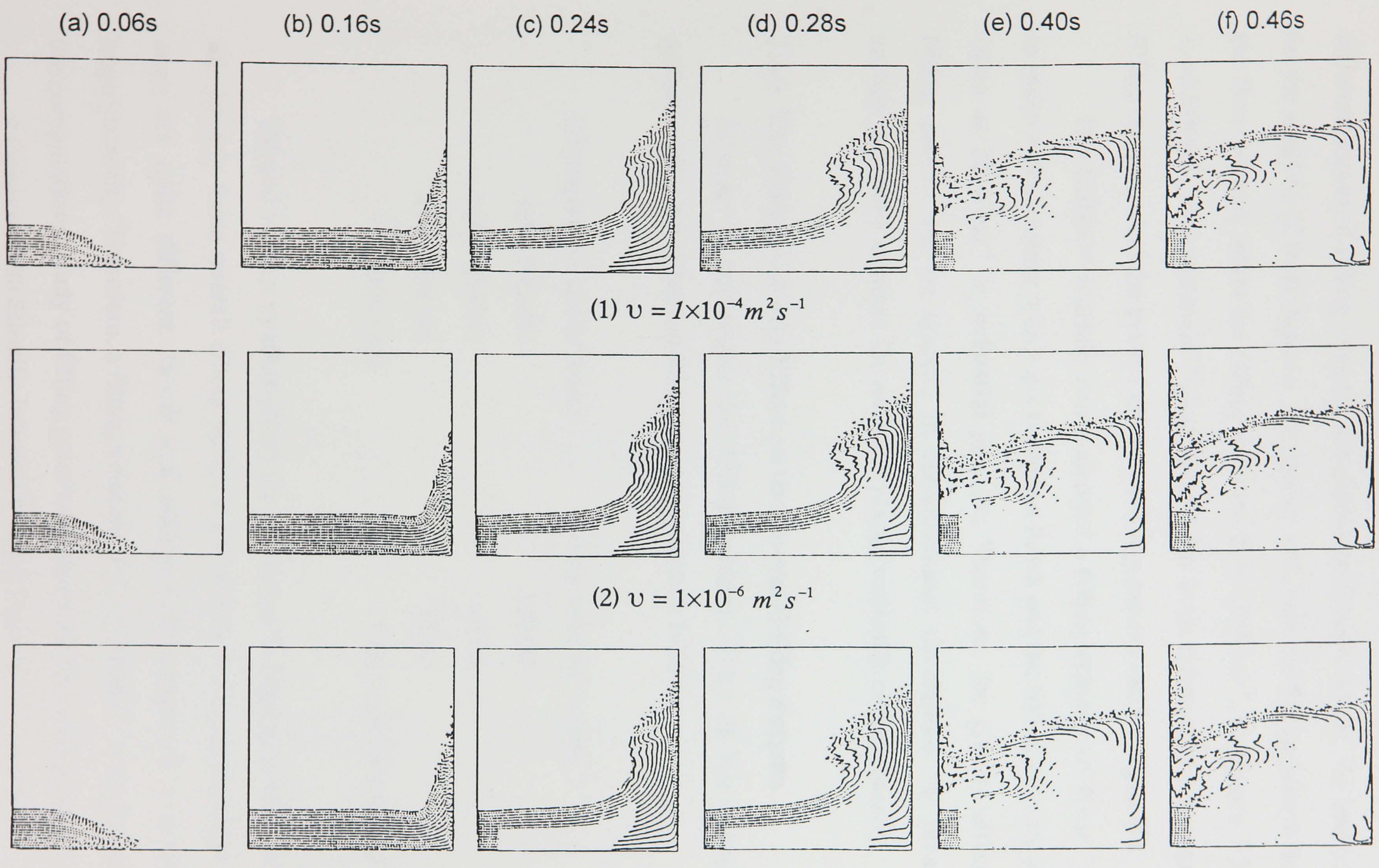

Figure 3-4 Computed marker plots of the same overall filling patterns for different viscosity of (1) $\upsilon = 1\times10^{-4} m^2 s^{-1}$, (2) $\upsilon = 1\times10^{-6}\ m^2 s^{-1}$ and (3) $\upsilon = 1\times10^{-9}\ m^2 s^{-1}$.

Three sets of figures (marker plots) in connection with the above three different inputs of filling velocity are shown in Figures 3-5(a), (b) and (c). Based on the analysis of these figures, the gravity effect on the filling pattern dominates the flow process when the filling velocity is v_f<5.00ms^{-1}. In Figure 3-5(c) with v_f=5.00ms^{-1}, a symmetrical filling pattern has been achieved for a symmetrical filling injection and the gravity effect on filling pattern can be neglected.

The CSIRO* recently recommended a filling velocity of 40ms^{-1} in order to make a zinc casting with a good surface finish and the filling velocity is always taken as 20-40ms^{-1} in industrial practice. Therefore, the gravity effect on the filling pattern can be ignored in computational simulations for pressure die casting processes whether the mould is placed vertically or horizontally.

3.6.3 The Filling Velocity Effect on the Overall Filling Pattern

In order to investigate the filling velocity effect on the overall filling pattern, four simulation models were designated as follows:

Dimension of model (*mm*)	Filling velocity v_f (ms^{-1})
100×100×10	120.00
100×100×10	60.00
100×100×10	30.00
79× 90×11.5	9.89 (water analogue)

Typical figures (marker plots) are illustrated in Figures 3-6(a), (b), (c) and (d). Clearly these overall filling patterns are almost the same although the time steps are quite different. Booth and Allsop (1983) reported a similar result experimentally. Therefore, a filling velocity of v_f=10.00ms^{-1} is recommended for the computational study of filling patterns in pressure die casting processes.

* Commonwealth Scientific Industrial Research Organization, Australia.

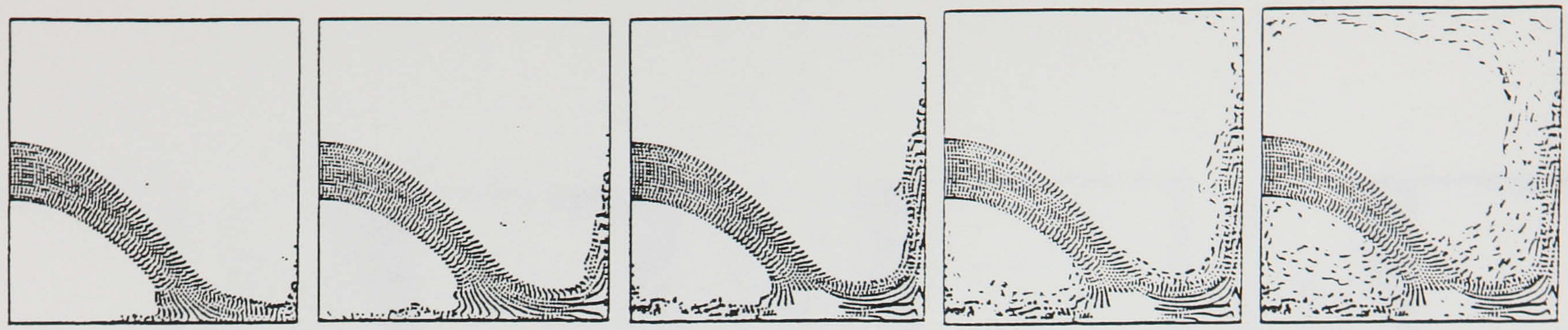

(a) 0.16s (b) 0.20s (c) 0.24s (d) 0.28s (e) 0.32s

(A) The overall filling pattern for filling velocity $v_f = 0.75ms^{-1}$

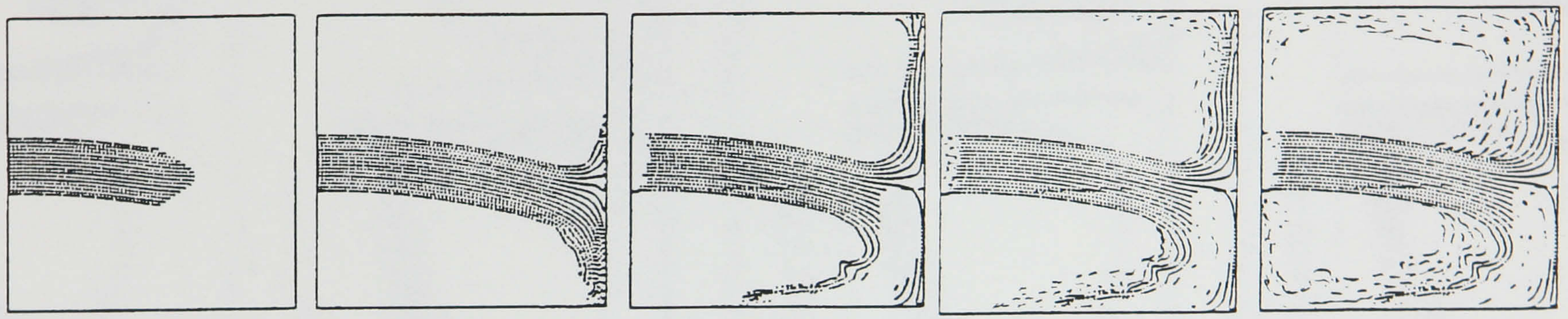

(a) 0.04s (b) 0.08s (c) 0.12s (d) 0.16s (e) 0.20s

(B) The overall filling pattern for filling velocity $v_f = 1.93ms^{-1}$

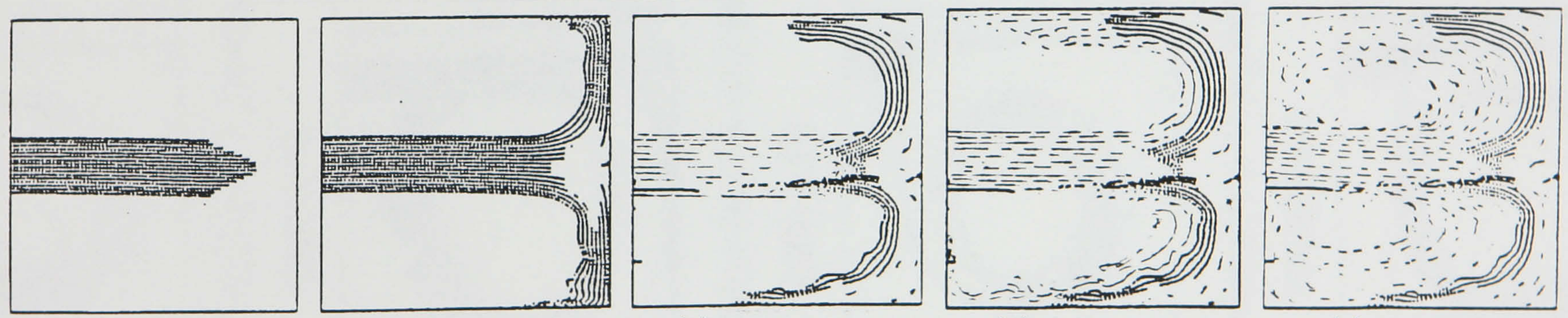

(a) 0.02s (b) 0.04s (c) 0.06s (d) 0.08s (e) 0.10s

(C) The overall filling pattern for filling velocity $v_f = 5.00ms^{-1}$

Figure 3-5 The gravity effect on the filling pattern.

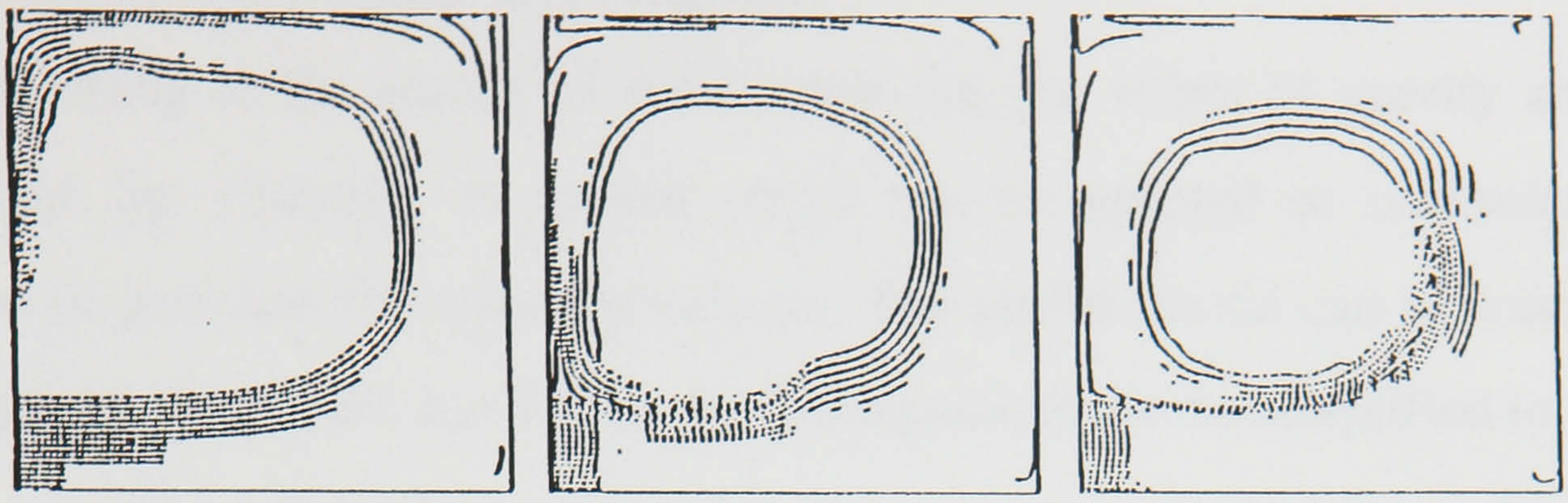

(a) 0.0025s (b) 0.0030s (c) 0.0035s

(A) The overall filling pattern for filling velocity $v_f = 120.00ms^{-1}$

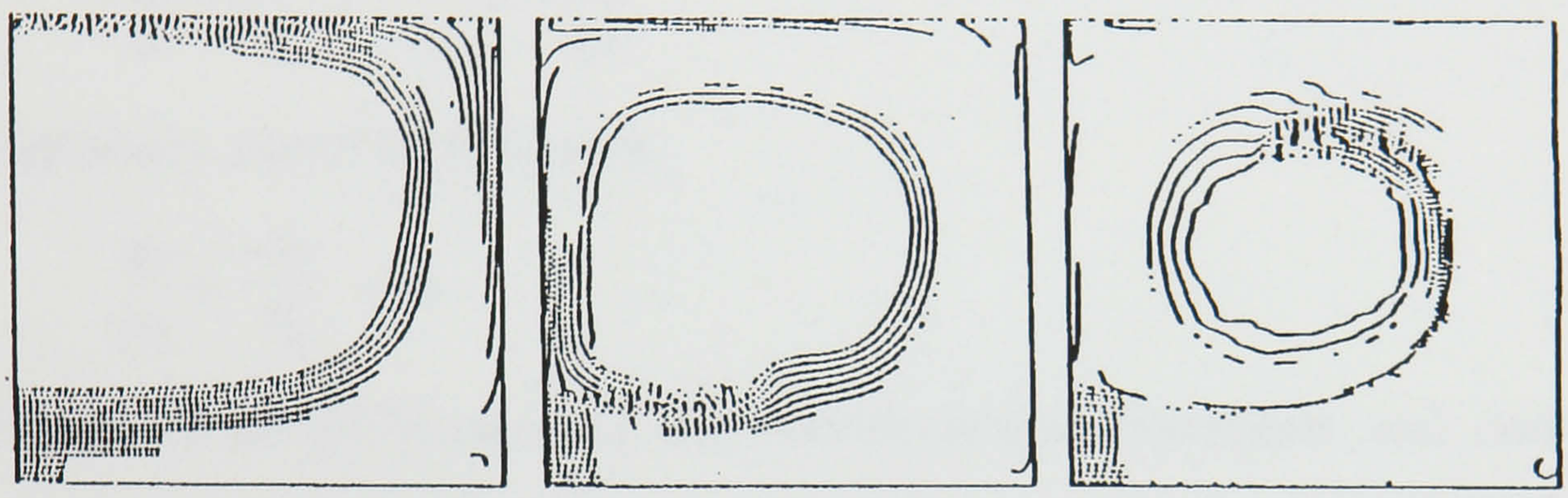

(a) 0.004s (b) 0.006s (c) 0.008s

(B) The overall filling pattern for filling velocity $v_f = 60.00ms^{-1}$

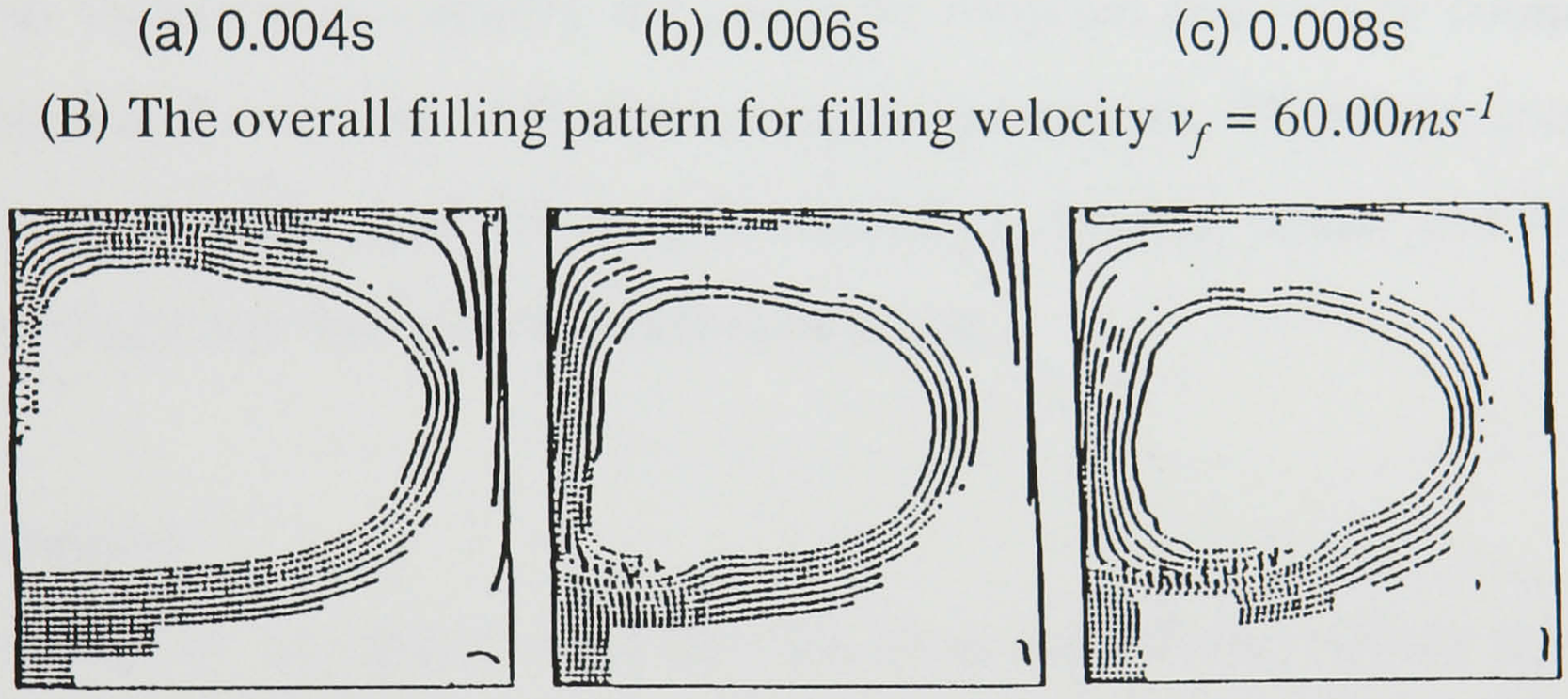

(a) 0.040s (b) 0.048s (c) 0.052s

(C) The overall filling pattern for filling velocity $v_f = 30.00ms^{-1}$

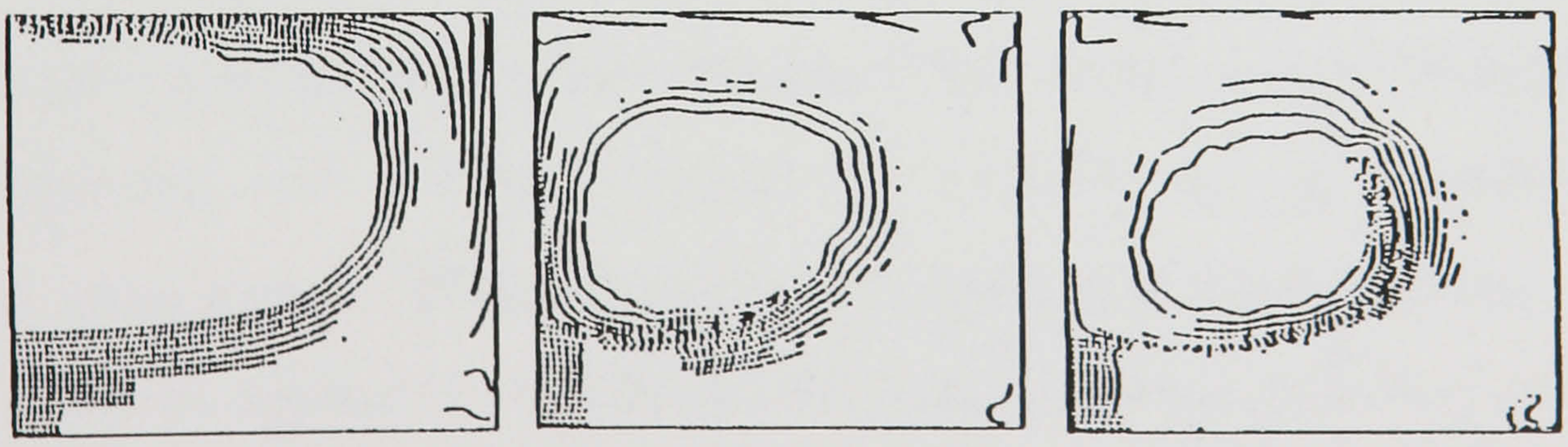

(a) 0.08s (b) 0.12s (c) 0.14s

(D) The overall filling pattern for filling velocity $v_f = 9.89ms^{-1}$

Figure 3-6 The filling velocity effect on the filling pattern.

3.7 Simplification of Computer Program

According to the results of the Section 3.6, the effect of gravity and the influence of the viscosity of molten metal can be ignored in computational simulation of pressure die casting processes. The molten metal can be treated as 2-D ideal fluid. Therefore, the Navier-Stokes equations can be simplified to:

$$\frac{\partial u}{\partial t}+u\frac{\partial u}{\partial x}+v\frac{\partial u}{\partial y}=-\frac{\partial p}{\partial x}$$
$$\frac{\partial v}{\partial t}+u\frac{\partial v}{\partial x}+v\frac{\partial v}{\partial y}=-\frac{\partial p}{\partial y} \qquad (3\text{-}35)$$

and the continuity equation becomes:

$$\frac{\partial u}{\partial x}+\frac{\partial v}{\partial y}=0 \qquad (3\text{-}36)$$

The above simplification of the Navier-Stokes equations and continuity equation do significantly simplify the computer program and reduce computing time of iteration for cavities with more complex geometries. Therefore, it can be extended to deal with quasi-3D or 3-D simulation models. Anzai and Uchida (1990) have tried this way with a satisfactory result.

3.8 Conclusions

In this study, the SMAC technique has been applied successfully to obtain information regarding the filling patterns of pressure die casting processes. On the basis of the computational analysis discussed in Sections 3.6.1, 3.6.2 and 3.6.3, the gravitational force and the viscous effect on the overall filling pattern can be neglected, and a filling velocity of v_f=10.00 ms^{-1} is suggested for convenient computation. These conclusions suggest that the hypothesis of an ideal liquid can be applied in the mathematical equations for modelling of filling flow patterns. The numerical simulation program can then be further simplified to achieve an accurate and cost-effective computation for the filling of a complex geometry cavity by quasi-3-D or 3-D models.

Annex 3-1 The Vorticity Field

The definition of vorticity for the 2 dimensional case is as follows (Hwang, 1985):

$$\omega = \frac{\partial u}{\partial y} - \frac{\partial v}{\partial x} \tag{3A-1-1}$$

or rewritten in finite difference form as:

$$\omega^{n+1} = \frac{u^{n+1}_{i+1/2,j+1} - u^{n+1}_{i+1/2,j}}{\Delta y} - \frac{v^{n+1}_{i+1,j+1/2} - v^{n+1}_{i,j+1/2}}{\Delta x} \tag{3A-1-2}$$

$$\omega^{n+1} = \frac{\overline{u}^{n+1}{}_{i+1/2,j+1} - \dfrac{\varphi_{i+1,j+1} - \varphi_{i,j+1}}{\Delta x} - \left(\overline{u}^{n+1}{}_{i+1/2,j} - \dfrac{\varphi_{i+1,j} - \varphi_{i,j}}{\Delta x}\right)}{\Delta y}$$

$$- \frac{\overline{v}^{n+1}{}_{i+1,j+1/2} - \dfrac{\varphi_{i+1,j+1,} - \varphi_{i+1,j}}{\Delta y} - \left(\overline{v}^{n+1}{}_{i,j+1/2} - \dfrac{\varphi_{i,j+1} - \varphi_{i,j}}{\Delta y}\right)}{\Delta x} \tag{3A-1-3}$$

$$\omega^{n+1} = \frac{\overline{u}^{n+1}{}_{i+1/2,j+1} - \overline{u}^{n+1}{}_{i+1/2,j}}{\Delta y} - \frac{\overline{v}^{n+1}{}_{i+1,j+1/2} - \overline{v}^{n+1}{}_{i,j+1/2}}{\Delta x}$$

$$- \frac{1}{\Delta x \Delta y}\left[(\varphi_{i+1,j+1} - \varphi_{i,j+1}) - (\varphi_{i+1,j} - \varphi_{i,j}) - (\varphi_{i+1,j+1} - \varphi_{i+1,j}) - (\varphi_{i,j} - \varphi_{i,j+1})\right]$$

$$= \overline{\omega}^{n+1} \tag{3A-1-4}$$

Thus it is proven that this final velocity carries the correct vorticity as the tentative velocity field.

Annex 3-2 The Surface Configuration

Depending upon the surface configuration shown in Figure 3A-2, surface cells are treated differently and forced to satisfy vanishing divergence. A brief description of the treatment is (Hwang, 1985):

If the surface has one empty face (No. 1, 2, 4 and 8 in the above configuration) or has two empty (configuration No. 2, 4, 8), the appropriate u or v on the empty faces may be calculated precisely. The other configurations involve more than one u and/or more than one v in the surface cell have no precise treatment. Thus one velocity is modified to assure that at least $D = 0$ in the surface cell.

The eight equations labeled (1) through (8) on the following page are used in the following arrangement for each of the 15 configurations.

Configuration No.	Equation (3A-2-1 to -8) used
1, 5, 11, 13, 15	(3A-2-1)
2, 7, 10, 14	(3A-2-2)
3	(3A-2-3) & (3A-2-6)
4	(3A-2-4)
6	(3A-2-5) & (3A-2-6)
8	(3A-2- 7)
9	(3A-2-3) & (3A-2-8)
12	(3A-2-5) & (3A-2-8)

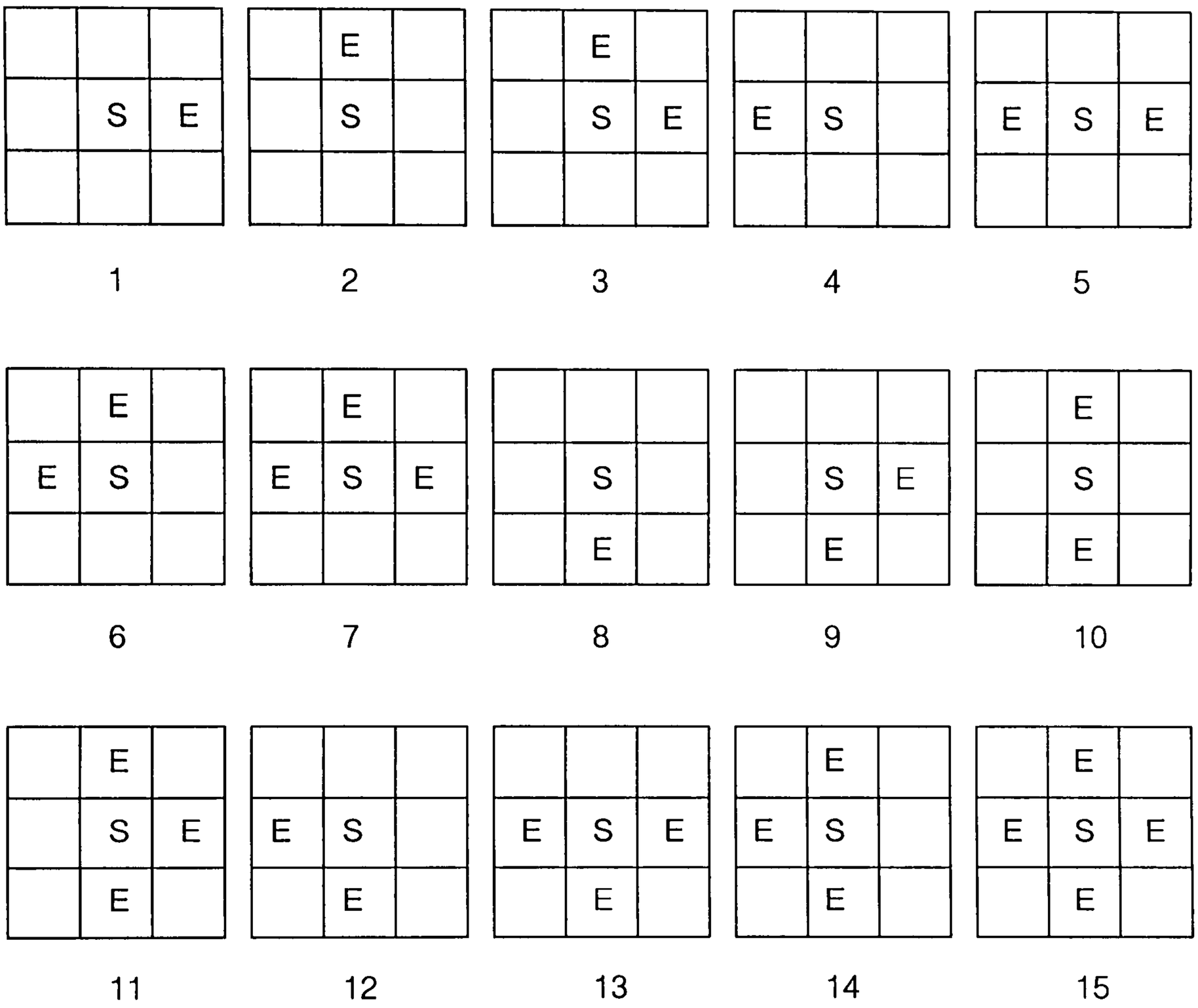

E = Empty cell S = Surface cell

Figure 3A-2 Arrangements of different surface cells.

$$u_{i+1/2,j} = u_{i-1/2,j} - \frac{\Delta x}{\Delta y}(v_{i,j+1/2} - v_{i,j-1/2}) \quad (3A\text{-}2\text{-}1)$$

$$v_{i,j+1/2} = v_{i,j-1/2} - \frac{\Delta y}{\Delta x}(u_{i+1/2,j} - u_{i-1/2,j}) \quad (3A\text{-}2\text{-}2)$$

$$u_{i+1/2,j} = u_{i-1/2,j} \quad (3A\text{-}2\text{-}3)$$

$$u_{i-1/2,j} = u_{i+1/2,j} + \frac{\Delta x}{\Delta y}(v_{i,j+1/2} - v_{i,j-1/2}) \quad (3A\text{-}2\text{-}4)$$

$$u_{i-1/2,j} = u_{i+1/2,j} \quad (3A\text{-}2\text{-}5)$$

$$v_{i,j+1/2} = v_{i,j-1/2} \quad (3A\text{-}2\text{-}6)$$

$$v_{i,j-1/2} = v_{i,j+1/2} + \frac{\Delta y}{\Delta x}(u_{i+1/2,j} - u_{i-1/2,j}) \quad (3A\text{-}2\text{-}7)$$

$$v_{i,j-1/2} = v_{i,j+1/2} \quad (3A\text{-}2\text{-}8)$$

Annex 3-3 The Basic Surface Cell Configurations

There are four basic surface cell configurations shown in Figure 3A-3 that must be checked to satisfy the vanishing of the normal derivative of tangential velocity at the surface and velocities are set to a function of three other velocities to satisfy the required conditions (Amsden and Harlow, 1970).

case I: $$v_{i+1,j+1/2} = v_{i,j+1/2} - \frac{\Delta x}{\Delta y}\left(u_{i+1/2,j+1} - u_{i+1/2,j} \right) \qquad (3A\text{-}3\text{-}1)$$

case II: $$u_{i+1/2,j+1} = u_{i+1/2,j} - \frac{\Delta y}{\Delta x}\left(v_{i+1,j+1/2} - v_{i,j+1/2} \right) \qquad (3A\text{-}3\text{-}2)$$

case III: $$v_{i-1,j+1/2} = v_{i,j+1/2} + \frac{\Delta x}{\Delta y}\left(u_{i-1/2,j+1} - u_{i-1/2,j} \right) \qquad (3A\text{-}3\text{-}3)$$

case IV: $$u_{i+1/2,j-1} = u_{i+1/2,j} + \frac{\Delta y}{\Delta x}\left(v_{i+1,j-1/2} - v_{i,j-1/2} \right) \qquad (3A\text{-}3\text{-}4)$$

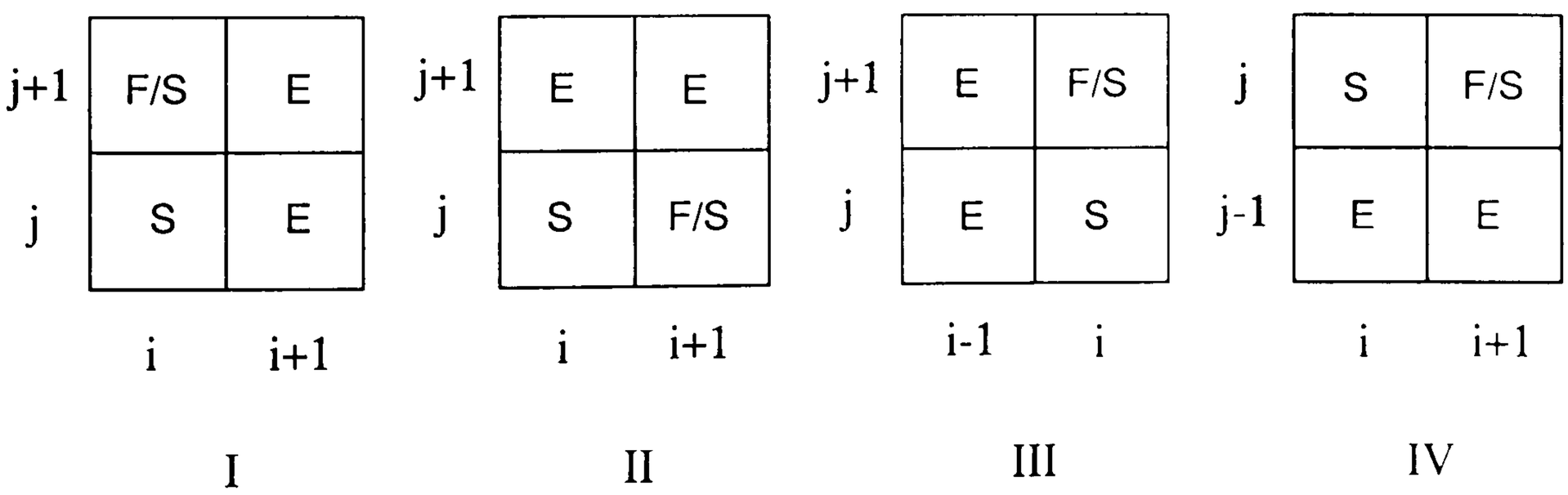

F = Full E = Empty S = Surface

Figure 3A-3 Four basic configurations of free surface cell.

Chapter 4

A study of the residual flow existing in pressure die casting processes

Chapter 4

A Study of the Residual Flow Existing in Pressure Die Casting Processes

Abstract

This chapter deals with the analysis of residual flow in the final fifth stage of a pressure die casting process. On the basis of hypotheses, the governing equation of residual flow is generated. The mathematical models of residual flow such as the maximum velocity and the decaying function for turbulent residual flow and laminar residual flow, the damping constant and decay time of the residual flow are derived. Section 5.3.4 introduces the experimental results and proves their agreement with theoretical equations, and the decay time coefficient of residual flow, c_r, is also obtained from water analogue experiments. For a solidification process of molten metal, two basic physical patterns of residual flow are illustrated and the mathematical equations are also derived against two different cooling conditions.

4.1 Inctroduction

The phenomenon of residual flow in pressure die casting processes exists over a short period during post-fill of the process until the molten metal is solidified completely. As investigated, at the third filling stage, the molten metal flows with a filling velocity of about 40-100 ms^{-1} filled the die cavity completely within 20-200 *ms* (Pokorny, 1977). Following the completion of the third stage, the filling pressure builds up rapidly (say above 1-5 *ms*) to the final pressure set up due to the liquid compressibility (Zeleniak, 1993; Kawaguchi and Tanaka, 1977; Robinson, 1977; and Segawa, 1977). Although the incoming flow is stopped, the momentum of molten metal flow at the last instance of the third

filling stage continues the molten metal flow within the cavity over a short period. This is the so-called residual flow. This residual flow is an unsteady flow that has its own characteristics, especially in that it links the filling and solidification processes. There are limited experimental data on residual flow in pressure die casting processes in the literature. Research performed by numerical simulations by Desai and Pagalthivarthi (1987) and Minaie (1989) may be taken for reference. There is thus a need to make further theoretical investigations of the residual flow phenomenon.

4.2 The Governing Equation of Residual Flow

4.2.1 Hypotheses

Based on the observation of the residual flow phenomenon as described above, the following hypotheses are made:

(1) the pressure of the molten metal in the cavity is maintained at a constant during the decay time of residual flow. This is because the molten metal pressure in the cavity has been built up already to the final pressure set up by the fluid power system of the pressure die casting machine. No pressure gradient exists (i.e., $\frac{\partial p}{\partial x} = 0$; $\frac{\partial p}{\partial y} = 0$; $\frac{\partial p}{\partial z} = 0$) within the cavity during the decay time of residual flow.

(2) because there is no energy source to drive the residual flow of the molten metal inside the cavity continuously, the Newtonian inertial force is balanced only by the shear stresses of liquid elements due to viscosity;

(3) in general practice, for a rectangular enclosure the thickness of the cavity is always much smaller than its length and width. Therefore, the residual flow in the cavity will be treated as 2-D motion between two parallel plates. The component of residual flow in the z-direction is ignored.

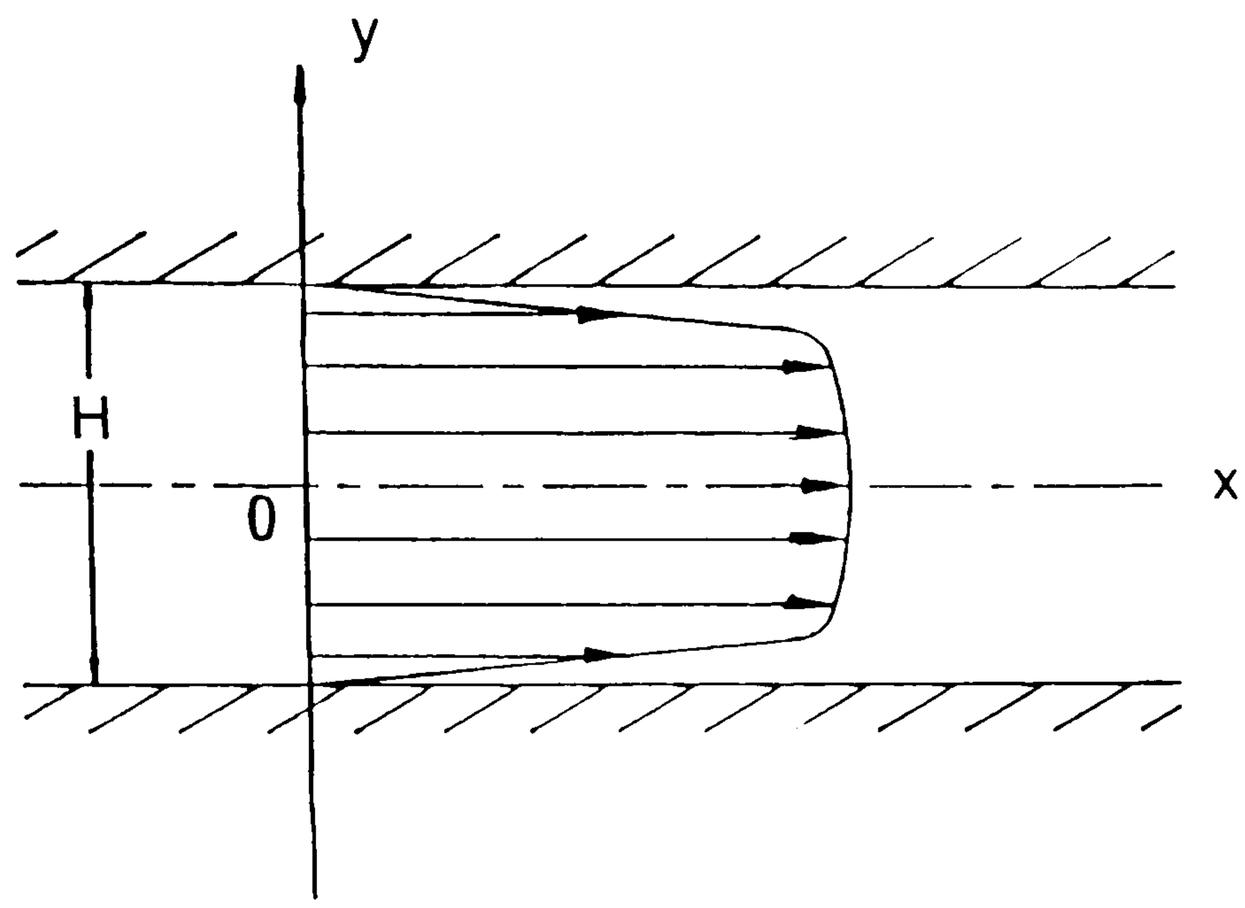

Figure 4-1 Velocity profile of turbulent residual flow.

4.2.2 The Governing Equations

Under the hypotheses above, the differential equation of the residual flow can be written on the basis that the Newtonian inertial force is balanced by the shear stresses of liquid elements:

$$\frac{dv_r}{dt} = \frac{1}{\varrho}\frac{d\tau}{dy} \tag{4-1}$$

Equation (4-1) is the differential equation of the residual flow in the cavity. It can be rewritten according to Newton's law of viscosity as:

$$\frac{dv_r}{dt} = \upsilon\frac{d^2v_r}{dy^2} \tag{4-2}$$

where the y direction is normal to the flow direction as shown in Figure 4-1.

4.3 Turbulent Residual Flow

4.3.1 Velocity Profile

At the completion of the filling stage of the pressure die casting process, residual flow follows immediately. Initially it is fully turbulent and the experimental one-seventh power law can be applied as the velocity profile between two parallel plates (Tennekes and Lumley, 1972; White, 1986). Due to the symmetric velocity profile, the study of residual flow is identified in a half upper part as shown below:

$$v_r = v_{r\max}(1-\frac{2y}{H})^{1/7} \tag{4-3}$$

where y=0, $v_r=v_{r\max}$ and y=H/2, v_r=0, which illustrates the boundary conditions at the centre line and upper wall respectively as shown in Figure 4-1. By substituting equation (4-3) into equation (4-2), a second differential equation can be obtained:

$$\upsilon\frac{d^2v_r}{dy^2} = v_{r\max}\frac{24\upsilon}{49H^2}(1-\frac{2y}{H})^{-\frac{13}{7}} \tag{4-4}$$

Equation (4-4) provides a general solution to find out the velocity of residual flow at each point. At the centre line, y=0, equation (4-4) can be simplified:

$$\upsilon \frac{d^2 v_r}{dy^2}\bigg|_{y=0} = v_{r\max} \frac{24\upsilon}{49H^2} \tag{4-5}$$

Equation (4-5) shows the shear stress of the liquid at the centre line which corresponds to the maximum residual velocity. While the $v_{r\max}$ is decaying to zero, the residual flow is disappearing. In fact, this is also the completion of the whole pressure die casting process in terms of the solidification of the molten metal. Thus, the history of the maximum velocity of residual flow at the centre is a typical representation of the whole decay process of the residual flow.

4.3.2 The Maximum Velocity of Turbulent Residual Flow, $v_{r\max}$

According to the nature of the orifice or jet flow, the actual maximum velocity of the residual flow is allocated in the contracted section of the jet flow and equal to:

$$(v_{r\max})_g = \frac{1}{c_c} v_f \tag{4-6}$$

where the coefficient of contraction, c_c, depends on the shape and size of the gate as well as the elevation of the free surface above the gate, and is usually from 0.61 to 0.63 for a turbulent flow (Davis and Sorensen, 1968). Thus, equation (4-6) is approximately equal to:

$$(v_{r\max})_g = 1.6 v_f \tag{4-7}$$

It should be noted that the $(v_{r\max})_g$ is the initial and maximum available velocity of the residual flow decaying with time, and the $v_{r\max}$ is the maximum velocity of the residual flow at any instant in time, thus there is a function linking the two, $(v_{r\max})_g$ and $v_{r\max}$, and this is explained in the following sections.

4.3.3 The Decaying Velocity

The equation of the decaying velocity can be obtained by substituting equations (4-5) into equation (4-2):

$$\frac{dv_{r\max}}{dt} = - v_{r\max} \frac{24\upsilon}{49H^2} \tag{4-8}$$

Integrating equation (4-8) gives equation

$$\int_{(v_{r\max})_g}^{v_{r\max}} \frac{dv_{r\max}}{v_{r\max}} = \int_0^t \frac{24\upsilon}{49H^2} dt \tag{4-9}$$

and $$v_{r\max} = (v_{r\max})_g \exp(-K_{ot}\, t) \tag{4-10}$$

where $$K_{ot} = \frac{24\upsilon}{49H^2} \tag{4-11}$$

Equation (4-10) indicates that the velocity of residual flow is an exponential function. The damping coefficient, K_{ot}, is proportional to the viscosity of molten metal and inversely proportional to the second power of the cavity thickness.

In order to expose clearly the decaying nature of the residual flow, Table 4-1 below shows the typical calculated values for the case of water analogue experiments in which the water temperature $T_w = 20^{\circ}C$, and the kinematic viscosity $\upsilon = 1.006\times10^{-6} m^2 s^{-1}$ according to equations (4-10) and (4-11).

Table 4-1 Examples of the decaying nature of the velocity during residual flow.

		t (second)				
		0.0	0.5	1.0	2.0	3.0
H (mm)	K_{ot}	$v_{r\max}/(v_{r\max})_g$ %				
1	0.4927	100	78	61	37	23
2	0.1232	100	94	88	78	69
5	0.0197	100	99	98	96	94
10	0.0049	100	99	99	99	98

Table 4-1 shows: one second after residual flow was initiated, the velocity of the residual flow for a cavity thickness *H=1mm* decays to $61\%(v_{r\max})_g$, whilst for the case of *H=10mm* it only decays slowly to $99\%(v_{r\max})_g$.

Further to the above calculations, Table 4-2 shows the maximum velocity, $v_{r\max}$, of residual flow for different cavity thickness, H, after one second of residual flow was initiated and assuming $(v_{r\max})_g = 20ms^{-1}$.

Table 4-2 Examples of the decaying nature for different cavity thickness after one second of residual flow initiated and assuming $(v_{r\max})_g=20ms^{-1}$.

H mm	1	2	5	10
$v_{r\max}/(v_{r\max})_g$ %	61	88	98	99
$v_{r\max}$ ms^{-1}	12.2	17.6	19.6	19.8

Obviously, the cavity thickness, H, is the dominating factor in influencing the decay function of the residual flow.

Yamamoto *et al.* (1988 and 1989) used molten aluminium alloy to study flow behaviour with filling velocities of 15 to 20 ms^{-1} at the gate of a die cavity for two thin walled pressure die castings. They reported that the molten metal velocity decreases abruptly within a passage of 20 to 25 *cm* and reaches 2 to 3 ms^{-1} at the final filling portion, **irrespective of the cavity shape** which is in agreement with the basic hypotheses mentioned at the section 4.2.1.

4.4 Laminar Residual Flow

As a classical topic, the turbulent flow decays from high velocity to low velocity characterized from high Reynolds number to lower Reynolds number. As the Reynolds number approaches the lower critical value (2000 for a circular

section, 1100 for a rectangular section) the turbulent flow changes to laminar flow (Shames, 1992).

4.4.1 Velocity Profile

When the turbulent residual flow changes to laminar flow, the one-seventh power law profile of velocity is no longer valid and needs to be replaced by a parabolic law. Using a similar approach to that given in section 4.3., the laminar residual flow can be expressed as:

$$v_r = v_{r\max}\ (1-\frac{4y^2}{H^2}) \tag{4-12}$$

4.4.2 The Maximum Velocity of Laminar Residual Flow $v_{r\max}$

Equation (4-12) can be integrated to calculate the flow rate of unit width in order to obtain the maximum velocity of laminar residual flow:

$$Hv_c = 2\int_0^{H/2} v_{r\max}(1-\frac{4}{H^2}y^2)dy \tag{4-13}$$

For laminar residual flow, the decay velocity can be expressed as:

$$v_{r\max} = \frac{3}{2}v_c\ \exp(-K_{ol}t) \tag{4-14}$$

where $$K_{ol} = 8\frac{\upsilon}{H^2} \tag{4-15}$$

Equations (4-11) and (4-15) indicate that both damping constants K_{ot} and K_{ol} have similar natures. The conclusion is clear that the thinner cavity thickness, H, is still a dominating factor in influencing the decay process of the residual flow. The ratio of the damping constants of laminar to turbulent residual flow can be obtained from equations (4-10) and (4-15):

$$\frac{K_{0l}}{K_{0t}} \cong 16 \tag{4-16}$$

Equation (4-16) indicates quantitatively that the damping coefficient of

the laminar residual flow is sixteen times the damping coefficient of the turbulent residual flow. That means that the laminar residual flow decay is faster than the turbulent residual flow decay with time.

4.5 The Decay Time of the Residual Flow

4.5.1 Water Analogue Experiments

In a water analogue experiment, the thickness, H, is a constant, and the water temperature can be controlled to be an approximately fixed value in order to maintain the condition of constant viscosity.

(1) The decay time of turbulent residual flow

Integrating equation (4--9), using the constants in equation (4-14) gives:

$$\int_{(v_{r\max})_g}^{\frac{3v_c}{2}} \frac{dv_{r\max}}{v_{r\max}} = \int_0^{t_{dt}} \frac{24\upsilon}{49H^2} dt \tag{4-17}$$

and this in turn, when integrated, gives the decay time of turbulent residual flow:

$$t_{dt} = \frac{1}{K_{ot}} \left| \ln \frac{3v_c}{2(v_{r\max})_g} \right| \tag{4-18}$$

(2) The decay time of laminar residual flow

Following a similar approach to that given above, the decay time of laminar residual flow t_{dl} is obtained:

$$\int_{\frac{3}{2}v_c}^{0} \frac{dv_{r\max}}{v_{r\max}} = \int_0^{t_{dl}} \frac{8\upsilon}{H^2} dt \tag{4-19}$$

$$t_{dl} = \frac{H^2}{8\upsilon} \left| \ln \frac{2v_{r\max} \to 0}{3v_c} \right| \tag{4-20}$$

It is noted that, $v_{r\max}$ can never be zero for a damping exponential function, and thus the decay time of laminar flow t_{dl} will be infinite theoretically.

(3) The decay time for water analogue experiments t_d

As shown in equation (4-18) and (4-20), the total decay time of residual flow for water analogue experiments is equal to t_d where

$$t_d = t_{dt} + t_{dl} \tag{4-21}$$

Thus
$$t_d = \frac{49H^2}{24\upsilon}\left|\ln\frac{3v_c}{2(v_{r\max})_g}\right| + \frac{H^2}{8\upsilon}\left|\ln\frac{2v_{r\max}\to 0}{3v_c}\right| \tag{4-22}$$

Equation (4-24) may be further simplified. By assuming the decay period of the residual flow is complete when $\frac{v_c}{v_f}$ = (1-5)%, then the decay time of residual flow can be treated from an experimental study and be shown in equation (4-23) as:

$$t_d = c_r \frac{H^2}{\upsilon} \tag{4-23}$$

where the decay time coefficient of residual flow, c_r, is a function of the geometry of the cavity and gate. Equation (4-23) indicates clearly that $t_d \propto H^2$ for the cases of using the same molten metal. An experimental study and experimental results are given in Chapter 5. The results shown in Table 5-4 and its graph (Figure 5-17) are in good agreement with equation (4-23) that $t_d \propto H^2$ and $t_d \propto \frac{1}{\upsilon}$. The decay time coefficient of residual flow, c_r, is approximately a constant. For the test example, an average value for c_r is 0.088.

Very often the residual flow co-exists with thermals during the period of post-fill of the cavity. An experimental study of the residual flow and thermals is presented in the Chapter 5. These flow patterns simulated by the water analogue experiments may be further treated to calculate the temperature distribution and the position of the mushy zone in predicting the formation of casting defects such as voids, porosity and cold shuts etc.

4.5.2 Solidification Time of a Pressure Die Casting Process

There are three basic physical models that can be established for depicting residual flow as shown in Figure 4-2 and 4-3. From which two basic residual flow patterns are presented.

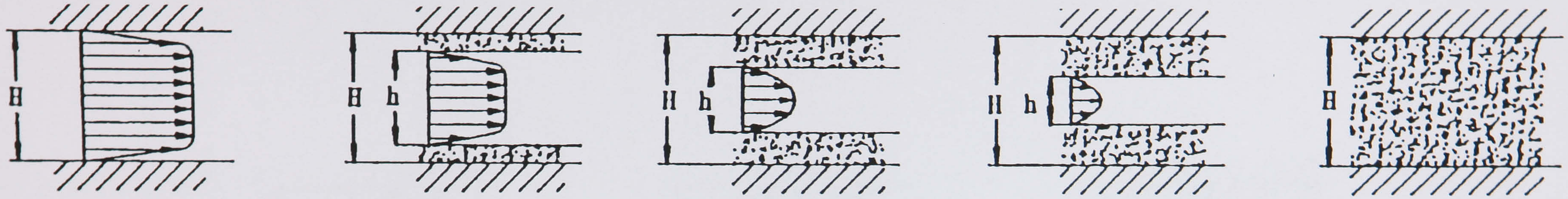

(a) R_e>>2300 (b) R_e>2300 (c) R_e=2300 (d) R_e<2300 (d) R_e=0

(a) Turbulent flow status, non-solidified

(b) Turbulent flow status, a layer of solidified metal developed at the cavity wall

(c) Laminar flow status, increasing thickness of solidified layer

(d) Laminar flow status, solidified layer further developed

(e) Fully solidified, $v_r = 0$.

Figure 4-2 A typical velocity profile of a decay process of residual flow.

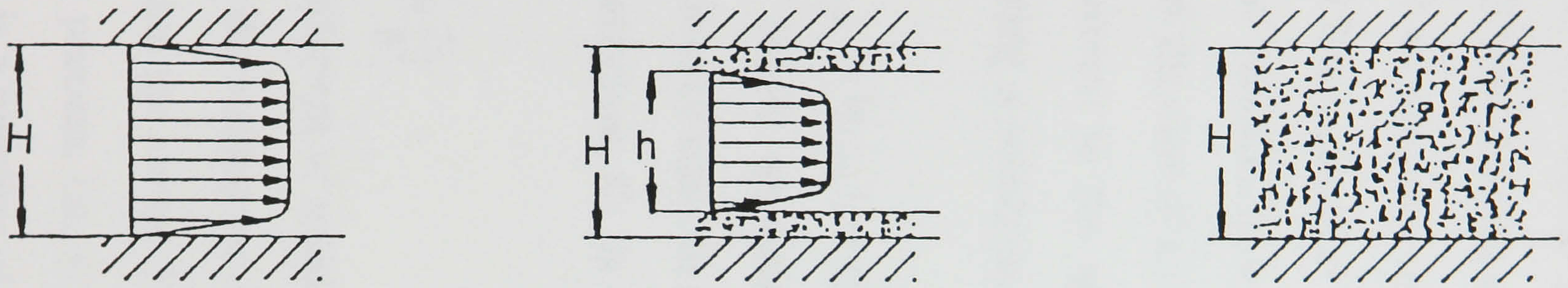

(a) R_e>>2300 (b) R_e>2300 (c) R_e=0

(a) Turbulent flow status, non-solidified.

(b) Turbulent flow status, a layer of solidified metal developed at the cavity wall.

(c) Fully solidified, $v_r = 0$.

Figure 4-3 A typical velocity profile of a decay process of residual flow without laminar flow.

(1) Figure 4-2 shows a complete process of residual flow that consists of turbulent and laminar flow. This represents castings with a relatively thick wall, a slower cooling rate, and thus a slower development of the solidified layer and zone. These kinds of residual flow may exist in sand casting.

(2) Figure 4-3 depicts the residual flow as turbulent dominating flow during the solidifying process of molten metal. This illustrates a relatively thin wall casting with an adequate cooling condition and a faster solidification rate.

The third basic physical model is a decay process similar to Figure 4-2, with full laminar residual flow during the solidification of molten metal. This mainly represents the case of a sand casting process.

With reference to the approach in section 4.3.3, the decay velocity of residual flow during a solidifying process of the molten metal can be determined as:

$$v_{r\max} = (v_{r\max})_g \exp(-Kt) \tag{4-24}$$

Equation (4-24) represents the decay velocity $v_{r\max}$ that is still an exponential function of time. In comparing this with equations (4-11) and (4-15), the damping coefficient, K, is not a constant and can be expressed as equation (4-25) below:

$$K = \frac{c_s}{h^2} \tag{4-25}$$

where c_s, the coefficient of solidification that is related to the physical properties and flow state of the molten metal, and h is the average casting thickness of the molten metal within the cavity. Both are nonlinear functions of the temperature T in the solidifying process, i.e., $c_s = f(T)$ and $h = f(T)$, whereas the temperature of the molten metal is a function of time, i.e., $T = f(t)$, c_s (or υ) $= f(t)$ and $h = f(t)$, that concerns mainly the cooling conditions and control, and the physical characteristics of the molten metal. This information can be found in the literature.

The differential equation of residual flow of molten metal in the solidifying process is then written as:

$$\frac{dv_{r\max}}{v_{r\max}} = \left(\frac{\upsilon t}{h^3}\frac{\partial h}{\partial T}\frac{\partial T}{\partial t} - \frac{t}{h^2}\frac{\partial \upsilon}{\partial T}\frac{\partial T}{\partial t} - \frac{\upsilon}{h^2}\right)dt \qquad (4\text{-}26)$$

4.5.3 Chvorinov's Rule

It is difficult to solve equations (4-24) or (4-26) due to uncertainties in the boundary conditions that mainly depend on the die cooling, and the properties of the metal. Flemings (1974) introduced the well-known Chvorinov's rule to estimate the time for solidification of simple-shaped castings as expressed in equation (4-27).

$$t_s = c_s \left(\frac{\overline{V}}{A}\right)^2 \qquad (4\text{-}27)$$

It is interesting that equation (4-27) is quite similar to equation (4-23). In the case of a thin wall die casting, $H \cong \frac{\overline{V}}{A}$, and the solidification time is equal to the decay time of residual flow during the solidification process of the molten metal, i.e., $t_s = t_d$.

Equation (4-27) can be further simplified for a 2-D flow for a relatively plate-type casting as:

$$t_s = c_s H^2 \qquad (4\text{-}28)$$

Many empirical formulae have a similar mathematical formation to equation (4-28). Two examples (Lin, 1983) are recommended below:

For aluminium $t_s = (0.017 \sim 0.034) H^2$ (4-29a)

For zinc $t_s = (0.025 \sim 0.032) H^2$ (4-29b)

The time for solidification of molten metal is proportional to H^2, where H representing the cavity thickness of the die. For those formulae in section 4.4 to be used to determine the solidification time, the coefficient of the solidification time c_s is different for each individual metal or alloy.

Nevertheless, the decay time of the residual flow in the water analogue experiment or the solidification time in a real solidifying process of molten metal is mostly proportional to the square of the mean cavity thickness, i.e., $t_d \propto H^2$ or $t_s \propto H^2$ as shown in equations (4-23) and (4-28)-(4-29b).

The solidification time of the molten metal is mainly dependent on the cooling conditions of the die and the properties of the metal.

4.6 Conclusions

This chapter studied the residual flow pattern of pressure die casting processes. Based on the hypotheses made, a differential equation of the residual flow is derived. The one-seventh power and parabolic laws are applied to the derivation of the velocity profiles for turbulent and laminar residual flow respectively. The maximum velocity of the residual flow is termed according to the nature of the orifice or jet flow. The velocity equation of the residual flow indicates that the decay of the residual flow is an exponential function. The decay time of the residual flow is proportional to the square of the cavity thickness.

The experimental results presented in the Section 5.3.4 prove the correctness of the derived equations concerning the residual flow in pressure die casting processes in this chapter, and also disclose the phenomena of thermals that co-exist with the residual flow.

Chapter 5

An experimental study of fluid dynamics in pressure die casting processes

Chapter 5

An Experimental Study of Fluid Dynamics in Pressure Die Casting Processes

Abstract

This chapter consists of two parts. The first part deals with the application of similitude laws in pressure die casting processes that direct the determination of model scales for the model-prototype relation and analysis of experimental results. The first part also provides a guide for experimental practice especially for the flow visualization by using a super video charge coupled device (CCD camera) in a study of flow patterns in pressure die casting processes. Detailed analyses and criteria on different relationships between model and prototype are given in order to correct previously offered formulae by Eckert (1989). This approach then determines the model scale factors for the model-prototype relation and the analysis of experimental results.

The second part presents the application of a CCD camera in the flow visualization for studing the diversity of fluid motion including the filling pattern, residual flow, thermals and air entrapment during cavity-fill and post cavity-fill in water analogue experiments of pressure die casting processes. The images are grabbed and stored on tape which can be studied in detail later. The CCD images are then compared with the typical computational results from Chapter 3 and give an immediate, qualitative sense of the filling patterns. The formulae characterizing the residual flows for the case of water analogue experiments are quoted from Chapter 4 for comparing the experimental results. Three kinds of thermals are classified, and a set of computer prints after image processing is introduced for a typical case study of the behaviours of air within the model cavity.

5.1 The Application of Similitude Laws to Experiments

The injection of molten metal in die casting is a complex process with high transient flow phenomena. A great deal of work has been done in an attempt to correlate the empirical knowledge of the die casting process with scientific principles. In recent years, research and development on pressure die casting processes have tried to adopt similitude laws that needed to deal with the problems of high transient flow for setting up physical models in order to improve die design, casting quality and thus reduce manufacturing costs. By carrying out such model experiments, the validity of mathematical simulation may be proved. The work of Eckert (1989) has pioneered the introduction of the use of similitude laws into the field of pressure die casting. A later paper written by Hu *et al.* (1992b) has also recommended this approach. Unfortunately, the formulae applied for similitude laws in the papers referred to above have been found by the present author to be incorrect in terms of dynamic similarity and result in unrealistic dimensional scales without a time scale. The present work deals with the development of similitude laws for pressure die casting processes, and comments are given on the papers cited above.

5.1.1 Similitude Laws

(1) Hypothesis

Figure 5-1 shows a typical filling process that is a highly transient flow for a whole process that can be classified as three stages of quasi-steady flow plus two stages of unsteady flow. There seems no doubt that the third filling stage is the most important, and plays a key role in completing the whole function of a pressure die casting process. Actually, the flow pattern of molten metal is approximately steady during the fill time and this can be treated as a quasi-steady flow process. The hypothesis of quasi-steady flow for the third stage of the

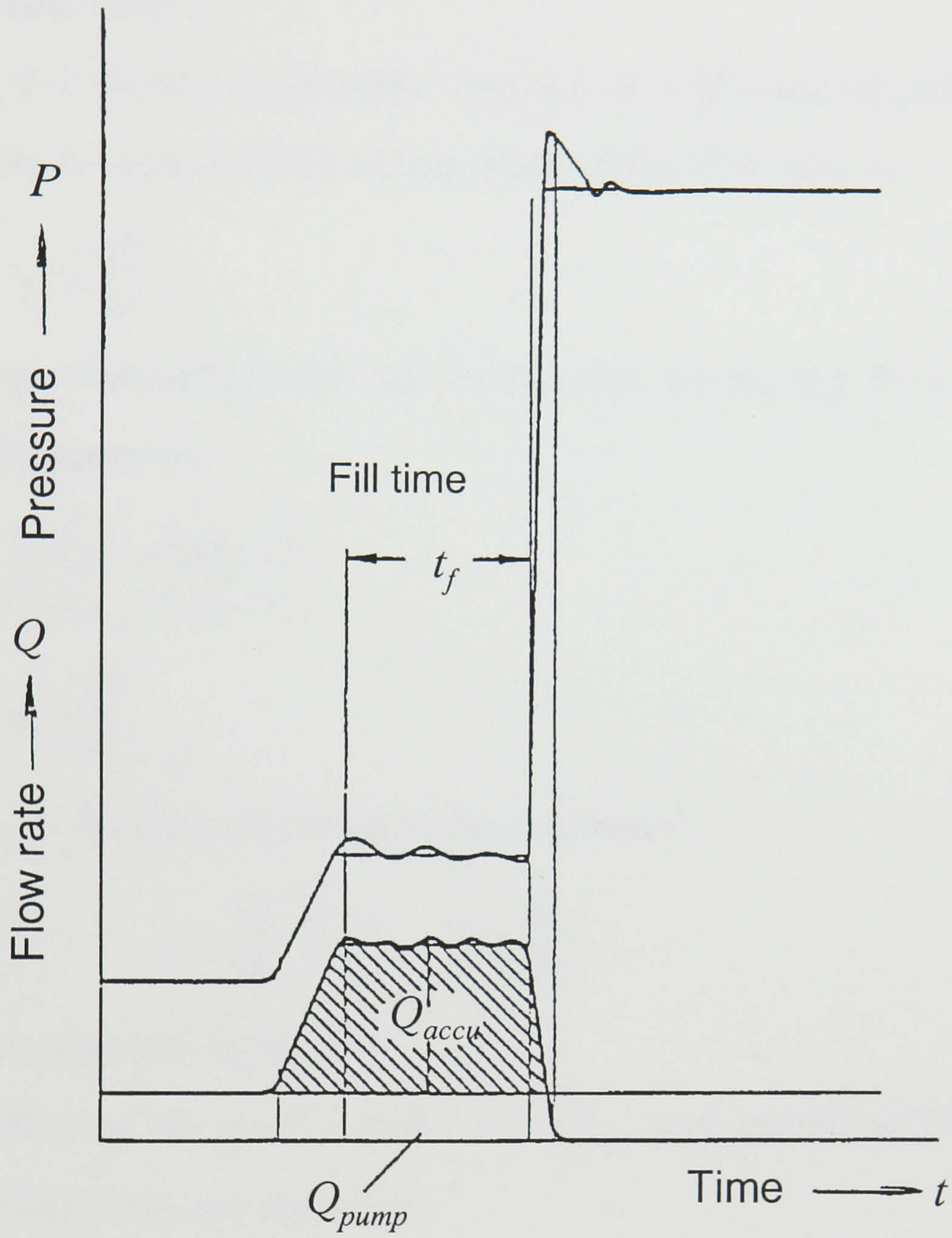

Figure 5-1 The typical history of molten metal pressure and flow rate of pressure die casting process.

process permits the use of similitude laws for simulating flow in the filling stage of pressure die casting processes.

(2) Geometric and Kinematic Similarity Criteria

(i) Fill time scale ratio S_t

Figure 5-2 shows a schematic diagram of a physical model in which the fill time, t_f, can be expressed by the equation of the flow rate, i.e.:

$$t_f = \frac{AH}{Q} \tag{5-1}$$

The following relationship can be written for simulating flow with similar geometric configurations:

$$\frac{(t_f)_m}{(t_f)_d} = \frac{A_m H_m}{A_d H_d}\frac{Q_d}{Q_m} \tag{5-2}$$

$$S_t = \frac{S_l^3}{S_q} \tag{5-3}$$

where S_t, S_q, S_l are defined respectively as follows:

$$S_t = \frac{(t_f)_m}{(t_f)_d}\ ; \qquad S_q = \frac{Q_m}{Q_d} \text{ and } \qquad S_l = \frac{L_m}{L_d}\ .$$

(ii) Scale ratio of cavity thickness

By substituting the gate velocity $v_f = Q/t_f$ into equations (5-2) and (5-3), the following equations are obtained:

$$\frac{H_m}{H_d} = \frac{(t_f)_m}{(t_f)_d}\frac{(v_f)_m}{(v_f)_d} \tag{5-4}$$

$$S_l = S_t\ S_v \tag{5-5}$$

where $S_v = \frac{(v_f)_m}{(v_f)_d}$ and $S_l = \frac{H_m}{H_d}$.

The cavity thickness is an important parameter, and the relationship of fill time, thickness and filling velocity scale ratio should satisfy equations (5-4) or (5-5). Equations from (5-2) to (5-5) express the most important relations between fill

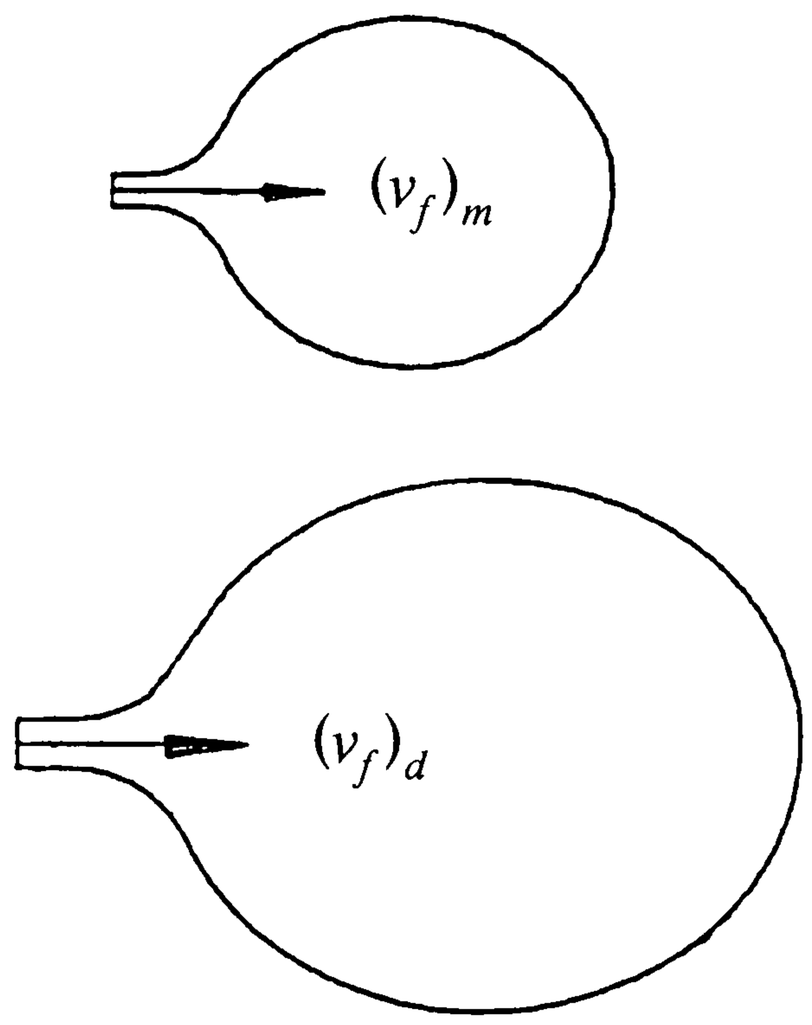

Figure 5-2 Schematic diagram for kinematic similarity flows.

$(v_f)_m$ Filling velocity at the gate of model

$(v_f)_d$ Filling velocity at the gate of die

time, thickness, gate velocity and flow rate between the model and actual die cavity. These formulae provide an engineering method to design an experimental model in the simulation of the die-filling process.

(iii) Proper procedures for design practice

The following procedures provide a practical guide in designing an experimental model. Whilst an experimental model for fundamental research may have a relatively simple geometric shape, the design principles will be the same.

(A) To determine the fill time of the model

The fill time is a basic parameter and should be always checked for an actual die and the model. For instance Pokorny (1977) has given data with a fill time varying from 0.020 to 0.200*s* as the volume through the gate varied 19.5-750 in^3 (320-12,290 cm^3). For the CCD camera employed in the modelling experiment performed by this study, the time interval for each image frame is 0.040 *s* and thus in order to obtain 5-8 frames to cover clearly the filling stage, the fill time of the model needs to be in the range of 0.200-0.320 *s*. Then other parameters should be adjusted to achieve this fill time.

With a fill time for a model $(t_f)_m$<0.20*s*, the number of frames of flow images recorded by the CCD camera will be less than five, and this cannot properly represent a filling process. If $(t_f)_m$>0.320*s* this may result in too small a gate velocity of the model such that the quasi-similitude condition may no longer apply to the model experiments.

Therefore, the determination of the model's fill time is a key factor in the use of similitude laws in the simulation of die casting processes.

(B) To obtain information on the actual process

When the geometric details and parameters of the die have been designed, it is best to obtain a history of the plunger speed from the machine by a dry shot test. A typical example of speed-time history on an injection cycle has been

shown in Figure 5-1. The flow rate, gate velocity and fill time of the actual process may be determined from the recorder chart.

(C) To select an adequate actuator

By reference to the available prototype information, an adequate actuator with known piston speed and stroke for the model test rig may be selected. In the general case, the model flow rate is smaller than that of the casting die (say 0.25-0.75). The dimensions of a suitable model are determined by the similitude laws given in equations (5-2) to (5-5). Typical examples are shown in Table 5-1 for fill time scales, S_t, of 10 and 1.

Table 5-1 Typical examples of the model-prototype scale.

Fill time (t_f)	Flow rate scale $S_q = Q_m / Q_d$	Dimension scale $S_l = L_m / L_d$	Velocity scale $S_v = v_m / v_d$
if $(t_f)_d = 0.02$s $(t_f)_m = 0.20$ s $S_t = 10$	1.00	2.15	0.215
	0.75	1.96	0.196
	0.50	1.71	0.171
	0.25	1.36	0.136
if $(t_f)_d = 0.20$ s $(t_f)_m = 0.20$ s $S_t = 1$	1.00	1.00	1.000
	0.75	0.91	0.910
	0.50	0.79	0.790
	0.25	0.63	0.630

As is seen in the Table 5-1 altering the flow rate scale, S_q, from 0.25 to 0.75, gives an alteration in the dimension scale, S_l, from 0.63 to 1.96 which indicates that the model can be bigger (S_l>1) or smaller (S_l<1) than the actual die.

5.1.2 Dynamic Similitude Problems

The basic dynamic equations expressing Newton's second law for fluid flow with constant density are described by the Navier-Stokes equations (Shames, 1992) for a liquid element as below:

$$\left.\begin{aligned}
\frac{\partial u}{\partial t}+u\frac{\partial u}{\partial x}+v\frac{\partial u}{\partial y}+w\frac{\partial u}{\partial z} &= \mathrm{X}-\frac{\partial p}{\partial x}+\upsilon\left(\frac{\partial^2 u}{\partial x^2}+\frac{\partial^2 u}{\partial y^2}+\frac{\partial^2 u}{\partial z^2}\right) \\
\frac{\partial v}{\partial t}+u\frac{\partial v}{\partial x}+v\frac{\partial v}{\partial y}+w\frac{\partial v}{\partial z} &= \mathrm{Y}-\frac{\partial p}{\partial y}+\upsilon\left(\frac{\partial^2 v}{\partial x^2}+\frac{\partial^2 v}{\partial y^2}+\frac{\partial^2 v}{\partial z^2}\right) \\
\frac{\partial w}{\partial t}+u\frac{\partial w}{\partial x}+v\frac{\partial w}{\partial y}+w\frac{\partial w}{\partial z} &= \mathrm{Z}-\frac{\partial p}{\partial z}+\upsilon\left(\frac{\partial^2 w}{\partial x^2}+\frac{\partial^2 w}{\partial y^2}+\frac{\partial^2 w}{\partial z^2}\right)
\end{aligned}\right\} \qquad (5\text{-}6)$$

According to the hypothesis of quasi-steady flow during cavity-fill, we have:

$$\frac{\partial u}{\partial t}=\frac{\partial v}{\partial t}=\frac{\partial w}{\partial t}=0 \qquad (5\text{-}7)$$

Assuming no rotation in the flow as the molten metal is injected:

$$\mathrm{X}=0,\quad \mathrm{Y}=-g,\quad \mathrm{Z}=0 \qquad (5\text{-}8)$$

The following dimensionless variables are introduced:

$$E_u=\frac{p}{\varrho V^2} \qquad u^*=\frac{u}{V},\quad v^*=\frac{v}{V},\quad w^*=\frac{w}{V} \qquad (5\text{-}9)$$

$$x^*=\frac{x}{L},\quad y^*=\frac{y}{L},\quad z^*=\frac{z}{L} \qquad (5\text{-}10)$$

Substituting equations (5-7), (5-8), (5-9) and (5-10) into Navier-Stokes equations (5-6), the full set of Navier-Stokes equations in the form of dimensionless variables may be obtained:

$$\left.\begin{aligned}
\frac{du^*}{dt} &= -\frac{\partial E_u}{\partial x^*}+\frac{1}{R_e}\nabla^2 u^* \\
\frac{dv^*}{dt} &= -\frac{\partial E_u}{\partial y^*}+\frac{1}{R_e}\nabla^2 v^*-\frac{1}{F_r} \\
\frac{dw^*}{dt} &= -\frac{\partial E_u}{\partial z^*}+\frac{1}{R_e}\nabla^2 w^*
\end{aligned}\right\} \qquad (5\text{-}11)$$

where E_u, R_e and F_r are three basic dimensionless numbers shown in Table 5-2.

The above full set of the Navier-Stokes equations (5-11) in the form of dimensionless variables govern the workings of a model, especially when the water analogue technique is employed.

Table 5- 2 The formulae, definition and significance of dimensionless numbers.

Dimensionless numbers	Formula	Definition	Significance
Reynolds Number	$R_e = \frac{vL}{\upsilon}$	$\frac{Inertial-force}{Frictional-force}$	Viscosity dominant
Froude Number	$F_r = \frac{v}{\sqrt{Lg}}$	$\frac{Inertial-force}{Gravitational-force}$	Gravity dominant
Euler Number	$E_u = \frac{p}{\varrho v^2}$	$\frac{pressure-force}{Inertial-force}$	Pressure dominant

One may establish force polygons at each point of the flow. By the rules of dynamic similarity of the model and prototype, two force polygons at two corresponding points of two similar streams should be similar and fulfill equation (5-11). This is always difficult to achieve. Therefore, the argument is always focused onto what force is dominant in the prototype which is now addressed. Put another way, it is necessary to examine what kind of force is dominant in the prototype in order to choose a proper dimensionless number.

Eckert (1989) proposed a simulation criterion for application to the die casting process. Hu *et al.* (1992c) again recommended this criterion and provided the technical data for determining model scales. The dimensions of the model and/or the die calculated from Eckert's criteria will be either unrealistically large or small. Typical calculations are shown in Table 5-3.

Table 5-3 Dimensions of the model and/or die calculated from Eckert's criteria.

	Aluminium	**Zinc**
dimension scale $S_l = L_m / L_d$	S_l = 18 (Hu *et al.*, 1992c)	S_l = 12 (Hu *et al.*, 1992c)
Case **1**: dimensions of model dimensions of die (based on Eckert's criterion)	170×115×10 *mm* (Hu *et al.*, 1992c) 9.44×6.39×0.56 *mm* (reduced 18 times, it is unrealistically small)	170×115×10 *mm* (Hu *et al.*, 1992c) 14.17×9.58×0.83 *mm* (reduced 12 times, it is unrealistically small)
Case **2**: dimensions of die dimensions of model (based on Eckert's criterion)	170×115×10 *mm* 3060×2070×180 *mm* (enlarged 18 times,it is unrealistically large)	170×115×10 *mm* 2040×1380×120 *mm* (enlarged 12 times,it is unrealistically large)

Table 5-3 shows the unacceptable nature of the criteria proposed by Eckert (1989) of dynamic similarity for studying pressure die casting processes. In order to examine Eckert's error, his derivation is quoted below:

" ---------- We divide both sides of the equation by the square of the respective Reynolds number *to eliminate the velocity* and obtain

$$\frac{\varrho_m \nu_m^2}{\sigma_m} \frac{1}{L_m} = \frac{\varrho_d \nu_d^2}{\sigma_d} \frac{1}{L_d} \quad "$$

The Navier-Stokes equations (5-6), (5-11) and Table 5-2 illustrate that the flow velocity is always representing the Newtonian inertial force in similitude theory. Unfortunately, Eckert disregarded this point and attempted "to eliminate velocity". In so doing the Newtonian inertial force is eliminated and this is a fundamental force in the filling stage of pressure die casting processes. Of course, this approach (using equation (13) quoted from his paper) only involved grouping some physical parameters (ϱ, υ and σ) of the liquid, which resulted an unrealistic dimensional scale for the model-prototype relation and do not include the time scale. The time scale is an important scale related to fill time that has been covered in equations (5-1) to (5-5) and should be applied to design practice of the experimental work.

5.1.3 Quasi-Similitude

The Reynolds number, R_e, plays a decisive role in the determination of the flow status especially for a closed fluid system, and R_e should not be disregarded in selecting models. However, as R_e increases and becomes greater than a critical value, the influence of R_e on the flow can be ignored and this is the state which is defined as quasi-similitude in fluid dynamics. Under the conditions of quasi-similitude, equation (5-11) can be simplified to:

$$\left.\begin{aligned} \frac{du^*}{dt} &= -\frac{\partial E_u}{\partial x^*} \\ \frac{dv^*}{dt} &= -\frac{\partial E_u}{\partial y^*} - \frac{1}{F_r} \\ \frac{dw^*}{dt} &= -\frac{\partial E_u}{\partial z^*} \end{aligned}\right\} \qquad (5\text{-}12)$$

The viscosity of molten metal is very small. For instance, the kinematic viscosity of aluminium is equal to 0.542 of that of water and that of zinc's is equal to 0.417 of that of water. On the basis of experimental data, the injection flow of molten metal is always fully turbulent. With reference to an orifice in a conduit similar to

a gate in a cavity, when the Reynolds number is greater than (10,000 - 20,000) depending upon the ratio of orifice area to the area of conduit, the velocity profile, velocity coefficient and discharge coefficient are stable and independent of Reynolds number (Davis and Sorensen, 1968). The influence of viscosity may then be ignored in the modeling experiments. The quasi-similitude criterion provides a very convenient testing condition which eliminates the influence of liquid viscosity. Nevertheless, in order to ensure the flow states are quasi-similitude in character, it is necessary to check the Reynolds number experimentally.

Figure 5-3 shows the dimension scale ranging from 0.4 to 3.0 depending on different fill time scales (from 0.5 to 30.0) and flow rate scales (from 0.1 to 1.0). These curves indicate that adequate and realistic experimental models may be enlarged or reduced in size from those in actual dies. Figure 5-4 shows that when the flow rate scale, S_q, is constant, the relation between velocity scale, S_v, and fill time scale, S_t, represents a hyperbolic function and varies over a narrow range.

The computational analysis presented in Chapter 3 shows that the overall filling pattern is unrelated to viscosity, it is also unrelated to gravity and velocity when the filling velocity $v_f > 5.00 ms^{-1}$ that is actually under the condition of the quasi-similitude criterion. Logically, these computational results have proved the truthfulness of the similitude criterion derived in the preceding sections.

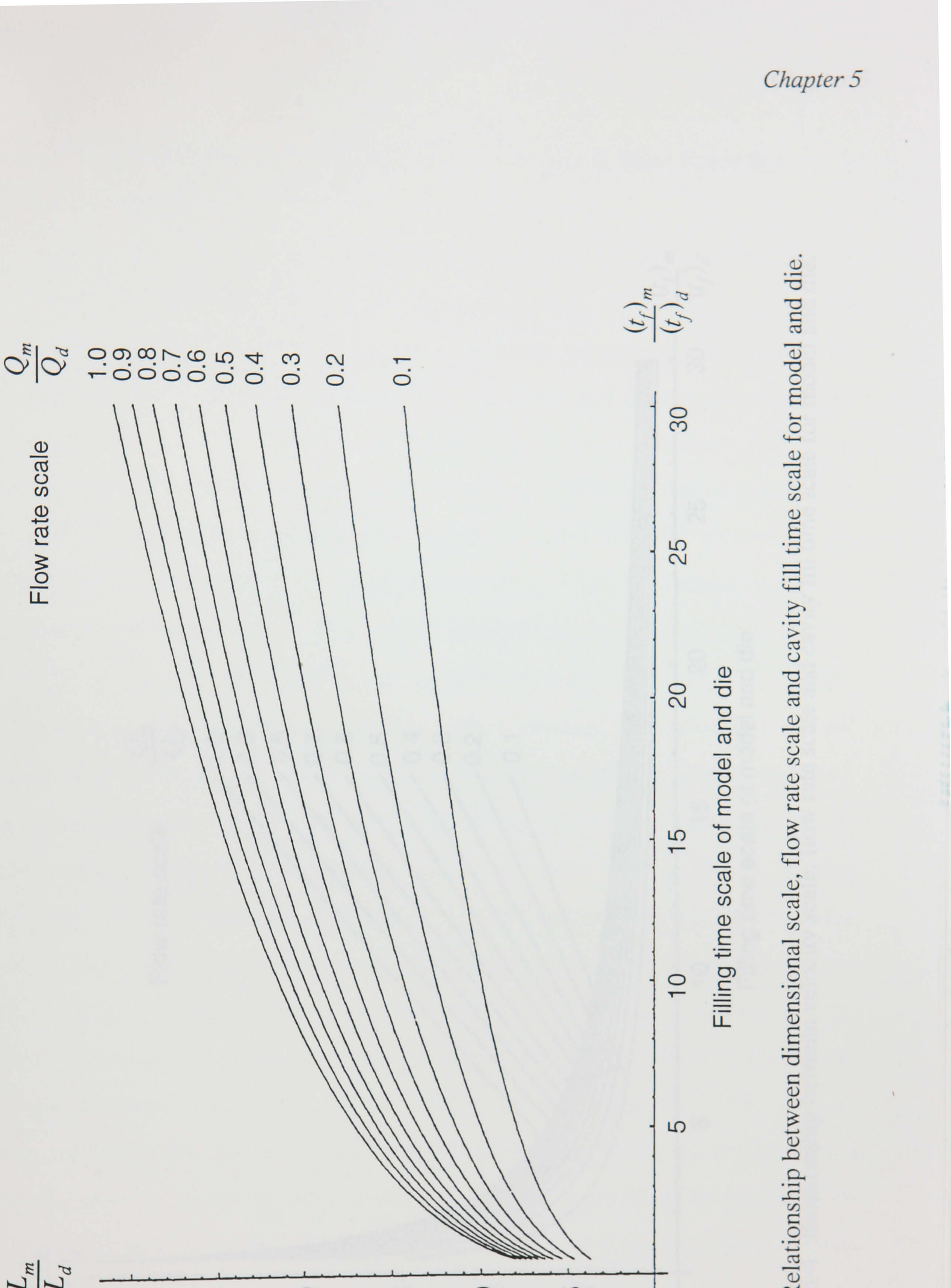

Figure 5-3 Relationship between dimensional scale, flow rate scale and cavity fill time scale for model and die.

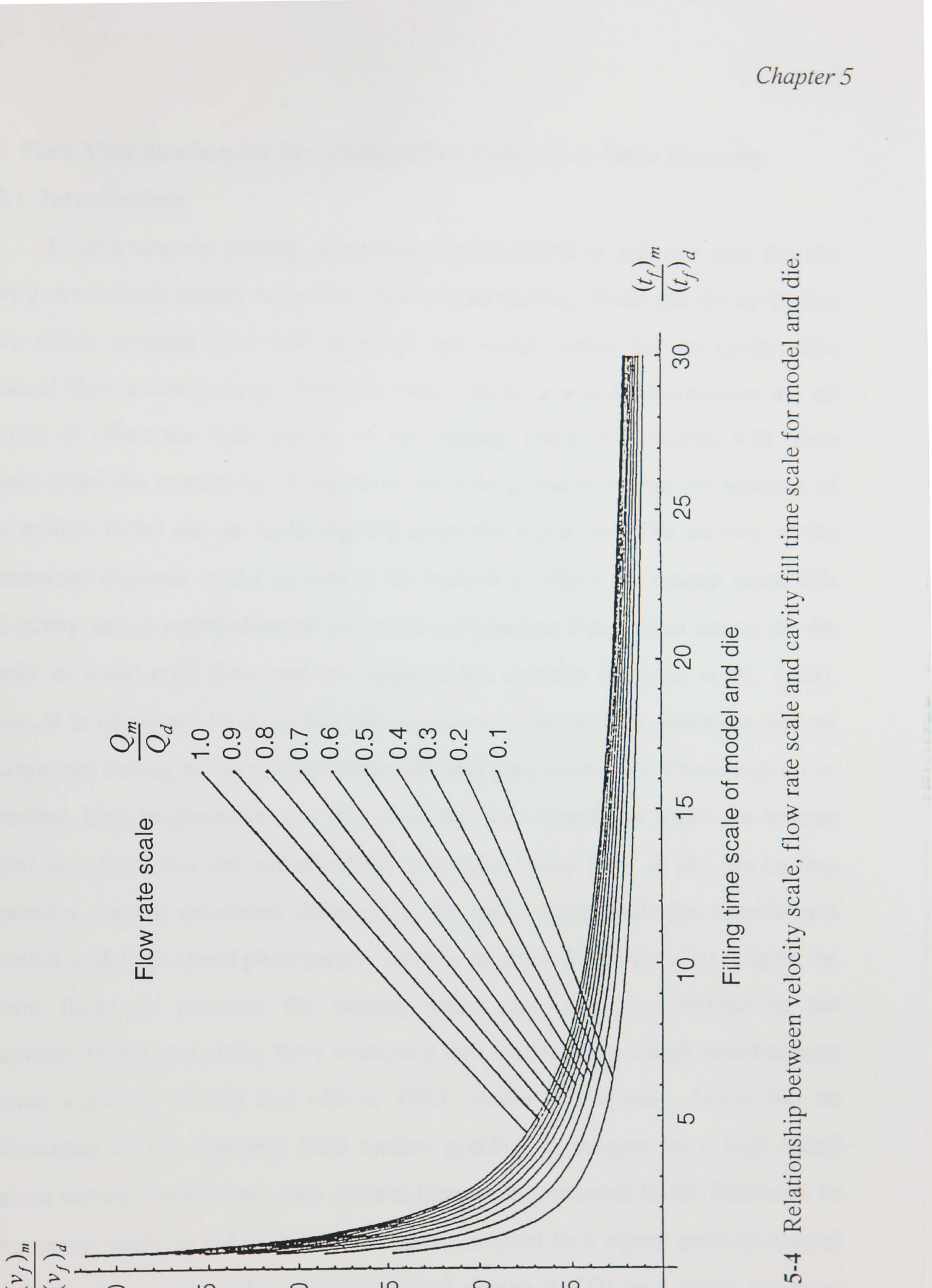

Figure 5-4 Relationship between velocity scale, flow rate scale and cavity fill time scale for model and die.

5.2 Flow Visualization for Simulating Flow Patterns & Flow Diversity

5.2.1 Introduction

In pressure die casting processes, molten metal is injected into the die cavity at relatively higher velocities than in sand casting. When the die cavity has been filled, residual flow with thermals still exists within the die cavity. The residual flow accompanying thermals, liquid droplets and air entrapment are all known to affect the final quality of the casting. Defective castings will often result under the conditions of turbulent die filling and/or premature freezing of the molten metal due to rapid chilling from the metal die. The success of the technology depends on the control of the manner in which the molten metal fills the cavity and in establishing an adequate temperature distribution across the die cavity to avoid cold shuts and hot spots in the castings (Nguyen *et al.*, 1988). Thus, it is necessary to study the filling pattern, residual flow, thermals and air entrapment during the period of cavity-fill and post cavity-fill. These extremely transient, high temperature and fast processes are carried out within an opaque metal die, therefore, the visualization of molten metal flow in the die casting processes present enormous difficulties. To date, water analogue experiments coupled with high speed photography have been applied widely to investigate the filling flows in pressure die casting which are well documented in the literature. In the past years, there were only still frames from a high speed motion picture available (Booth and Allsop, 1983; Stoehr and Hwang, 1983), but no information of the diversity fluid motion grabbed as images by a high speed camera during a whole one shot process have been presented in the literature. In the present study, a polarizing He-Ne laser coupled to a signal pick-up system consisting of a super video charge coupled device (CCD) in a water analogue model is introduced. The advantage of this combination of instrumentation is that it is the ability to visualize the diversity of fluid motion existing in the cavity-fill and post cavity-fill processes in a cost-effective manner.

5.2.2 Experimental Apparatus

(1) Test rig

A schematic diagram of the apparatus is shown in Figure 5-5. The test rig consists of a plexiglass (perspex) die assembly, a hot water supply tank and a pneumatic control circuit. The transparent plexiglass (perspex) plates were used to form a rectangular or circular model cavity with a variety of boundary conditions, gating and cavity thicknesses. In order to identify a cold boundary, hollow copper or aluminium square tubes filled with cold water were fitted so as to surround the model die cavity. These water-filled tubes were refrigerated before the start of each experiment. The plexiglass model die assembly was firmly held onto a supporting stand in a vertical position by several clamps. The hot water was kept in a tank at a constant prescribed temperature for each experimental shot and this was used to investigate the residual flow accompanying the thermals at different Reynolds and Rayleigh numbers. An actuator with a capacity of 0.3 litre was selected to meet the desired range of volume flow and fill time for the model cavity. The actuator was coupled to a pneumatic control system and was connected to a compressed air supply with a pressure range up to 10 bar.

The determinations of model scaling factors, fill times and actuator capacities have been directed by the laws of similitude offered in the preceding section 5.1.

All water analogue experiments were conducted without any other additives such as aluminium powder, hydrogen bubbles and ink dots etc.

(2) Optical set up

Figure 5-6 shows the schematic optical layout. A polarizing He-Ne laser assembly was employed with the inclusion of a beam expansion section. The laser beam after passing through the expansion section was filtered, collimated,

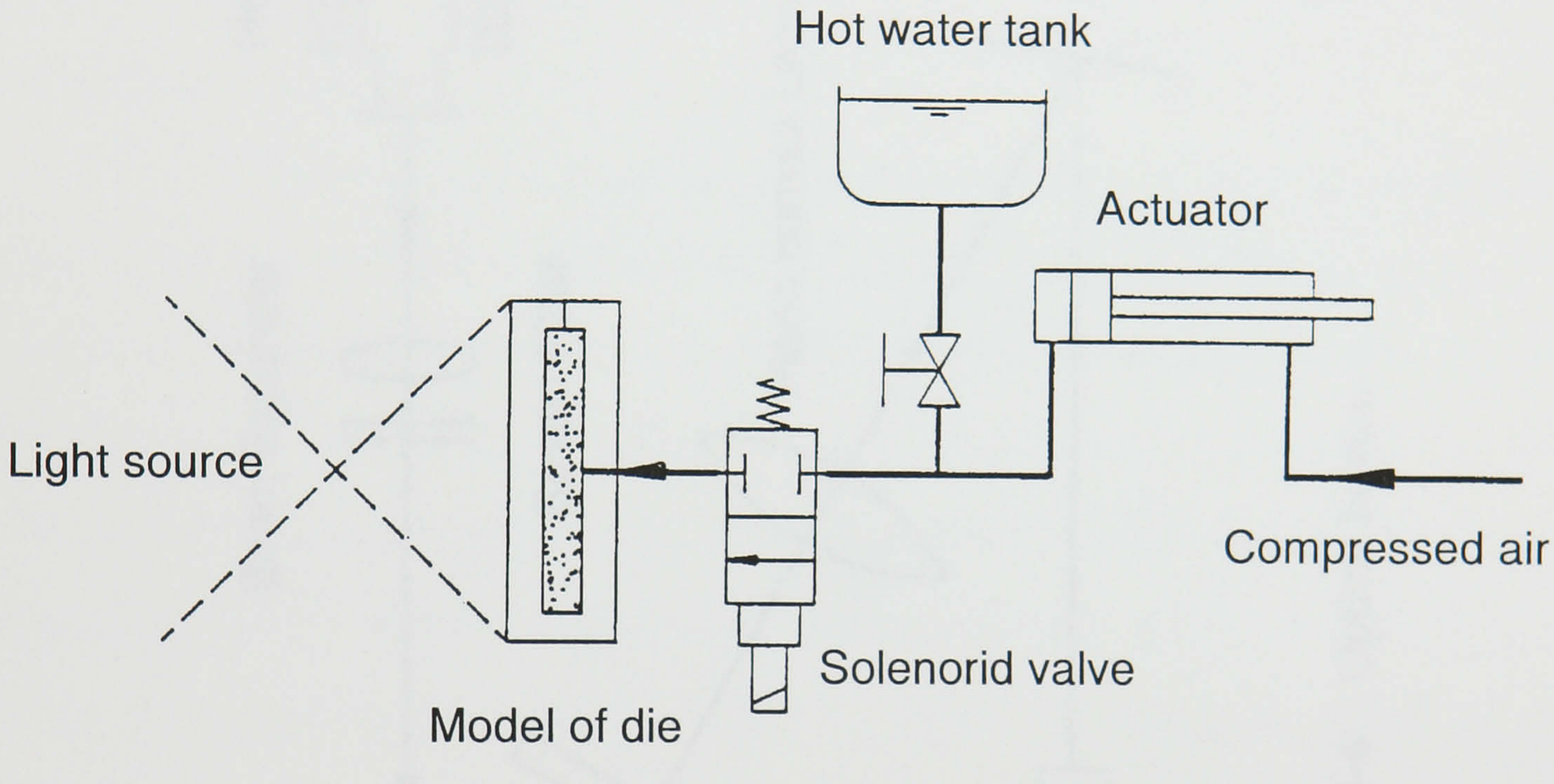

Figure 5-5 Experimental apparatus set up.

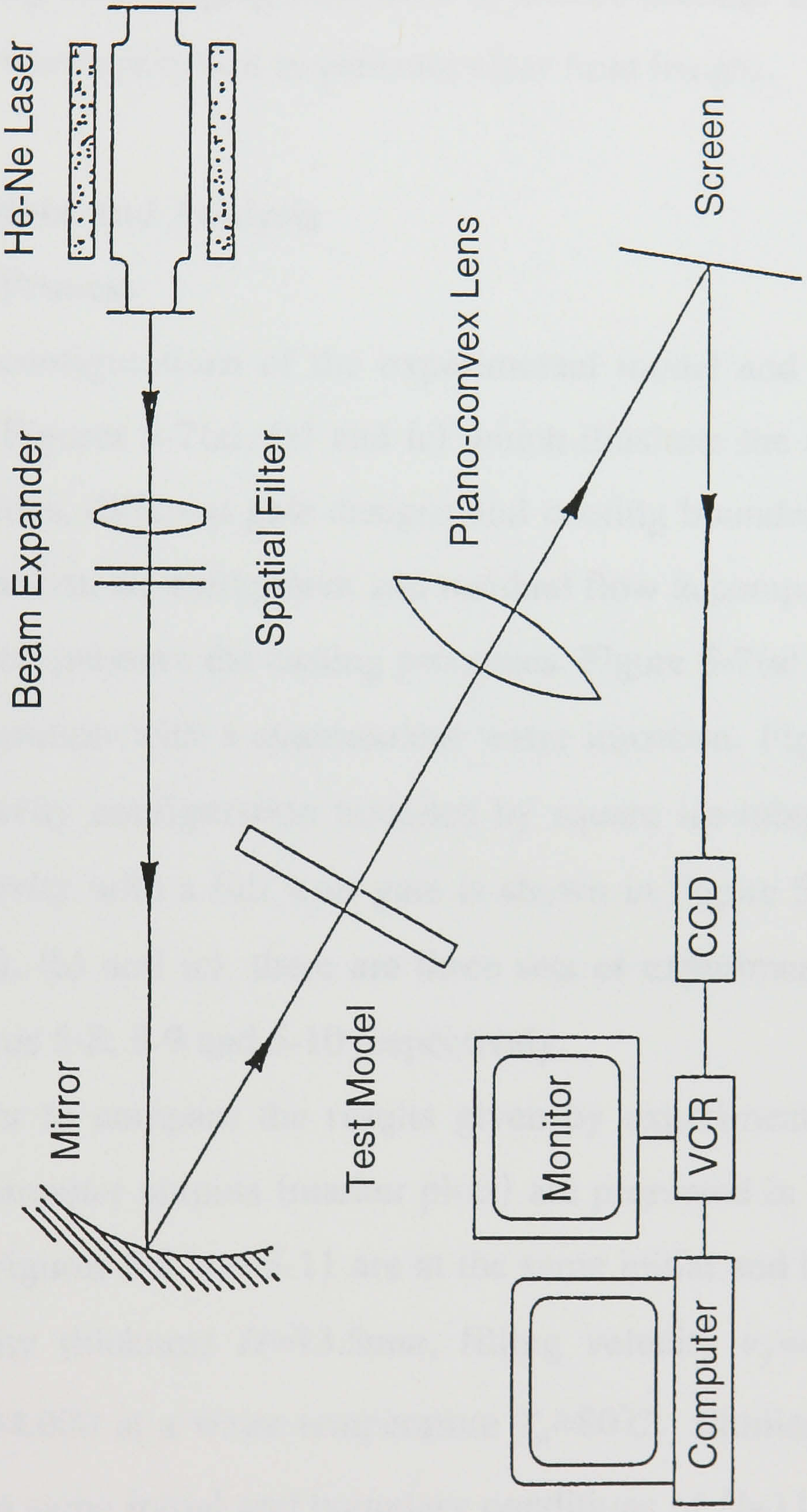

Figure 5-6 Optical layout.

and travelled to reach a mirror that acted as a reflector. The laser beam was then reflected to pass through the plexiglass model die assembly under observation. A plano-convex lens enlarged and made clear the optical field fringes which were displayed on the screen. Recording of the images was effected by a CCD camera with a recording time ranging from 1/50 to 1/2000 second. The characteristics of the laser tube were optimized to generate clear field fringes.

5.3 Observations and Analysis

5.3.1 Filling Process

Three configurations of the experimental model and their flow sketches are shown in Figures 5-7(a), (b) and (c) which illustrate the different geometries of model cavities, different gate designs and cooling boundaries for the study of filling flow pattern, air entrapment and residual flow accompanying thermal flow of the simulated pressure die casting processes. Figure 5-7(a) illustrates a circular cavity configuration with a symmetrical water injection. Figure 5-7(b) shows a rectangular cavity configuration bounded by square ice-tubes. A variant of this rectangular cavity with a full weir gate is shown in Figure 5-7(c). Correlated to Figures 5-7(a), (b) and (c), there are three sets of experimental records that are given in Figures 5-8, 5-9 and 5-10 respectively.

In order to compare the results given by experiments and computation, two sets of computer outputs (marker plots) are presented in Figures 5-11 and 5-12. The two Figures 5-8 and 5-11 are at the same initial and boundary conditions with the cavity thickness H=13.5mm, filling velocity v_f=1.93ms^{-1}, Reynolds number R_{ef}=94,000 at a water temperature T_w=80$^{\circ}C$. Similarly, Figures 5-9 and 5-12 are at the same initial and boundary conditions of H=11.5mm, v_f=9.9 ms^{-1}, R_{ef}=123,500 and at T_w = 80$^{\circ}C$. Actually the spike images shown in Fig.5-8 (a), (b), (c) and (d) are the condencing water vapour sticking onto the outside surface of the cavity as the cavity assembly taken out from the refrigerater.

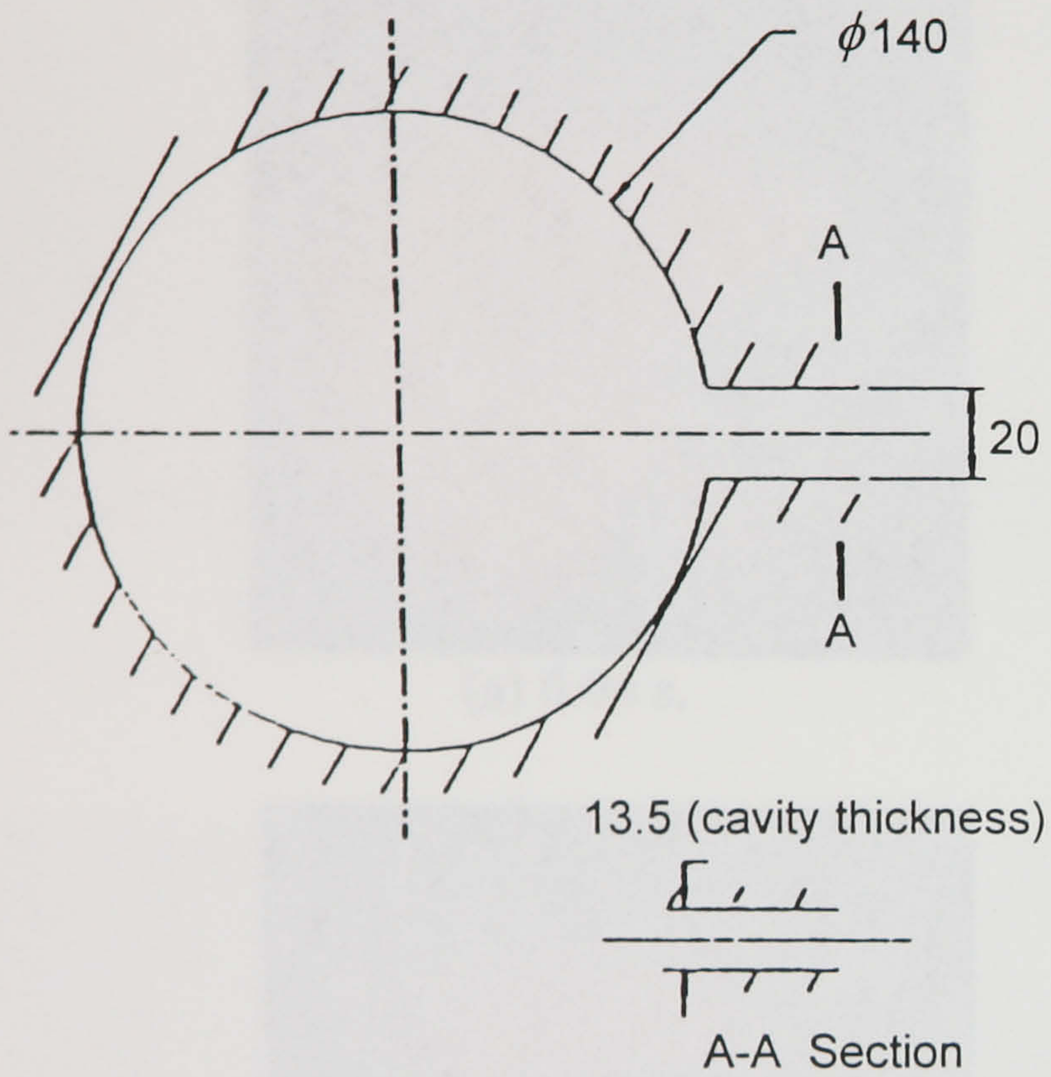

(a) Circular cavity

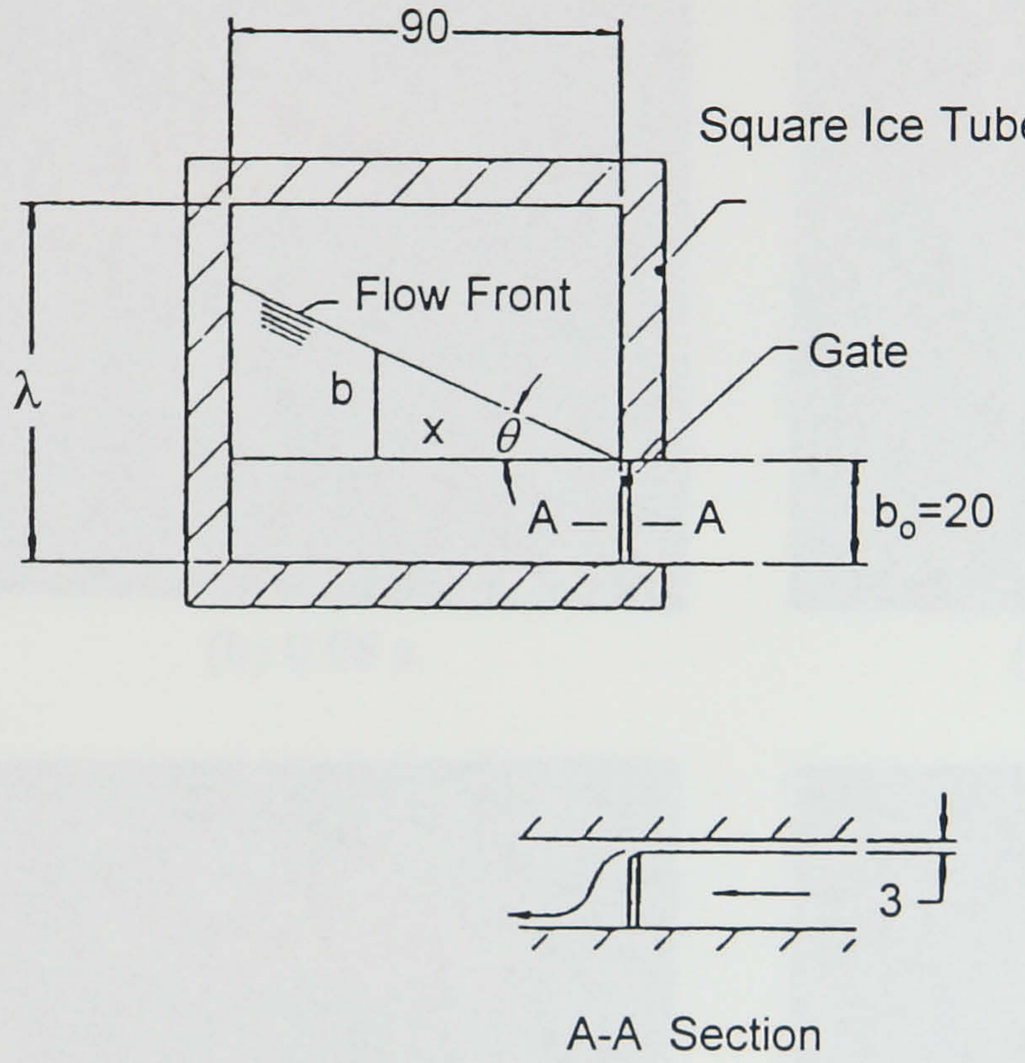

(b) Rectangular cavity and filling sketch

$\lambda = 79\ mm$

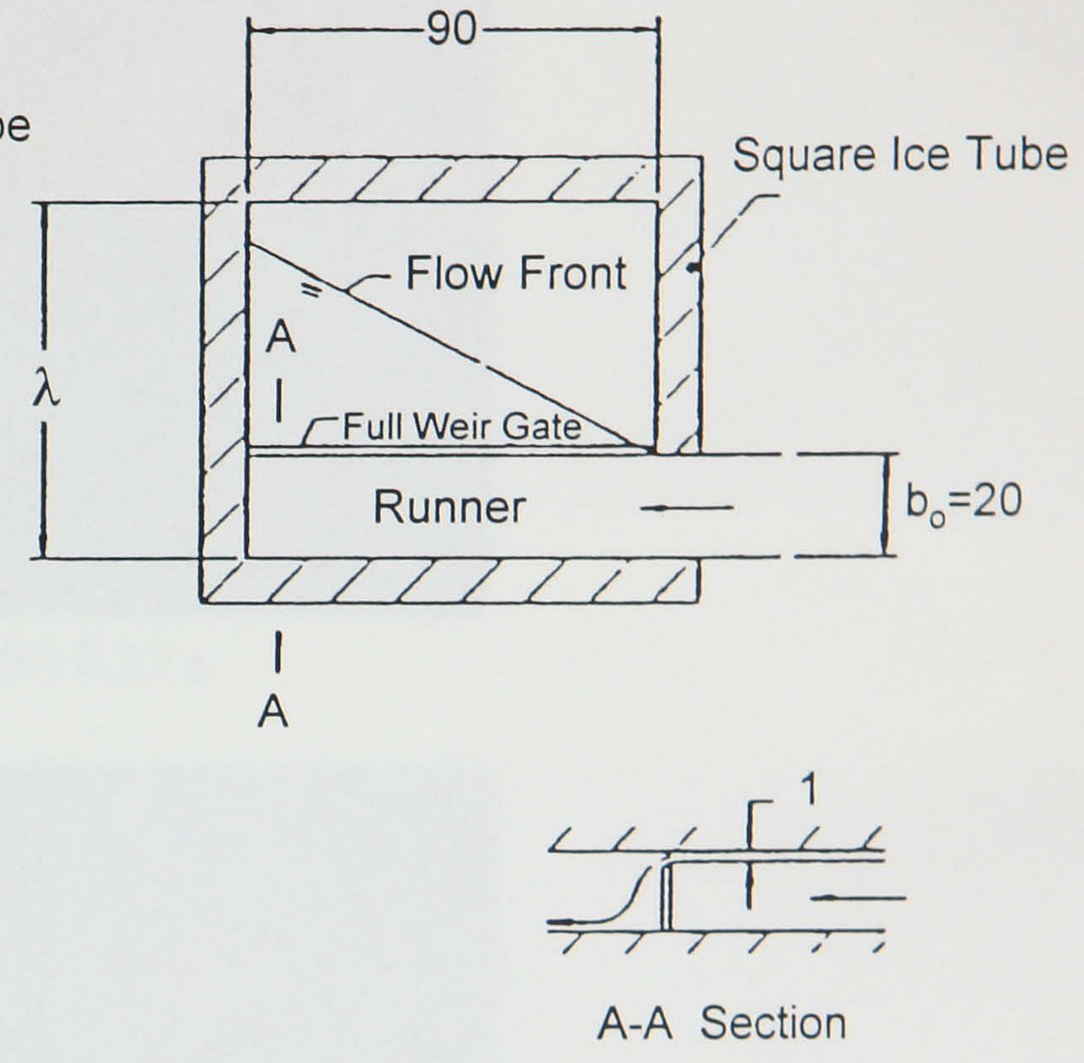

(c) Rectangular cavity and filling sketch

$\lambda = 93\ mm$

Figure 5-7 The configuration and filling sketch of the test model.

(dimensions: *mm*)

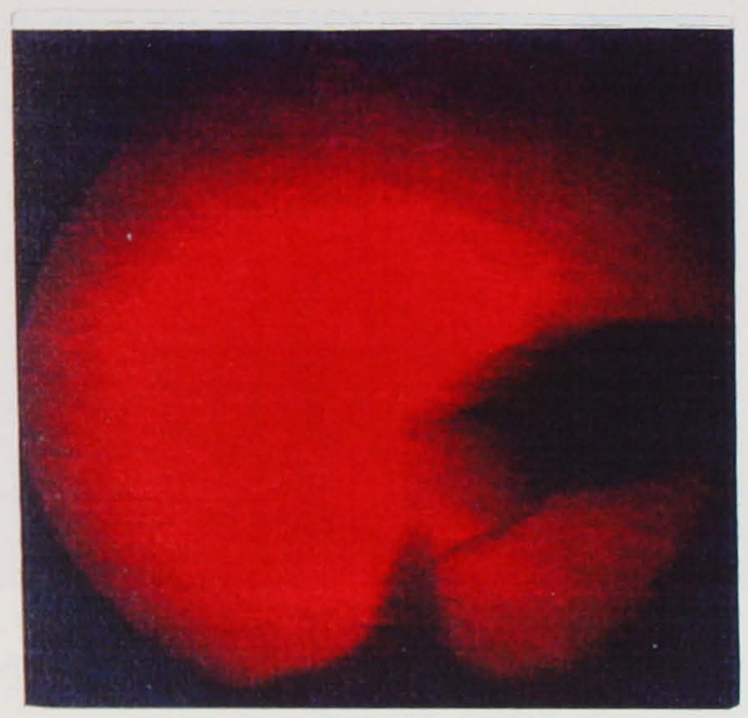

(a) 0.04 s.

(b) 0.08 s.

(c) 0.12 s.

(d) 0.16 s.

(e) 0.20 s.

(f) 0.24 s.

(circular cavity diameter: 140*mm*)

Figure 5-8 Filling pattern in a circular cavity from video-print

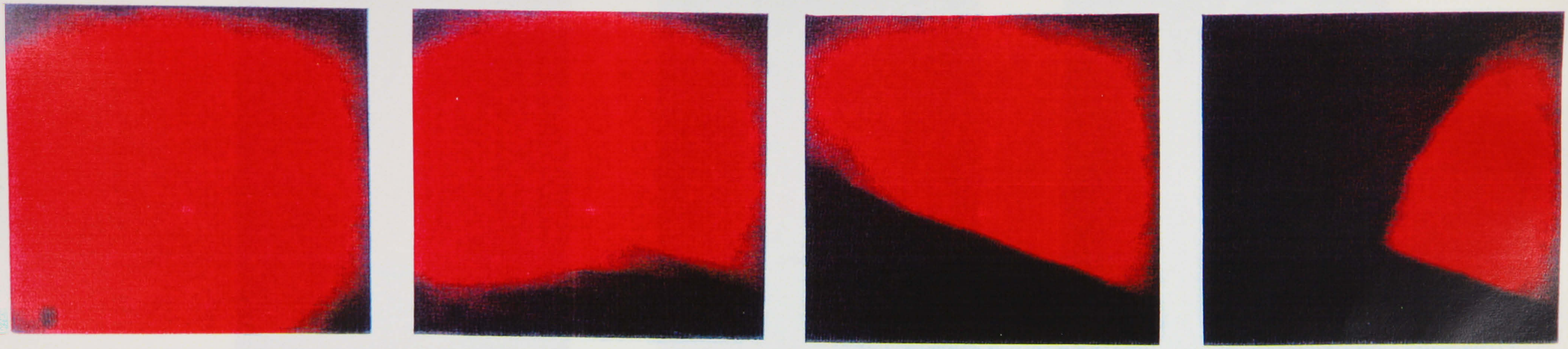

(a) 0.00 s. (b) 0.04 s. (c) 0.08 s. (d) 0.12 s.

(e) 0.16 s. (f) 0.20 s. (g) 0.24 s. (h) 0.28 s.

(rectangular cavity dimension: height 79*mm*, width 90*mm*)

Figure 5-9 Filling pattern in a rectangular cavity from video print

(rectangular cavity dimension: height *93mm*, width 90*mm*)

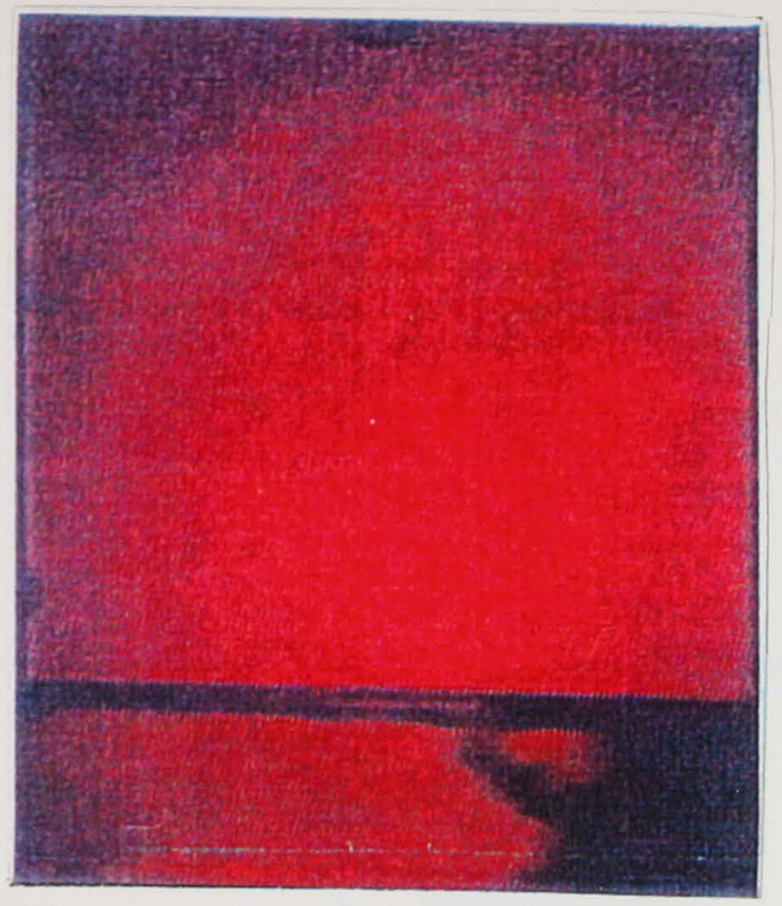

(a) 0.04 s. flow in runner

(b) 0.08 s. flow in runner

(c) 0.12 s.

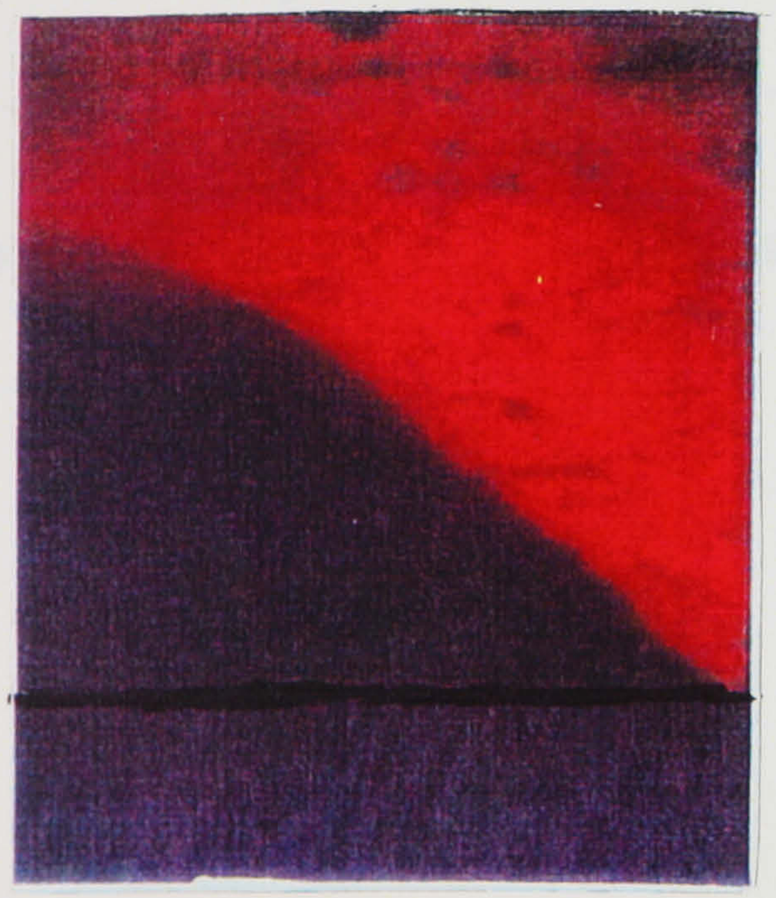

(d) 0.16 s.

(e) 0.20 s.

(f) 0.24 s.

Figure 5-10 Filling pattern in a rectangular cavity with a full weir gate from video print

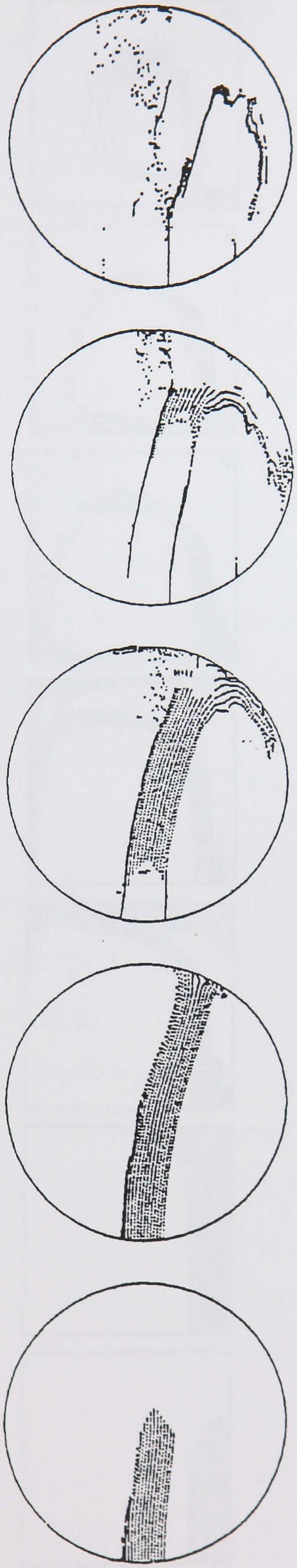

(a) 0.04s (b) 0.08s (c) 0.12s (d) 0.16s (e) 0.20s

Figure 5-11 Filling pattern in a circular cavity from computation

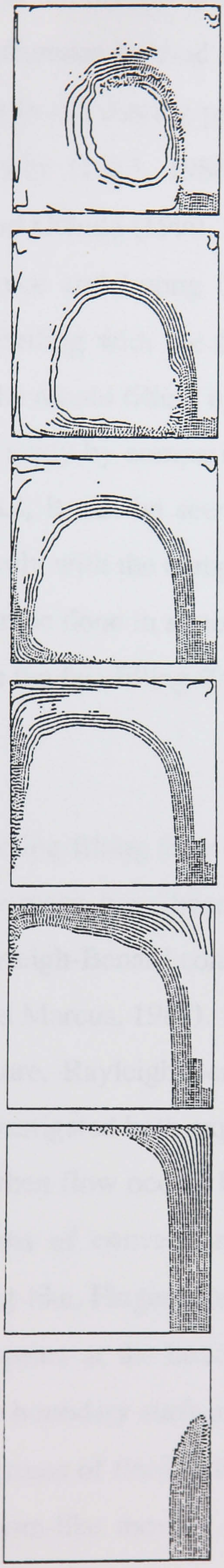

Figure 5-12 Filling pattern in a rectangular cavity from computation.

The numerical simulation used was based on the SMAC technique and applied the finite difference method to the numerical simulation of molten metal filling flow patterns in die casting processes. Recent studies have been reported by Hwang and Stoehr (1983, 1988); Hwang (1985); Minaie (1989) of 2-D modelling, Anzai and Uchida (1990, 1991); Jong and Hwang (1991a, b) of quasi-3-D modelling, Frayce and Loong (1991); Muttin *et al.* (1992). Lewis *et al.* (1992) of 2-D modelling with the finite element scheme and a Flow-3D fluid dynamics study of the mould filling by Hirt (1991) has also been reported.

In the present study by comparing Figure 5-8 with Figure 5-11; and Figure 5-9 with Figure 5-12, it can be seen that the experimental results are in good agreement qualitatively with the computation output. However, there is still some further work that can be done in simulating the highly irregular and complex free surface that exists in the fast filling flow of pressure die casting processes.

5.3.2 Thermals

While conducting filling flow visualization experiments, some interesting fluid dynamic phenomena have been observed. The structures of the thermals appear to be the Rayleigh-Benard convection flow in an enclosure space (Tritton, 1977; Humphrey and Marcus, 1987).

In the literature, Rayleigh-Benard convection and flow instability have been extensively investigated both experimentally and theoretically. The accurate information about when flow occurs has been provided by theoretical work. The detailed flow patterns of convection cells, thermals or plumes such as the Mushroom-like, Ring-like, Finger-like etc. come from experiments.

A thermal appears at the boundary that is driven by buoyancy forces to move away from the boundary surface into the bulk of the fluid stream. A typical thermal is a moving mass of fluid with the leading front blunted and folded back producing a mushroom-like moving part (Sparrow *et al.*, 1970; Tritton, 1977;

Humphrey and Marcus, 1987). Such patterns of thermals are influenced by the variation of fluid viscosity with temperature. The primary characterizing parameter for the natural convection flows can be expressed by the Rayleigh number R_a (Thomas, 1992):

$$R_a = G_r P_r = \frac{g\beta\Delta T c_p \varrho L^3}{k\upsilon} \tag{5-13}$$

The Rayleigh number is a ratio characterizing the relative magnitudes of buoyancy and viscous forces in the fluid layer. Instability occurs when the Rayleigh number exceeds a critical value of R_a about 1700. Above this the fluid layer becomes unstable (Tritton, 1977).

For observation of thermals the test apparatus, the optical set up and three test model configurations are shown in Figures 5-5, 5-6 and 5-7 respectively. The present experimental method used to observe thermals flow has advantages over the methods recommended in the literature, which required additives of aluminium powder or dye in the fluid. Moreover, water can be used as the test liquid to obtain very clear thermal plume flow structures.

The R_a is 3.2×10^9 for the test model configuration of Figure 5-7(b), in which the water temperature was 80 $^{\circ}C$, the cavity wall temperature was 18 $^{\circ}C$, and the cavity wall surrounded by hollow copper square tubes was at 0 $^{\circ}C$. The flow regime was turbulent. This is in agreement with Thomas' report (1992) that natural convection flow over a vertical surface is generally turbulent for $R_a > 10^9$.

Experimental evidence indicates that after completion of the cavity-fill, various patterns of thermals appear. Three of the thermal flow patterns are presented and shown in Figure 5-13:(i) Mushroom-like (Figure 5-13(a)): (ii) Earthworm-like (Figure 5-13(b)); (iii) Wave form (Figure 5-13(c)). The Earthworm-like thermals are quite similar to one kind of thermals that reported by Humphrey and Marcus (1987). From their illustrated picture, this kind of thermals which mark a spot tips as they rise in the flow.

(circular cavity: ϕ*140mm*)

(rectangular cavity: height *93mm*, width *90mm*)

(a) Mushroom-like

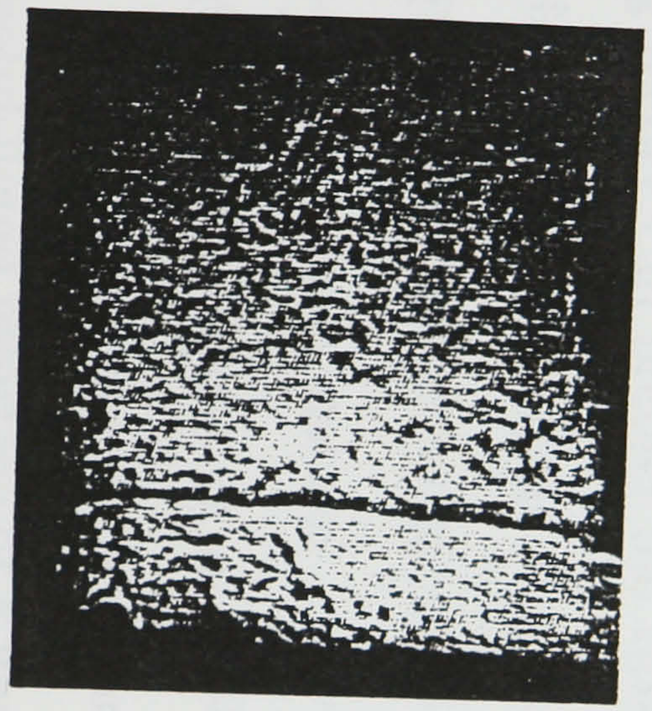

(b) Earthworm-like

(c) Wave form

Figure 5-13 Thermal flow pattern

The video output shows that the residual flow is co-existing with the thermal plumes (Gebhart *et al.*, 1988) from its beginning to fade out. All the model experiments were under the same conditions of the water temperature and the cavity wall temperature, and the decay pattern of the residual flow changes its structure in a similar manner of four steps:

(i) the rotational residual flow decays promptly in a short period;

(ii) the Mushroom-like thermal plumes appear and buoying up;

(iii) then thermals decay further to be the Earthworm-like thermals;

(iv) finally thermals decay to the Wave-form until totally fade-out.

The length of time of visual images can be counted to determine the decay time of the residual flow.

No existing theory can predict the flow structures of thermals within a cavity especially for moderate-to-large Rayleigh numbers (Christopher, 1991). There is little experimental information available on the thermals in a metal casting processes. Only some natural convection limit criteria have been developed for liquid metals (Buhr *et al.*, 1968). The pattern of thermals is important in the analysis of the interaction of residual flow and natural convection at the solid-liquid interface of a metal casting process (Adrian *et al.*, 1986). By obtaining the patterns of thermals from water analogue experiments, these data may be further processed to correlate the variation of molten metal viscosity with the temperature, and predict the locations of the mushy zones of solidification for a metal casting process. The present preliminary results show that the experimental method described in Section 5.2.2 is able to capture sequential thermal images and provide information on the residual flow history and the time interval for the whole filling flow period. On the other hand, the preliminary results of the convection flow structures are of special interest to researchers developing non-linear stability experimental methodologies.

5.3.3 The Air Entrapment

The flow visualization technique described here provides an efficient way to examine the dynamic behaviour of the air entrapment history. The variations of size and displacement of air bubbles, and the air-to-water fraction etc. may be examined. With the cavity configurations of Figures 5-7(b) and (c), the sequential movement of air bubbles are shown in Figure 5-14 and 5-15. Figure 5-14 is the print out after image processing via a program that interprets the input of the CCD tapes to computer. Figure 5-15 involves no images processing. There are two major phenomena to be observed for the patterns of air entrapment.

(i) In general, the larger bubbles move away via the vent of the model cavity (Figure 5-14), while the smaller bubbles move relatively slow with the residual flow stream (Figure 5-15). Here (in Figure 5-15) the air bubbles are seen as black spots in the images corresponding to the instant of injection. Some of the smaller bubbles then become blisters that stick to the inner wall of the model cavity as shown in Figure 5-16. This is quite similar to the research results from flat shaped aluminium die castings examined by X-ray photography (Anzai *et al.*, 1990).

(ii) In some cases the plume of bubbles can be compressed and hidden somewhere in the feed system during the filling of the cavity. Here, the residual flow, air bubbles and thermals are co-existing in a multiphase state within the model cavity. The motion of the bubble plume then dominates, and may influence the direction of the residual flow and the thermals; even reversing the rotation of the residual flow visualized by the thermals. The case of the hidden bubbles that cannot escape within a certain time period may provide one of the reasons to form porosity in castings. In other words, information on the sequential air entrapment is useful in the design of vents for the die and in one way predicts the location of porosity.

(rectangular cavity dimension: **height** *93mm*, **width** *90mm*)

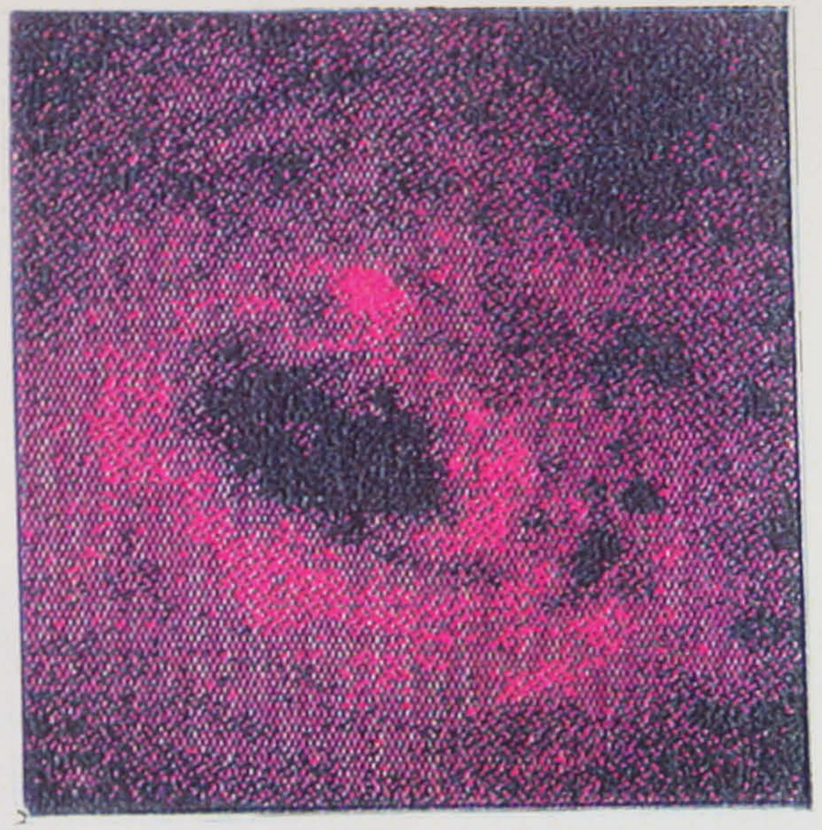

(a) 01:36

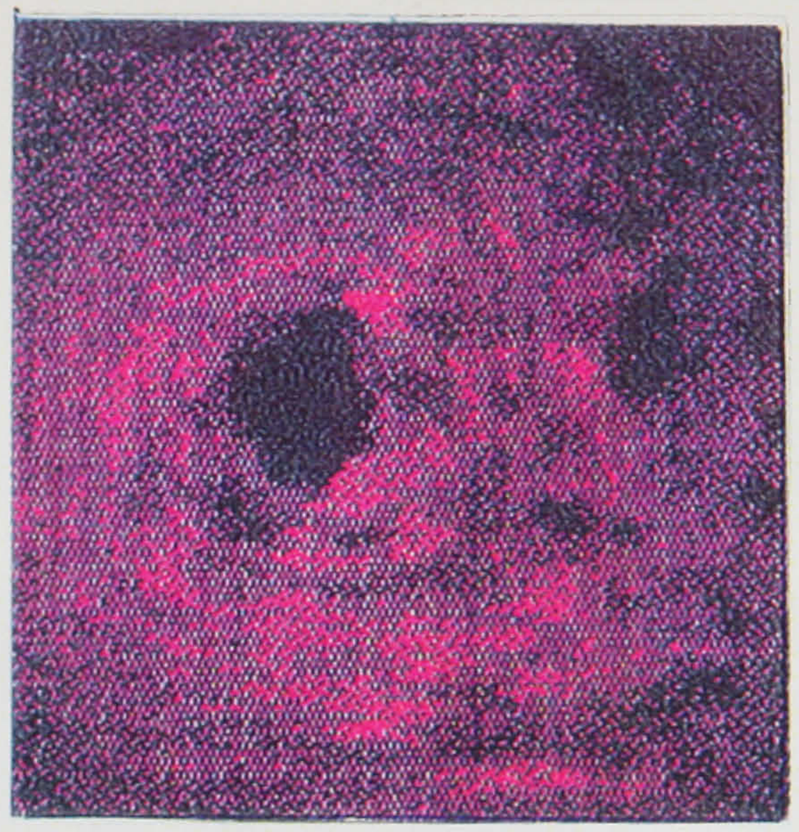

(b) 01:40

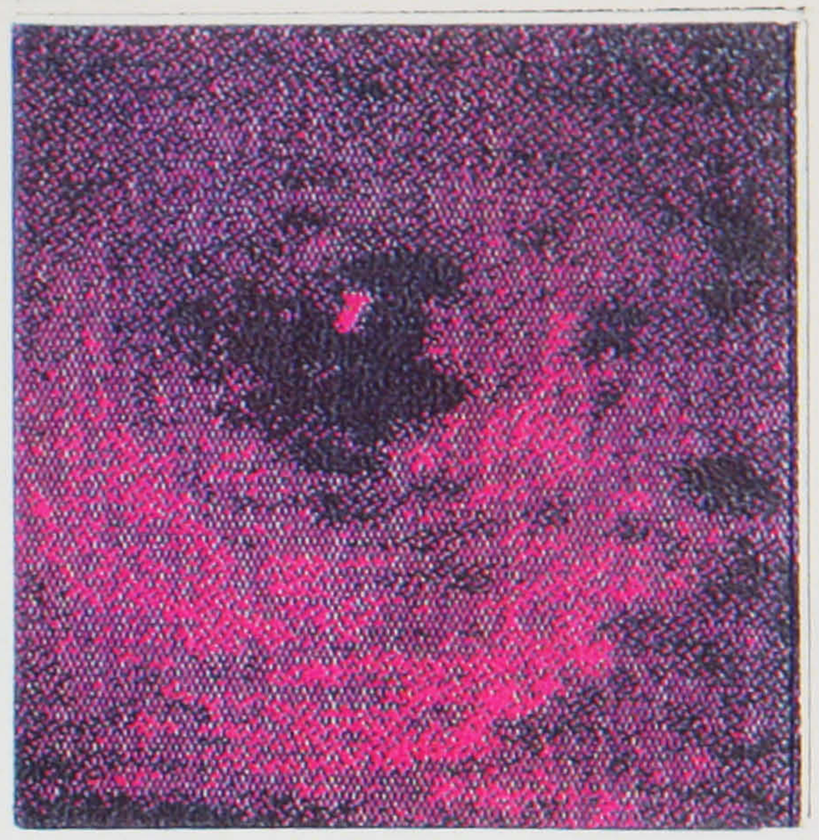

(c) 01:52

(d) 01:56

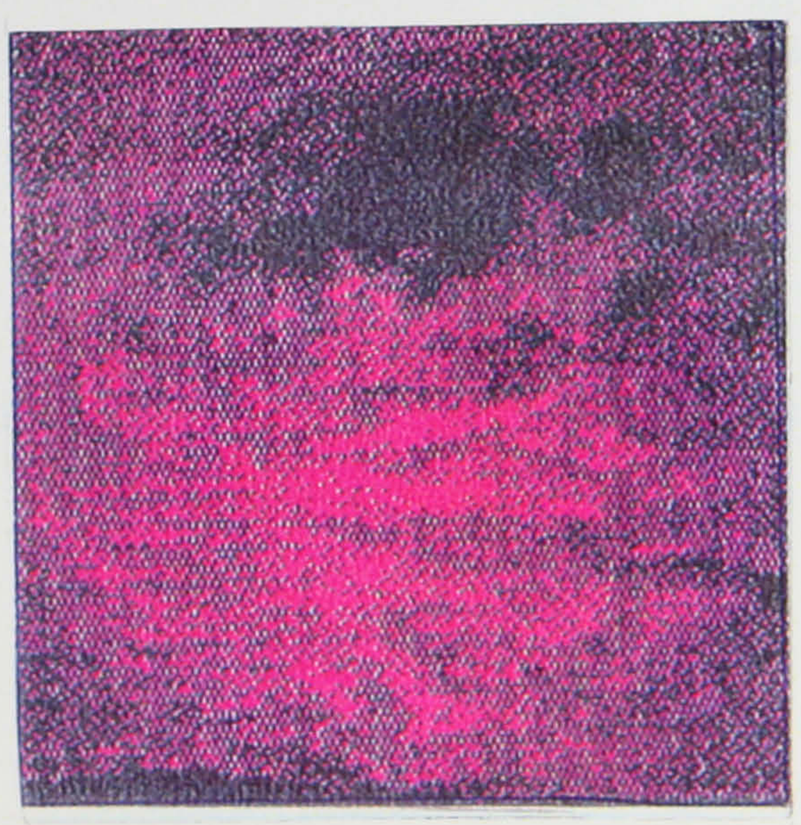

(e) 01:68

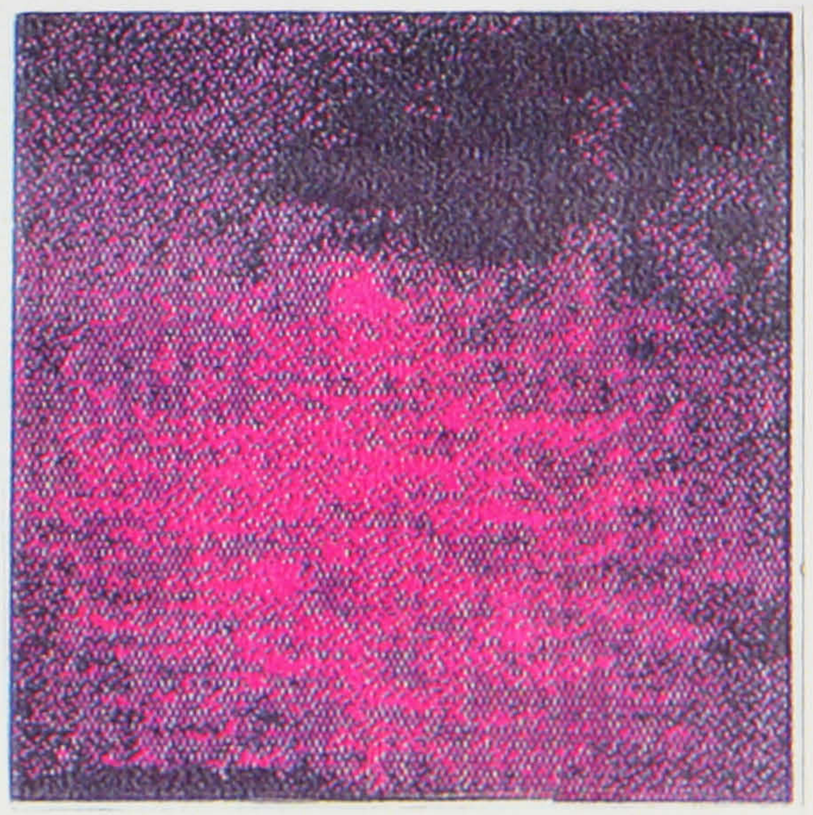

(f) 01:72

Figure 5-14 Dynamic behaviours of air entrapment from computer image processing

(rectangular cavity dimension: height 65*mm*, width 90*mm*)

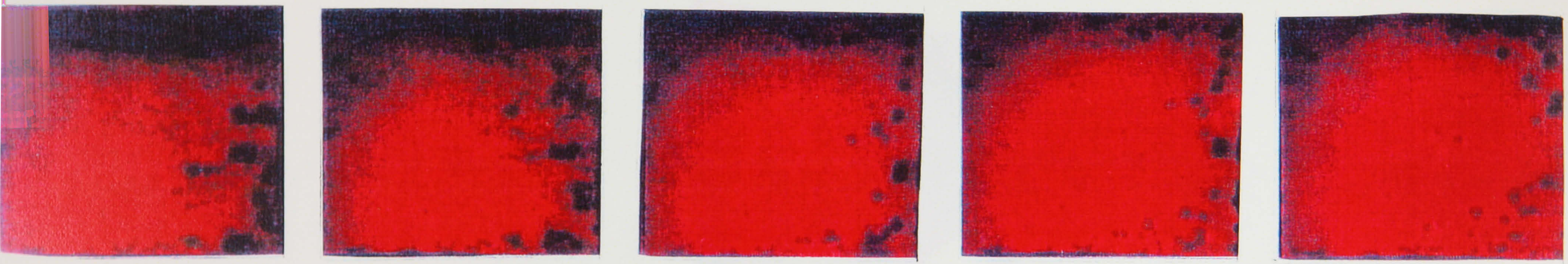

(a) 1.16 s. (b) 1.20 s. (c) 1.24 s. (d) 2.08 s. (e) 2.16 s.

Figure 5-15 Dynamic behaviours of air bubbles from video-print

(an inclined surface of the rectangular cavity test model: height 93*mm*, width 90*mm*)

Figure 5-16 Smaller bubbles become blisters that stick onto the inner wall of the cavity

5.3.4 Residual Flow

There is little available experimental information on residual flow in the pressure die casting processes (Desai and Pagalthivarthi, 1987; Minaie, 1989). The present study attempts to produce some insights into the residual flow that immediately follows the cavity-fill.

Table 5-4 lists the information obtained from the experiments for the configuration of the rectangular model illustrated in Figure 5-7(b) and other related parameters are given in Annex 5-1.

Table 5-4 The decay time of residual flow obtained from experiments.

H (mm)	v_f (cms^{-1})	t_f (ms)	t_d (s)	T_w $(^{\circ}C)$	υ $10^{-6}(m^2 s^{-1})$	c_r
11.5	869	221	29	80	0.367	0.0805
11.5	869	221	9	10	1.308	0.0890
5.2	869	99	6	80	0.367	0.0814
5.2	869	99	2	10	1.308	0.0967
2.0	1303	38	1	80	0.367	0.0918

Table 5-4 and its graphs (such as Figure 5-17) confirm that the correlation of decay time, t_d, and cavity thickness, H, is: $t_d \propto H^2$; and the correlation with kinematic viscosity υ is: $t_d \propto \frac{1}{\upsilon}$ for the cases of water analogue tests. The decay time coefficient of residual flow, c_r, is approximately a constant, the mean value of c_r is 0.088 from the data in Table 5-4.

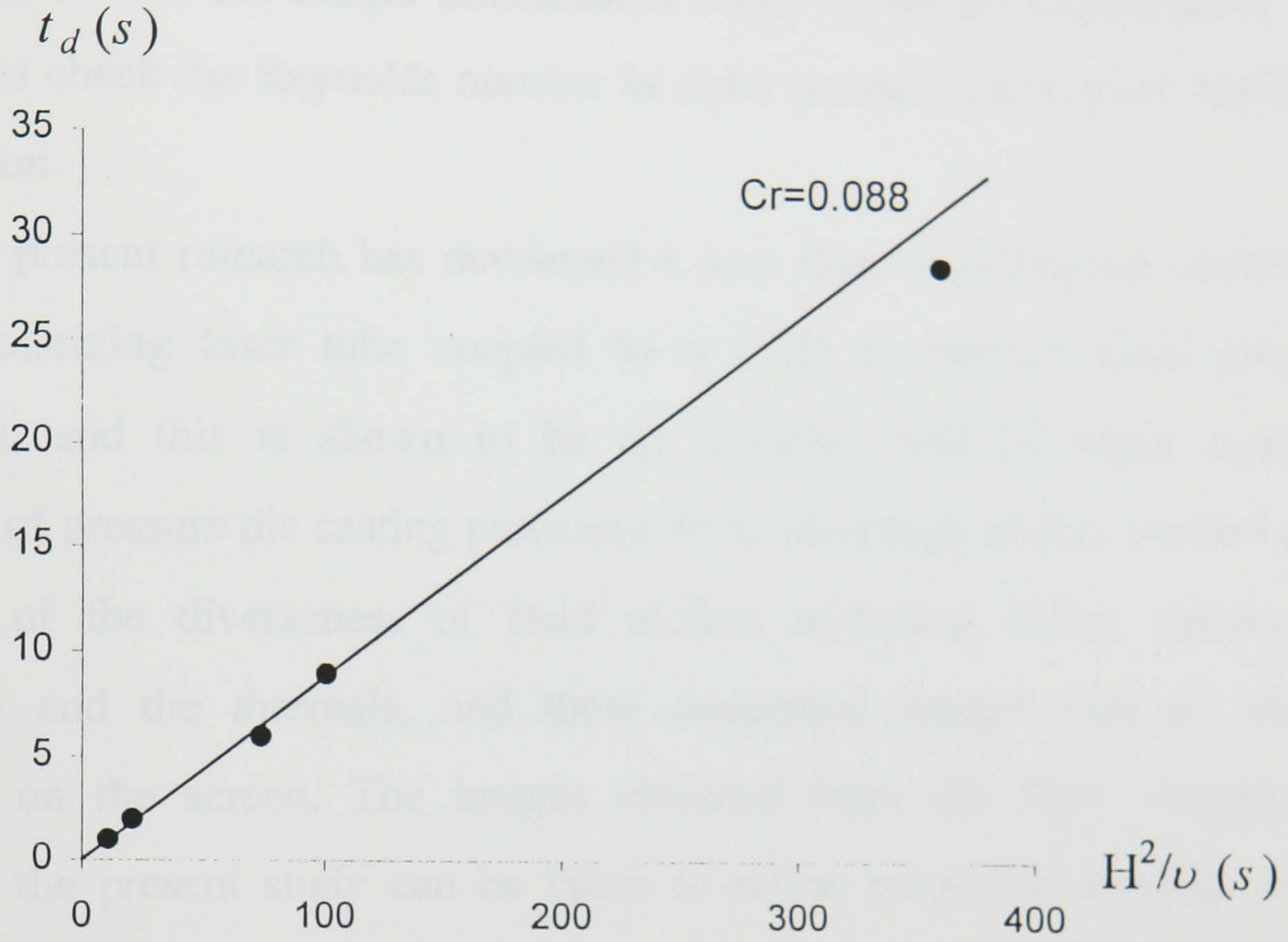

Figure 5-17 The relation between decay time, cavity thickness and kinematic viscosity.

5.4 Conclusions

Under the hypothesis of quasi-steady state, the similitude laws can be applied for simulating flow for the filling stage of pressure die casting processes. Equations (5-2) to (5-5) then can be recommended for water analogue experiments. The charts obtained from computation are also recommended as a means to determine the model dimensional scale. In model experiments, it is necessary to check the Reynolds number in order to maintain a quasi-similitude test condition.

The present research has developed a new flow visualization method by using a polarizing laser tube coupled to a CCD to capture fluid dynamic phenomena, and this is shown to be an effective way of water analogue simulation of pressure die casting processes. One advantage of this method is the disclosure of the diverseness of fluid motion including filling pattern, air entrapment and the thermals, and these sequential images can be studied repeatedly on the screen. The images obtained from the flow visualization method of the present study can be taken to refine numerical models, and to predict prototype information in multiphase-flow and other fluid engineering applications. This technique also could be recommended as one of the experimental methodology for the study of non-linear stability flow structures in fluid dynamic systems.

Annex 5-1

The data of the rectangular model cavities as shown in Figure 5-7(b) are given below as:

	Case one	**Case two**
Dimension:	90×79 *mm*;	90×79 *mm*;
Cavity thickness:	2 mm ;	11.5 *mm*;
Cavity volume:	14.3 cm^3 ;	82.2 cm^3 ;
Gate area:	40 mm^2 ;	60 mm^2 ;
Hydraulic diameter of gate:	3.636 mm;	5.217 mm;
Fill time t_f :	38 *ms* ;	221 *ms* ;
Gate velocity v_f :	13 ms^{-1} ;	8.7 ms^{-1};

The above two cases were carried out by using water with the same flow rate: 391cm^3s^{-1} but with two different temperatures of T_w=80$^\circ C$ or 10$^\circ C$; the following information is given against these cases as:

(i) when the kinematic viscosity: $\upsilon = 0.367\times10^{-6}m^2s^{-1}$;

(at a water temperature: $T_w = 80^\circ C$):

Reynolds number at the gate R_{ef} =128,800 for case one;

Reynolds number at the gate R_{ef} =123,700 for case two;

(ii) when the kinematic viscosity: $\upsilon = 1.308\times10^{-6}m^2s^{-1}$;

(at a water temperature: $T_w = 10^\circ C$):

Reynolds number at the gate R_{ef} = 36,100 for case one;

Reynolds number at the gate R_{ef} = 34,700 for case two;

The above data show that Reynolds number at gate

R_{ef} = 128,800 --- 34,700 > 20,000

which is in agreement with the conditions of quasi-similitude.

Chapter 6

Discussion

Chapter 6

Discussion

6.1 Discussion on the Study of Reclassification of the Processes

1. Figure 2-1 results from the sensitive electronic and mechanical instruments in experimental studies. Because of the dynamic errors existing in various instruments during measurement and the different initial and boundary conditions which always influence the experiments, a repeatability of the experiments is difficult to obtain. Nevertheless, Figure 2-1 is redrawn according to the analysis of the existing information from the literature covering the past half century. Although the repeatability of such data is not good, information in the literature showed similar profiles and common performance trends of pressure die casting machines. Figure 2-1 characterizes an overall profile of a pressure die casting process that can be used for reclassification of the whole process and as the basis for a mathematical approach to each stage.

Figure 2-1 shows the pressure-time and flow rate-time history represents the main characteristics of the molten metal feed system; also the dynamic characteristics of the oil pump, accumulator and control valves will be illustrated sensitively in such a figure. Also many effects occurring in association with the die casting cavity system such as air entrapment, plunger creeping, serious oil leakage etc. will be reflected sensitively in the dynamic profiles. Therefore, the study of these profiles will help to solve the problems encountered in research, design, machine setting and trouble shooting.

2. As described in Chapter 2, a set of mathematical formulae has been derived in order to tackle the fluid dynamic problems encountered in research, design and performance prediction in pressure die casting processes. Those formulae are created on a common background illustrated in Figure 2-2, which shows a functional systematic sketch for the hydraulic circuit consisting of a single oil pump and a single accumulator. In industrial practice, a pressure die casting machine may have one oil pump or two or even a group of pumps, and the flow rate of an oil pump may be constant or varied. Similarly a machine can be without accumulator, or may have one accumulator or two or even a group of accumulators. Eventually, the main hydraulic circuit shown in Figure 2-2 can be further simplified to that given as Figure 6-1 which omits the oil pump, accumulator and control valves. Thus Figure 6-1 becomes a diagram of a functional molten metal feed system. The flow rate, Q_a and pressure, P_a at the inlet of the cylinder shown in Figure 6-1 characterise the performance of the hydraulic system and thus the formulae contained in Chapter 2 are completely the same despite the paticular numbers of oil pumps, accumulators and control valves in a hydraulic casting system. In other words, the performance of pressure die casting machine can be improved by altering the static and dynamic characteristics of the flow rate, Q_a and pressure, P_a at the inlet of the cylinder. Once the oil pump and accumulator have been selected, changing the control valves in order to improve machine performance can be a cost-effective method in practice.

3. In section 2.5.4, a total of nineteen formulae uses the main parameters of fluid compressibility occurring in pressure die casting processes. In fact, there is a common background based on the following hypotheses:

(i) the pipe line of the molten metal feed system is very short and of a small diameter;

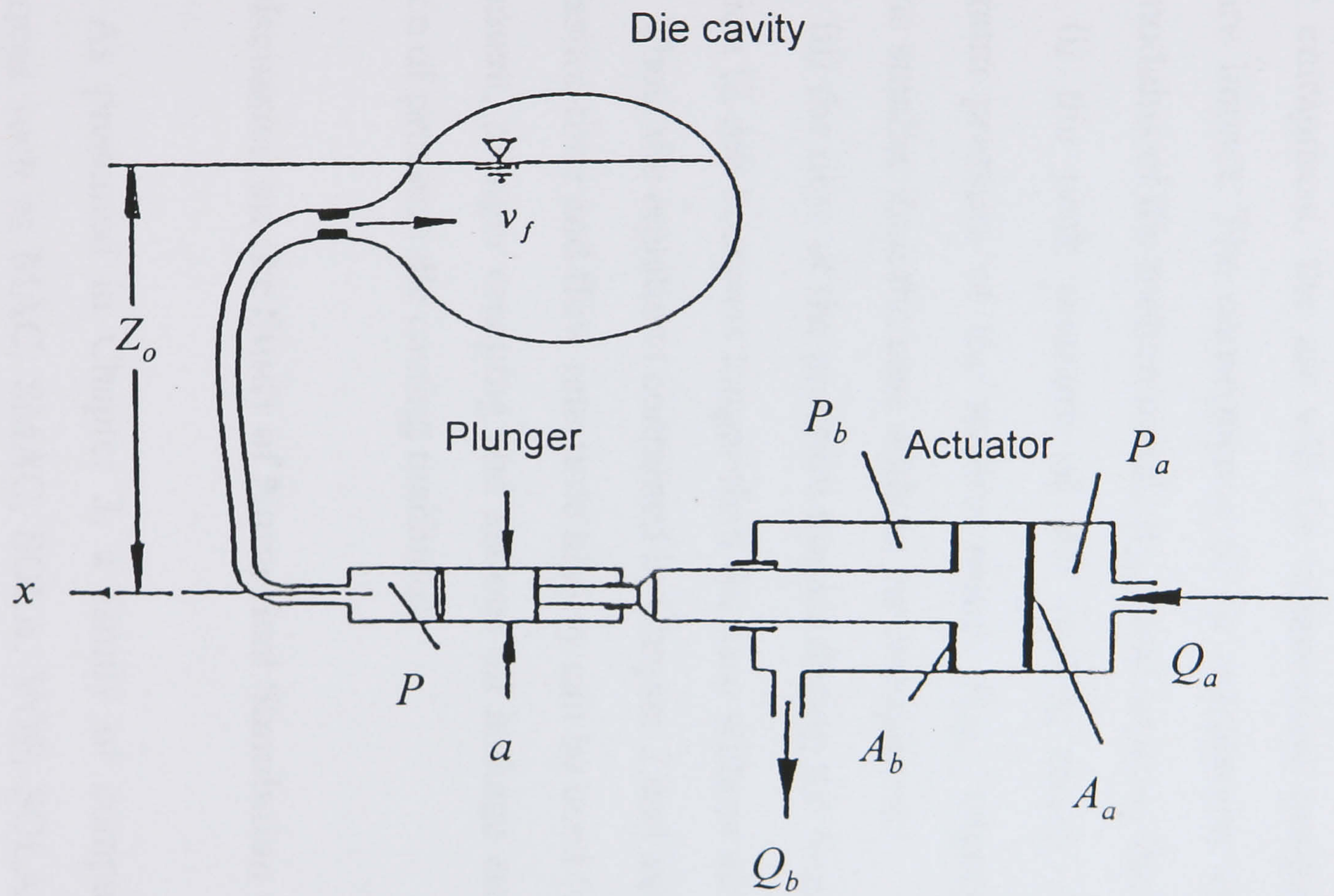

Figure 6-1 The molten metal feed system.

(ii) the material of the pipe line is absolutely rigid;

(iii) the feed system is full of molten metal without air entrapment.

Hypotheses (i) and (ii) are in good agreement with the real situation in pressure die casting machines. This is why the mathematical approach in this section is different to the approach of the water hammer phenomenon.

Hypothesis (iii) is removed from operating practice sometimes. In the case of air entrapment, the air will be compressed becoming tiny bubbles under pressure impact. The consequence of air entrapment will be a reduction in the bulk modulus of the molten metal, β_{met} and result in the following phenomena:

(i) the peak pressure of the molten metal, $(P_p)_{met}$ and the steady maximum pressure of the molten metal, $P_{\max}$ expressed in Equation (2-35) become smaller than the case without air entrapment;

(ii) the time of the pressure impact during the fourth stage, t_p expressed in Equation (2-39) becomes longer than the case without air entrapment.

Thus, the equations contained in Chapter 2 and associated with the profiles of pressure-time and flow rate-time history can be used for trouble shooting of air entrapment, plunger creeping and serious oil leakage etc. occurring in operating practice of pressure die casting machines.

6.2 Discussion on the Study of Numerical Simulation of Filling Pattern

1. As presented in Chapter 3, a family of computational fluid dynamics techniques such as MAC, SMAC, SOLA, VOF, SOLA-VOF and SIMPLE has been developed during the period from 1965 to 1982. During these years, the pioneers (Welch *et al., 1965;* Amsden and Harlow, 1970; Hirt *et al.*, 1975; Hirt and Nichols, 1981; Nichols *et al.*, 1980; Patankar, 1980 and so on) initiated the principles, created the mathematical models, amended the computational techniques and solved many difficult problems. The Finite Difference Method

has then been applied and is one of the two basic methods in numerical simulation which is used to solve various problems in fluid dynamics. In fact, Hwang and Stoehr (1987a) developed their specific codes for filling patterns of casting processes, and then others like Minaie, 1989; Anzai *et al.*,1988, 1990 and 1991; Hu *et al.*, 1992a,b,c; Lu, 1993 etc. extented the technique to pressure die casting processes. Despite the advantages of the finite element method, FEM, it requires large amounts of storage and longer computer operation times to compute flow patterns with complex boundaries and thick cavities. Therefore one of the aims of the present study was to try to reduce the amounts of storage and shorten the operation time by simplifying the computer programs. In order to achieve this aim, the SMAC technique was used for the analysis of the overall filling patterns and important conclusions resulted as discussed in the next paragraph.

2. It is nesseccary to highlight the important conclusions presented in section '3.7 Computational results and analysis':

(1) The effect of the kinematic viscosity on the overall filling pattern can be ignored in computational studies of pressure die casting processes.

In computation of the 'Broken-dam' project (Amsden and Harlow, 1970), a value of $\upsilon = 3000\times10^{-6}m^2s^{-1}$ that is about 3000 times of the kinematic viscosity of water was required for numerical stability in numerical simulation. Hirt and Cook (1972) pointed out that input of the artifitially high viscosity is a necessary feature of all finite-difference methods.

One way to overcome the instabilities and reduce the artificially high viscosty to a realistic viscosity of a working fluid is to search for improved finite formulae. Hirt (1968) examined certain kinds of truncation errors, explained the origin of instabilities in calculation and proposed a simple method for improving non-linear stability of finite difference equations in 2-D fluid flow calculation.

Fromm (1968) demonstrated a simple average of the central difference method and upwind difference method that produced a scheme with stability, and sharply reduced dispersion.

The present study benefited from solving the problems of instabilities and artificially high viscosity, which enabled the author to alter the input of the kinematic viscosity from $\upsilon = 1\times10^{-9} m^2 s^{-1}$ to $\upsilon = 1\times10^{-4} m^2 s^{-1}$ in order to investigate the effect of kinematic viscosity on the overall filling pattern of pressure die casting processes. This was validated from the computation experiments, the influence of the viscosity of the molten metal on the overall filling pattern can be ignored by assuming $\upsilon = 0$ at the filling stage and in advance of solidification.

(2) The effect of gravity on the overall filling pattern can be ignored in numerical simulation for pressure die casting processes whether the mould is placed vertically or horizontally, and this is not difficult to prove theoretically. Nevertheless the present study provides the related data using computational analysis, and its output pictures give the clear images with a conclusion that assuming acceleration due to gravity tends to be unimportant when the filling velocity $v_f \geq 10.00\, ms^{-1}$.

(3) In connection with the above sections (1) and (2), the computational experiments proved that the molten metal can be treated as an ideal fluid when the filling velocity of the molten metal $v_f \geq 10.00\, ms^{-1}$. Applying this hypothesis (sections 3.6 and 3.7) in the numerical simulation of filling patterns for pressure die casting greatly simplify the computer programs, and thus reduce the required storage capacity and running time of the computer.

(4) The influence of the filling velocity on the overall filling pattern is less important over a certain filling velocity range in the computational simulation for pressure die casting processes. This means that the overall filling pattern will be quite similar with different filling velocities provided these are greater than

$10.00ms^{-1}$. The way to get an expected filling pattern is to alter the geometric boundary conditions of the die cavity and the gate design.

The more important extension of the above (1)-(3) conclusions is to validate computationally the following approach:

(i) for pressure die casting processes, the molten metal can be treated as an ideal fluid which is a significant hypothesis to be used in computer programs for simulating filling patterns using 2D, quasi-3D or 3D simulation models;

(ii) to prove the quasi-similitude criterion presented in Section 5.1.3.

6.3 Discussion of the Study of the Residual Flow in the Post-Fill Stage

1. The residual flow is an unsteady fluid flow. Under the hypotheses presented in Section 4.2.1, the governing equations (4-2) and (4-3) are obtained. Firstly, the mathematical approach is to focus on the maximum available velocity of the residual flow $(v_{r\max})_g$. It should be noted that the filling velocity, v_f is a mean velocity at the gate, and is the maximum average velocity within the molten metal feed system. The maximum available velocity of the residual flow, $(v_{r\max})_g$ represents a real maximum available velocity at the centre point of the gate. The time to start counting the maximum available velocity of the residual flow, $(v_{r\max})_g$ is the instant when cavity fill is complete, which is also the first instant of the post-fill stage as well as the beginning of the pressure impact.

2. Chapter 4 reveals that an exponential function characterises the decay in motion with time for turbulent and laminar residual flow. A pendulum has a motion which also decays exponentially with time. Even though residual flow has a completely different nature to the motion of a pendulum, there is a common mathematical formulation in expressing their decaying nature.

3. It is well known that the lower characteristic Reynolds number to identify the transition from turbulent flow to laminar flow is always 2000 for a circular pipe section and 1100 for a rectangular pipe section. In the normal case, the molten metal flow across the gate section is rectangular, and this is used to calculate the Reynolds number. However, after completion of the cavity fill, it is difficult to identify the cross section of the residual flow inside the cavity. In Chapter 4, the residual flow is still treated as its motion is along an infinitely long tunnel formed by two parallel plates, where the gap between two parallel plates equals the cavity thickness with unit width. In fact, this is the physical model for the residual flow, from which the formulae presented were derived.

4. On the basis of the difference between turbulent and laminar flow, the laminar residual flow decays with time faster than the decay of turbulent residual flow. That can be explained qualitatively from their velocity profiles in associated with the one-seventh power law and the parabolic power law. Nevertheless, equation (4-16) indicates initially and quantitatively that the ratio of the damping constant of the turbulent residual flow is sixteen times that of the laminar residual flow. This is a contribution to the field of fluid dynamics.

5. The study of residual flow presented in Chapter 4 provides fundamental information in investigating the residual flow and its relation to solidification of the molten metal. For the case of the water analogue experiments, the decay time of the residual flow is proportional to the second power of the cavity thickness. This theoretical conclusion is in good agreement with experimental results. Also the mathematical formulation is similar to the well-known Chvorinov's rule and some other empirical formulae for the solidification time of molten metal. Because the solidified layer of metal developed with time non-linearly from the instant of completion of the cavity fill; the temperature of the cavity boundary

and the physical characteristics of the molten metal are also non-linear functions of time which presents the mathematical difficulties in investigating metal solidification processes. The transient temperature field, heat transfer, shrinkage-induced fluid flow, residual flow, thermals and air entrapment etc. should be integrated into a model in order to deal with their interactions with the solidification process. The Finite Element Method and Finite Difference Method should be applied in parallel through a computational study to get more accurate solutions for the improvent of the quality of pressure die castings. Eventually, the advanced design and manufacturing technology would result in increasing the production yield.

6.4 Discussion of the Experimental Study

1. As shown in Chapter 5, the similitude laws have been established to build the parametric relationships between model and prototype, and this idea has been widely applied in experimental studies of the steady flow process in past years. Eckert (1989) tried to extend the similitude laws to a study of unsteady flow in pressure die casting processes. He recommended the incorrect equation in his paper which gave an unrealistical dimensional scale of the model-prototype without a time scale. However, he still made a considerable contribution in his paper. He concluded that the heat transfer problems involved in the filling stage can be ignored because the process is too fast. This conclusion is convenient in a mathematical approach to the similitude laws applied to pressure die casting processes.

2. The equations relative to the similitude laws presented in Chapter 5 are more classical, where the fill time scale is a dominate factor in determining the scales of the test model and the experimental conditions.

For the whole of an experimental study, the first phase is to derive the model-prototype relation under the hypothesis of quasi-steady flow during the third filling stage in order to determine the dimensions of the test model. The second phase is then to perform the experiments to investigate the diversity of unsteady flow in pressure die casting processes. The logic in dealing with such unsteady flow problem is complicated. The conclusions drawn from the outcomes of computational experiments of unsteady flow are in a logical form from which to prove the absolute truth of the hypothesis of quasi-steady flow under the condition of quasi-similitude.

3. Figure 5-5 shows a schematic diagram of the experimental apparatus. The function of the test rig was able to simulate the main functions of a pressure die casting machine. The volume of the cylinder was slightly larger than the volume of the cavity-feed system. The control circuit of the test rig should give the piston a constant speed in order to keep a constant filling velocity approximately as in a real machine. The test rig proved to be simple, reliable, efficient and cost-effective; also it has the good characteristic of repeatability.

4. The experiments show that it is easy to fit hollow copper or aluminium square tubes filled with water or some other medium into the boundaries of the model cavity. Because the media-filled tubes can be heated or refrigerated before the start of the experiment, the temperature of the boundary can be controlled. Further work is suggested to look at the transient response of the thermocouples set into the model to investigate the relation of the thermals and the temperature fields.

5. Figure 5-6 shows the schematic optical layout used which is simple and inexpensive but reliable and effective. Nevertheless, some experimental skill is required to adjust the optical path in order to have clear images on the screen.

6. The experimental results can be repeatedly viewed in order to analyse and catalogue the data.

7. Previously the author employed a high speed camera to study the filling patterns for pressure die casting processes. More accurate photographs can be obtained by a high speed camera than those images gained by a CCD camera. However, a CCD camera is much better in studying the diversity of fluid dynamics during the filling stage and post-fill stages over a relatively long period in a water analogue model in a cost-effective way than employing a high speed camera.

8. Over the past years, research interest in pressure die casting processes has been focussed on filling patterns using experiments and numerical simulation. In this connection, the present study obtained good agreement between the experimental results and computational output qualitatively. However, there is still some further work that can be done in simulating the highly irregular and complex free surfaces that exists in the fast filling flow of pressure die casting processes. Therefore, it is recommended to adopt the hypothesis of an idea liquid for numerical simulation of the processes.

9. In the present study, it was not difficult to discover the phenomenon of the residual flow from the CCD tapes. The problem then is to determine precisely the total decay time of the residual flow in the post-fill stages.

10. Experimental evidence from the present study indicate that a wide range of dynamic behaviour of the working liquid exists during the residual flow in the post-fill stages. Three types of thermals are classified to match the appearance of the images obtained from the experiments:

(i) Mushroom-like;

(ii) Earthworm-like;

(iii) Wave form.

Three types of thermals were co-existing with the main stream of the residual flow and appearing not simultaneously in the sequence of fluid dynamic events depending on the temperature field of the liquid layers within the cavity. The Earthworm-like thermals correspond to the 'Ring-like' or 'Finger-like' thermals reported in the literature (Humphrey and Marcus, 1987). The 'Wave form' thermals really exist in the last phase of the residual flow and can be identified at the end of residual flow in the water analogue experiments.

There is still not a common classification of thermals in the literature, this means a lot of further work should be done in this field in the future.

11. The effects of air entrapment are associated with porosity and this has a direct effect on the quality of pressure die castings. Studies on the dynamic behaviour of air entrapment, path design of molten metal and venting layout would be needed to find a way to prevent porosity.

Chapter 7

Conclusions and suggestions for further work

Chapter 7

Conclusions and Suggestions for Further Work

This research deals with the development of mathematical models for the fluid dynamics of pressure die casting processes. The research has involved the analysis of the fluid dynamics problems in a whole process, has found the restrictions caused by the traditional classification of 'three stages' in interpreting the physical phenomena, and reclassified the total process to create a new basic tenet in constructing theoretical and practical investigations. Further, a study of numerical models for the flow patterns in the dominating cavity-fill stage and unsteady residual flow in post cavity-fill, a study of similitude laws for simulating molten metal flow in the processes have been performed and given a fundamental grounding for the experimental work. To cope with the theoretical study, a new application of a CCD in flow visualization for the simulation of flow patterns within the mould cavity has been developed successfully for the experimental work in order to verify the mathematical modelling and expose the diversity of fluid dynamics phenomena in pressure die casting processes. The computed results using the Simplified Marker And Cell (SMAC) technique have been compared with experimental data. On the basis of the computational analysis, valuable conclusions have been made that can be recommended for numerical modelling of the filling flow into complex geometry moulds in a more efficient way.

In this chapter, a summary of the major contributions drawn from this research is given briefly. For future extensions of the present work, recommendations are also made.

7.1 Contributions of the Theoretical Study

1. In the first phase of the research, the work focused on the analysis of the fluid dynamics problems of a whole pressure die casting process and found that the traditional 'three stages' classification of a filling process restricts the development of mathematical models for interpreting the physical phenomena existing in the whole process. Therefore, it was necessary to reclassify the whole process to create a new basic tenet in constructing theoretical and practical investigations.

A physical model has been drawn up for a typical molten metal injection machine, that links the molten metal filling system and oil power main circuit together as a physical background that enables one to carry forward the development of mathematical models.

Based on the analysis of the experimental data in the literature, the flow-rate-time and pressure-time history of a one shot process have been identified by fluid dynamics' profiles, thus a reclassification of the whole process is formulated by three quasi-stable stages plus two unstable stages according to the fluid dynamics' profiles. The present study breaks through the traditional classification of 'three stages', that enables one to distinguish two different phenomena of incompressibility and compressibility of fluid flow during cavity-fill and at pressure impact. The consequence of the reclassification leads to the development of mathematical models including formulae which interpret directly the problems involved in the five stages of a whole process, especially for the fourth stage of pressure impact.

2. A study of the dominating cavity-fill stage of the process was successfully made using the SMAC technique for numerical simulation of the filling flow pattern of the stage. The resulting filling patterns have been compared with

experimental studies presented in Chapter 5 that are in good agreement qualitatively. On the basis of the computational analysis of the influence of viscosity, gravity and filling velocity on the overall filling patterns, the molten metal can be treated as an ideal fluid and this important hypothesis has been proved computationally. Therefore, the hypothesis of an ideal fluid can be applied to the numerical simulation of filling flow patterns for pressure die casting processes. This contribution will simplify significantly computer programing, shorten the run time of iterations and reduce the amount of computer storage space. Furthermore, it can be extended to deal with quasi-3-D or 3-D simulation models. In addition, the computational results have contributed also to prove the validity of the similitude laws as applied in pressure die casting processes.

3. There was little information in the literature concerning the residual flow existing in the period of post cavity-fill inside the mould, and also there were no equations quoted for its study. Therefore it was necessarily to develop formulae for the phenomenon. On the basis of the observation of the residual flow phenomena from the experimental investigations of this study, the relevant hypotheses are: (1) no pressure gradient exists within the cavity during the decay time of the residual flow; (2) a Newtonian inertial force is balanced only by the shear stress for each liquid element of the residual flow; (3) the residual flow within the cavity is treated as 2-D motion. Under the above three hypotheses, the relevant differential equations, turbulent and laminar velocity profiles, decaying velocity and decay time of the residual flow have been formulated. The resulting velocity of the residual flow decays with time as an exponential function. The damping constant, K_{ot}, is inversely proportional to the second power of the cavity thickness H that is a dominating factor which influences the decay velocity of the residual flow. The decay time of the residual flow is proportional to the

square of the cavity thickness for the case of the water analogue experiment discribed. The formulated mathematical model of the residual flow has been verified by experimental results. The study also proved some empirical formulae used to calculate the solidification time of the molten metal. This contribution has resulted in a total of twenty eight fomulae presented in Chapter 4. The information contained in Chapter 4 is useful in finding the interaction of the residual flow and solidification process in order to improve the quality of pressure die castings.

4. In a study of the similitude laws for directing the experimental work, it was found that the previously offered formulae by Eckert (1989) were incorrect. The flow velocity always represents the Newtonian inertial force in similitude theory. Unfortunately, Eckert disregarded this point and attempted "**to eliminate velocity".** In so doing the Newtonian inertial force is eliminated and this is a fundamental force in dynamic similitude. Of course, this approach only involved grouping some physical parameters of the liquid, which resulted in an unrealistic dimensional scale for the model-prototype relation and did not include the time scale. The time scale is an important scale related to fill time that has been covered in relevant equations presented in Chapter 5, and should be counted into design practice of the experimental work.

Standing on the hypothesis of quasi-steady flow during the third filling stage, the analysis and criterion on different relationships between model and prototype are provided. The computational analysis presented in Chapter 3 shows that the overall filling pattern is unrelated to viscosity, it is also unrelated to gravity and velocity when the filling velocity $v_f > 5.00 ms^{-1}$ that is actually under the condition of quasi-similitude criterion. Logically, the truthfulness of the similitude criterion has been proved computationally. The development of

similitude laws directs the determination of model scales and analysis of experimental data, and provides a guide for experimental practice.

7.2 Contributions of the Experimental Study

In the past, there were only still frames from high speed motion pictures available, but no information of the diversity of fluid motion is available such as in the images grabbed by the high speed camera during a whole one shot casting process presented in the literature. In this research, a CCD together with a polarizing He-Ne laser coupled with a signal pick-up system in a water analogue model has been developed. This combination of instrumentation has been shown to be an effective way to visualize the diversity of fluid motion such as the several kinds of convection thermal plumes existing in cavity-fill and post cavity-fill processes. Another advantage of this method is the direct interpretation of the results on diversity of fluid motion, and these results can be studied repeatedly. The system also could be recommended for the study of other fluid dynamics systems specially for the case where the time interval between two images is longer than 0.04*s*. The large number of images obtained from the new flow visualization method can be used to refine numerical models, and to predict prototype information in multiphase-flow and other fluid engineering applications.

7.3 Recommendations for Further Study

1. Although the contributions made in the development of mathematical models for the residual flow contained in Chapter 4 are extensive, further work is needed in this area in terms of computational modelling of the interaction of the residual flow and solidification process. In addition, experimental research is also

needed for a better understanding of the solidification process involving convection thermals flow, that will be helpful in providing more accurate information for improving the quality of pressure die castings.

2. The heat transfer mechanisms at the mould casting interface have a complex nature and influence the whole process and the resulting quality of castings. Therefore, linking heat transfer mechanisms with the residual flow and the shrinkage-induced fluid flow require further research in this area to improve the performance of mathematical models for solidification process.

3. Experimental work with the digitized flow visualization method is needed in order to measure high velocity during cavity-fill for gaining a more accurate velocity field of the flow pattern and low velocity distribution of the residual flow. The accurate transient temperature measurement system also needs to be developed in order to obtain the temperature distribution within the mould cavity and at the boundary. Large numbers of images with more accurate data could be used to refine numerical models, and to predict the prototype information for die casting processes, solidification, multiphase-flow and other fluid engineering application.

References

Adrian R.J., Ferreira R.T.D.S. and Boberg T. (1986): "A review: Turbulent thermal convection in wide horizontal fluid layers", Experiments in Fluids, Vol. 4, p.121-141.

Allsop D.F. and Kennedy D. (1983): "Pressure Diecasting, Part 2, The technology of the casting and the die", Pergamon Press, p.45-48.

Amsden A.A. and Harlow F. H. (1970): "The SMAC mehtod: A numerical technique for calculation incompressible fluid flow", Report LA-4370, Los Alamos Scientific Laboratory, University of California.

Andersen S. T. and Ingerslev P. (1983): "A study of pouring a symmetrical casting by means of film shots and pressure measurements", 50th. Int'l. Foundry Congress, Cairo, Paper 7.

Andresen W.T. (1986): "Meltflow: computer aids for die casting", Die Casting Engineer, No.5, p. 38-43.

Andresen W.T. (1987): "Computer simulation and analysis of liquid metal flow and thermal condition in die casting dies", SDCE 14th Int'l Die Casting Congress and Exposition, Paper G-T87-019.

Anzai K. and Uchida T.(1990): "Extended quasi three dimensional mold filling simulation method for die casting", Imono, Vol.62, No.2, p.90-95.

Anzai K. and Uchida T. (1991): "Analytical solutions of die casting mold filling problems with ideal fluid model", Imono, Vol.63, No.6, p.528-533.

Anzai K., Uchida T. and Kataoka K. (1988): "Prediction of defects in die castings by quasi three dimensional flow analysis", Imono, Vol.60, No.12, p.763-769.

Anzai K., Uchida T. and Kataoka K. (1990): "Mold filling simulation of plate die casting by quasi three dimensional model", Imono, Vol.62, No.3, p.174-177

Ashton M.C. and Buhr R.K. (1973) "Direct observation of the flow of molten steel in sand moulds", Internal Report, TM-M-73-5, Canmet, Energy, Mines and Resources.

Barton H.K. (1964): "The pressure die casting of metals", Metallurgical Review, Vol.9, No.36, p.305-414.

Beckermann C. (1997): "Modeling segregation and grain structure development in equiaxed solidification with convection", Journal of Metallurgy, March 97, p.13-17.

Bennett F.C. (1961): Foundry, Vol.19, No.11, p.105.

Booth S.E. and Allsop D.F. (1983): "Cavity flow studies at BNF Metals Technology Centre using water modelling technique", SDCE 12th. Int'l Die Casting Congress and Exposition, Paper G-T83-033.

Brandt W.R. (1938): "Tech: Zeit Prackt. Metallarbeit", Machinery, Aug. and Nov. No.52, 53, p.1-87.

Buhr H.D., Carr A.D. and Balzhiser R.R.(1968): "Temperature profiles in liquid metals and the effects of superimposed free convection in turbulent flow", Int'l Journal Heat Mass Transfer, Vol.11, p.641

Chen Y.H. (1990): "Study of solidification, shrinkage and natural convection in casting processes", Ph.D. Thesis, The Ohio State University, USA.

Chen Y.H. and Im Y.T. (1990): "Analysis of solidification in sand and permanent mold casting and shrinkage prediction", Int'l. Journal of Machine Tools & Manufacture , Vol.30, No.2, p.175-189.

Chiang K.C. (1990): "Studies on the shrinkage-induced transport phenomena during alloy solidification", Ph.D. Dissertation. University of Missouri, USA .

Chiang K.C. and Tsai H.L. (1992a): "Interaction between shrinkage-induced fluid flow and natural convection during alloy solidification", Int'l Journal of Heat and Mass Transfer, Vol.35, No.7, p.1771-1778.

Chiang K.C. and Tsai H.L. (1992b): "Shrinkage-induced fluid flow and domain change in two-dimensional alloy solidification", Int'l Journal of Heat and Mass Transfer, Vol.35, No.7, p.1760-1770.

Chiou I.J. and Tsai H.L. (1990): "Modeling of porosity formation in castings ", AFS Trans. Vol.98, p.823-830.

Christopher J.F. (1991): "Numerical flow visualization of natural convection flows", FED, Vol.128, Experimental and Numerical Flow Visualization, ASME, p.307-310.

CSIRO (1992): Commonwealth Scientific Industrial Research Organization, Australia, "Die casting a problem? DMT-CASTFLOW relieves the pressure", Seminar on 27, Nov. 92, Hong Kong Productivity Council, Hong Kong.

Davis A.J. and Siauw H. (1977): "The significance of metal pressure in hot chamber die casting of zinc. Part I-Theoretical estimation of the pressure required to inject molten zinc into die cavities", SDCE 9th Int'l Die Casting Congress & Exposition, Paper G-T77-072.

Davis A.J., Siauw H. and Payne G. N. (1977a): "The significance of metal pressure in hot chamber die casting. Part II--Experimental determination of the pressure required to inject molten zine into die cavity", SDCE 9th Int'l Die Casting Congress and Exposition, Paper G-T77-073.

Davis A.J., Cunningham A. and Robinson P.M. (1977b): "The influence of injection cycle on casting quality. Part II--The effect of first stage conditions on cavity fill and casting porosity", SDCE 9th. Int'l Die Casting Congress & Exposition, Paper G-T77-012.

Davis A.J., Murray M.T. and Bennett W.J.(1980): "The effect of runner-gate design on the flow in a flat plate", Trans. of Society of Pressure Die Casting, No.80-10.

Davis A.J., Siauw H., and Cope M.A. (1985): "METFLOW- a system for the design and manufacture of metal flow systems for dies". SDCE 13th. Int'l Die Casting Congress & Exposition, Paper G-T85-065.

Davis C.V. and Sorensen K.E. (1968): Handbook of Applied Hydraulics, McGraw-Hill, p.2-27.

Desai P.V. and Pagalthivarthi K.V. (1987): "Modeling of combined fluid flow and heat/mass transfer," American Metal Handbook, 9th Edition, Vol.15, p.877-882.

Desai P.V., Berry J.T. and Kim C. (1984): "Computer simulation of forced and natural convection during filling of a casting", AFS Trans., p.519-528.

Doehler H. H. (1951): "Die casting", McGraw Hill, New York

Domanus H.M., Liu Y.Y. and Sha W.T. (1984): "Fluid flow and heat transfer modeling for casting", Proc. Engg. Foundation Conference on Casting and Welding Processes, p.361-375.

Eckert E.R.G. (1989): "Similarity analysis applied to the die casting process", Journal of Engineering Material and Technology, Vol.111, p.393-398.

Erickson J. L. (1945): "Light Metals", April, No.8, p.173.

Fink, R.(1987): "Quality Assurance by Microprocessor control of die casting machines", SDCE 12th Int'l Die Casting Congress and Exposition, Paper G-T87-016.

Flemings M. C. (1974): "Solidification Processing", McGraw-Hill.

Frayce D. and Loong C.A. (1991): "Mathematical modelling of the die casting process", Proceedings of 120th TMS Annual Meeting, p.873-902.

Fromm J.E. (1968): 'A method of reducing dispersion in convective difference schemes", Journal of Computational Physics, Vol.3, p.176-189.

Frommer L. (1933): "Handbuch der Spritzgubtechnik", Chapter 2, 3, 4, Academic Press.

Garber L.W. (1981): "Filling of the cold chamber during slow shot travel", Die Casting Engineer, p.36-38.

Garber L.W. (1982): "Theoretical analysis and experimental observation of air entrapment during cold chamber filling", Die Casting Engineer, Vol.26, No.3, p.14-20.

Gebhart, B., Jaluria Y., Mahajan L. and Sammakia B.(1988): "Buoyancy-induced flow and transport", Hemisphere Publishing Corporation.

Hansen P.N.(1991): "Fluid flow, Mould filling, and Gating", Cast Metals, Vol.4, No.3, p.155-158.

Hernandez F. and Hamar R. (1985): " Experimental study of mold filling in precision casting ", Memories et Etudes Scientifiques Revue de Metallurgy, Vol.82, No.1, p.37-45.

Hirt C.W. (1968): "Heuristic stability theory for finite-difference equations", Journal of Computational Physics, Vol.2, p.339-355.

Hirt C.W. (1991): "A Flow-3D study of the importance of fluid momentum in mold filling", Numerical Simulation of Casting Solidification in Automotive Applications, Published by The Minerals, Metals & Materials Society, p.173-187.

Hirt C. W. and Shannon J. P. (1968): "Free-surface stress conditions for incompressible-flow calculations", Journal of Computational Physics, Vol.6, p.403-411.

Hirt C.W. and Cook J. L. (1972): "Calculation three-dimensional flow around structure and over rough terrain", Journal of Computational Physics, Vol.10, p.324-340.

Hirt C.W. and Nichols B.D. (1981): "Volume of Fluid (VOF) method for the dynamics of free boundaries", Journal of Computational Physics, Vol.39, p. 201-225.

Hirt C.W., Nichols B.D., Romero N.C. (1975): "SOLA-A numerical solution algorithm for transient fluid flows", Report LA-5852, Los Alamos Scientific Laboratory, University of California.

Hu J., Eckert E.R.G. and Goldstein R.J. (1992a): "Numerical simulation of flow, heat transfer and solidification in pressure die casting". Modern Developments in Numerical Simulation of Flow and Heat Transfer, ASME HTD, Vol.194, p.67-74.

Hu J., Goldstein R.J. and Ramlingam S. (1992b): "Numerical simulation of filling flows in pressure die casting of thin walled components", The 2nd. Int'l. Conf.on Advanced Manufacture Technology, Sunderland, UK, Paper 11.2, p1-5.

Hu J., Ramlingam S., Meyerson G., Eckert E.R.G. and Goldstein R. (1992c): "Experiment and computer modeling of the filling flows in pressure die casting", Proc. of 1992 ASME Int'l Conf. and Exhibition on Computers in Engineering, Vol.1, p.401-410.

Humphrey J.A.C. and Marcus D.L. (1987): "Some observations of a sheared Rayleigh-Taylor/Benard instability", Experiments in Fluids, Vol.5, p235-239.

Huppert H.E. (1990): "Fluid mechanics of solidification", Journal of fluid Mechanics, Vol.212, p. 209-240.

Hwang W.S. and Stoehr R.A. (1983): "Fluid flow modeling for computer-aided design of castings", Journal of Metals, Vol.35, p.22-29.

Hwang W. S.(1985): "Computer aided fluid flow analysis of the filling of casting system", Ph.D. Thesis, University of Pittsburgh, USA.

Hwang W. S. and Stoehr R. A. (1987a): "Modeling of fluid flow", American Metals Handbook, 9th.Edition, Vol.15, p.867-876.

Hwang W.S. and Stoehr R.A. (1987b): "Computer simulation for the filling of castings", AFS Trans. 87-141, p.425-430.

Hwang W. S. and Stoehr R. A. (1988): "Molten metal flow pattern prediction for complete solidification analysis of near net shape castings", Materials Science and Technology, Vol. 4, p.240-250.

Iwahori H., Nakamura M., Tozawa K. and Yamamoto Y. (1985): "Metal flowing behavior in die cavities & defects in Aluminum die castings", Trans. of SDCE, Paper G-T85-072, p.1-7.

Iwata Y. and Yamamoto Y. (1986): "Molten metal flow through multiple gates in the runner of die casting", Journal of Japan Institute of Light Metals, Vol. 36, No. 9, p.577-581.

Jacobi E. (1950): "Flow calculation for die casting applied to the ASTM Committee B-6 test casting die", ASTM Bulletin, p.65.

Jong S. H. and Hwang W. S.(1991a): "Measurement of flow pattern for the mold filling of castings", AFS Trans. Vol.99, p.69-75.

Jong S. H. and Hwang W. S.(1991b): "Three-dimentional mold filling simulation for casting and its experimental verification", AFS Trans. Vol.99, p.117-124.

Jong S. H. and Hwang W. S. (1992): "Measurement and visualization of filling pattern of molten metal in actual industrial castings", AFS Trans. Vol.100, p.489-497.

Jonsson P., Saluja N., Ilegbusi O.J. and Szekely J.(1991): "Fluid-flow phenomena in the filling of cylindrical molds using Newtonian (turbulent) and non-Newtonian (power law) fluids", AFS Trans. Vol.91, p.291-297

Kawaguchi T. and Tanaka T. (1977): "New Ube-FF flash-free injection system", SDCE 9th Int'l Die Casting Congress & Exposition, Paper G-T77-041.

Kayama N. and Ichida M.(1953): "Report on the Casting Process Laboratory", Waseida University, No.4, p.13.

Koster J.N. (1997): "Visualizing convection and solidification in metallic alloys", Journal of Metallurgy, March 97, p.31-35.

Koester W. and Gohring K. (1941): "The study of the flowing and filling process in die casting by means of motion pictures", Giessergi, Vol.28, No.26, p.521-527.

Launder B. E. and Spalding D.B. (1972): “Lectures in mathematical models of turbulence”, Academic Press, London.

Lewis R.W., Usmami A.S. and Cross J.T. (1992): "An efficient finite element method for filling simulation in metal casting", Proc. Int'l. Conf. on Num. Methods in Engineering, University of Swansea. UK. p.273-283.

Lieby G. (1957): “Design of die castings”, American Foundrymen's Society.

Lin H. J. and Hwang W.S. (1988): "Combined fluid flow and heat transfer analysis for the filling of castings", AFS Trans., 88-144, p.447-457.

Lin Y. K. (1983): "Practice of the pressure die casting technology", Shu's Foundation Press, p.177-182.

Lindberg B., Hensen P. N. and Hensen S. N. (1991): "High speed filming of mould filling process of Al alloys in high pressure die casting", Proc. of Modelling of casting, welding and advanced solidification processes, Vol. 5, p.763-769.

Lipinski M., Schaefer W. and Andersen S. (1991): "Modeling of combined heat and fluid for determination of filling sequence for real complex shape castings", Proc. Engineering Foundation Conference on Modeling of Casting, Welding and Advanced Solidification Processes, Davos, Switzerland, p.771-776.

Lu H.Y.(1993): "Computer simulation of metal flow in thin-wall diecasting dies", MPhil. Thesis, Hong Kong Polytechnic, Hong Kong.

Lu H.Y., Lui Y.B. and Lee W.B. (1992): "Computer modeling of the effect of gating design on the metal flow in thin-wall die casting dies", Proc. Int’l Conf. on Manufacturing Automation, Hong Kong. p.536-541.

Maxworthy T., Gnann C., Kurten M. and Durst F. (1996): “Experiments on the rise of air bubbles in clean viscous liquids”. Journal of Fluid Mechanics, Vol.321, p. 421-441.

Minaie B. (1989): "Filling pattern and solidification analysis in die casting process", Ph.D. Thesis, University of Minnesota, p.1-104.

Minaie B. (1991): "Porosity-based prediction of forced convection coupled with solidification", ASME/JSME Thermal Engineering Proc., Vol.4, p.309-314.

Minaie B. (1992): "Modeling of fluid flow and phase change in cavities: a manufacturing/materials processing overview". Heat Transfer-ASME, Proc. of 1992 Energy Systems Design and Analysis Conf., Vol. 47, pt.3, p.109-112.

Minaie B., Stelson, K. A. and Voller V. R. (1987): "Fluid flow and solidification modeling of die castings", Proc. of Modeling of Materials Proc., ASME Materials Division, Vol.3, p.35-49.

Minaie B., Stelson K.A. and Voller V.R. (1991): "Analysis of flow patterns and solidification phenomena in the die casting process", Journal of Engineering Materials and Technology, Trans. of ASME, Vol.113, No.3, p.296-302.

Muttin F., Bellet M. and Chenot J.L. (1992): "Numerical simulation of inertial effects in Newtonian flows: application to the filling stage of the die-casting process", Journal of Material Processing Technology, Vol.31, No. 1-2, p.65-74.

Nguyen T.T., Siauw T.H. and Williams A.M. (1988): "Thermal analysis in diecasting", CSIRO Australia, Materials Australia, p.18-22.

Nichols B. D., Hitand C. W. and Hotchkiss R. S. (1980): "SOLA-VOF: A solution algorithm for transient fluid flow with multiple free boundaries ", Report LA-8355, Los Alamos Scientific Laboratory. University of California.

Nomura H., Terashima K. and Keishima K (1991a): "Prediction of die casting behavior by three dimensional simulation", Imono. Vol.63. No.5, p.425-431.

Nomura H, Keishima K.and Terashima K. (1991b): "Analysis of die casting filling behavior by use of water model", Imono. Vol.63. No.5, p.431-436.

Nussey I.D. and Kondic V. (1964): "A review of the theories of the pressure die casting process", Metallurgia, September, p.101-109 and October, p.165-171.

Ohtsuka Y., Ono T., Mizuno K. and Matsubara N. (1990): "Computer simulation system of molten metal flow in diecasting", Proc. of 57th World Foundry Congress, Part 9, p.1-10.

Patankar S.V. (1980): "Numerical heat transfer and fluid flow", Hemisphere Publishing Corporation.

Pickin J. E.J. and Travers S.M.P. (1991): "Practical experience with the MAGMAsoft mould filling and solidification simulation program", The Institute of Metals, April 91, p.22-23.

Piwonka T.S. (1995): "Investment casting" edited by Beeley P.R., and Smart R.F., The Institute of Materials, p.150-182.

Pokorny H. H. (1977): "Shot and performance of die casting machines-standardization and test", SDCE 9th Intl. Die Casting Congress & Exposition &, Paper G-T77-043.

Porter F. (1991): "Zinc Handbook: properties, processing, and use in design", Marcel Derkker Inc.

Randolph J., Hayner P. F., Thompson T.W. and Reichard D. (1977): "New developments in thin-wall zinc die casting equipment", SDCE 9th Int'l Die Casting Congress & Exposition, Paper G-T77-076.

Robinson P. M. (1977): "Assessing the performance of metal feed system", SDCE 9th Int'l Die Casting Congress & Exposition, Paper G-T77-71.

Rollez D. (1993): "The energy needs for thin wall die casting of zinc alloy", Hong Kong Diecasters Association Exposition and Symposium, April 22-24, Hong Kong.

Sachs B. (1952): "An analytical study of the die casting process", Ph.D. Thesis, Columbia University, USA.

Sachs B. (1967):"A practical scientific look at die casting", Die Casting Engineer, Vol.2, No.1.

Salloum G., Charland D. and Vinet A.(1987): "CASTFEED: interative design of feeding systems for die casting molds", SDCE 14th Int'l Die Casting Congress and Exposition, Paper G-T87-018.

Salloum G., Kappel V., Vinet A. and Loong C.A. (1989): "Die casting simulation and the automotive industry application of computer integrated materials processing", Int'l. Journal of Vehicle Design, IAVD Congress on Vehicle Design and Components, p.41-61.

Sanders S. D., Bruton R. C., Rodman C. W., Kaiser W. D. and Frost P. D. (1970): "Die casting process instrumentation study", The 6th Int'l Die Casting Congress, Paper No.51, p.1-8.

Sauki S. and Onada H. (1960): "Nippon Kinzoku Gakkai-Si", Vol.24, No.5, p.279.

Scott P., McConkey and Clark D. Skinner (1991): "SOLCAST: Implementation and successes", Numerical Simulation of Casting Solidification in Automotive Applications, Published by The Minerals, Metals & Materials Society, p. 335-338.

Segawa K. (1977): "A new gas-intensified die casting injection system", SDCE 9th Int'l Die Casting Congress & Exposition, Paper G-T77-042.

Shames I.H. (1992): "Mechanics 0f Fluids", McGraw-Hill, Third Edition.

Shawki G.S.A.and Kandell, A.Y.(1988): "A review of design parameters and machine performance for improved die casting quality", Journal of Mechanical Working Technology, Vol.16, p.315-333.

Sheptak N. (1963): "Water analogy study of fluid flow in the cold chamber", AFS Trans., Vol.71, p.349-357.

Smith W.E. and Wallace J.F. (1963) : "Gating of die castings", AFS Trans., Vol. 71, p.325-348.

Sparrow E.M., Husar R.B. and Goldstein R.J. (1970): "Observation and other characteristics of thermals", Journal of Fluid Mechanics, Vol.41, part 4, p.793-800.

Stoehr R.A. and Hwang W.S. (1983): "Modeling the flow of molten metal having a free surface during entry into molds", Proc. of Modeling of Casting and Welding Processes, II, p.47-58.

Stoehr R.A. and Ingerslev P. (1986): "Flow analysis of mold filling using Marker-And-Cell", Publication TM 86.09, The Laboratory of Thermal Processing of Materials, The Technical University of Denmark, p.1-21.

Street A.C. (1986): "The die casting book", 2nd edition, Potcullis Press Ltd, p.326-337 and p.647-653.

Stuhrke W.F., and Wallace J. F. (1965): "Gating of die castings", AFS Trans. Vol.73, p.569-597.

Tennekes T. and Lumley J. L. (1972): "A first course turbulence", MIT Press, Massachusetts, USA.

Thomas L.C. (1992): “Heat Transfer”, Prentice Hall, Inc., p.364-455.

Thome M.C. and Brevick J.R. (1993): "Modeling fluid flow in horizontal cold chamber diecasting shot sleeves", AFS Trans., Vol.101, p.343-348.

Tritton D.J. (1977): "Physical fluid dynamics", ELBS, p.127-161.

Veinik A. I. (1958): "Theory of special casting methods", Maschods, Moscow, p.143-242.

Walter H. and Sahm P.R. (1986): "A model for the computer simulation of liquid metal flow into moulds", Giesserei Forschung, p.119-124.

Wang J., Hansen S. F. and Hansen P. N.(1988): "3-D Modeling and simulation of mold filling using PC's", Proc. of Modeling of Casting and Welding Processes, edited by A.F.Giamei and G.J.Abbaschian. The Minerals, Metals & Materials Society, Vol.IV, p.741-753.

Welch J. E., Horlow F. H., Shannon J. P. and Dally B. J. (1966): " The MAC method: a computing technique for solving viscous, incompressible, transient fluid flow problems involving free surfaces", Report LA-3425, Los Alamos Scientific Laboratory. University of California.

White F.M. (1986) "Fluid Mechanics" McGraw-Hill.

Xue X., Hansen S.F. and Hansen P.N. (1993a): "Water analog study of gating designs on inclusion separation and mould filling control", AFS Trans., Vol.101, p.199-209.

Xue X., Hansen S.F. and Hansen P.N. (1993b): "Numerical simulation and experimental verification of mold filling processes through depressurized and less-depressurized gating system", AFS Trans., Vol.101, p.549-558.

Yamamoto Y., Iwata Y., Tozawa K. and Nakamura M. (1988): "Molten metal velocities and gas pressures in die cavity of commercial aluminum pressure die-casting", Journal of Japan Institute of Light Metal, Vol.38, No.3, p.129-133.

Yamamoto Y., Iwata Y. and Nakamura M. (1989): "Gas pressure in finally filled region in die cavities and defects in aluminum die casting", Journal of Japan Institute of Light Metals, Vol.39, No.1, p. 21-24.

Yeh J.L., Jong S.H. and Hwang W.S. (1993): "Improved 3-D mold filling model for complex castings and experimental verification", AFS Trans., Vol.101, p.1055-1063

Zeleniak M. (1993): "Die casting machine instrumentation", Hong Kong Diecasters Association Exposition and Symposium, April, 22-24, Hong Kong,